UCRL-19518

c.2

RATES OF GROWTH OF CRYSTALS FROM SOLUTIONS

Cheng T. Cheng
(Ph.D. Thesis)

December 1969

AEC Contract No. W-7405-eng-48

UCRL-19518

LAWRENCE RADIATION LABORATORY
UNIVERSITY of CALIFORNIA BERKELEY

DISCLAIMER

RATES OF GROWTH OF CRYSTALS FROM SOLUTIONS

Contents

LIST OF FIGURES

Chapter II

Chapter III

LIST OF TABLES

ABSTRACT

Studies of the rates of crystal growth from undercooled binary liquid mixtures of organic substances were conducted in two systems, a simple eutectic mixture of salol and thymol, and bibenzyl and trans-stilbene which form nearly complete solid solubility.

The newly designed temperature-gradient microscope stage, which incorporates facilities for a quantitative determination of the interfacial liquid and solid compositions and temperature through the use of interferometric techniques, has been successfully used for the first time to study the interfacial rate phenomena of crystallization.

A new theory is developed by modifying the Eyring's absolute-rate-theory-concept to interpret the experimental results for the growth of mixed crystal from the binary mixture in terms of a separation factor. This factor, representing the deviation from equilibrium, is found to depend on the growth rate and interface conditions.

The experimental results have shown that considerable departures of interfacial compositions and temperatures from the phase diagram can occur. The results suggest that the assumption of instantaneous phase equilibrium usually should not be used in design calculation for crystallization equipment.

The adaptation of Eyring-type theory in the prediction of rates of crystal growth by Kirwan and Pigford has been further tested and its application to crystal growth for various molecules of different structural complexity has been found to be good for an order-of-magnitude estimate.

CHAPTER I

INTRODUCTION

Crystallization is a very common phenomenon and is one of the most popular separation techniques being applied in many chemical process industries. The subject of crystal growth has been studied with an enthusiastic interest, both scientifically and technologically, for many years. However, the mechanisms by which crystals grow have not yet been understood completely.

In his opening remark in the 1948 Bristol International Conference on Crystal Growth, Mott (1948) referred to two types of problems in trying to understand crystal growth: (a) problems of understanding the atomic mechanisms at surfaces of crystals and (b) problems related with bulk heat flow and diffusion processes. These two types of problems were still pertinent and were re-emphasized by Cabrera (1967) in his closing address in the 1966 Boston International Conference on Crystal Growth. Frank (1958) in his introductory lecture in the 1958 Cooperstown International Conference on Crystal Growth stressed that the key to understanding the kinetics of crystal growth was to fully understand the morphology of the growing crystal. On the other hand, the failure in understanding the behavior of undercooled liquids quantitatively, which is an obstacle in understanding the crystallization phenomena, is, according to Turnbull (1965), attributed to lack of understanding the liquid structure at the solid-liquid interface. Both problems still need to be solved completely.

As a separation tool, crystallization possesses certain unique advantages as long as the freezing point of desired product is not too low. Among them are: (1) to provide products with high purities; (2) to purify thermally unstable compounds; (3) to separate close-boiling, chemically

similar isomers; (4) to offer a theoretical possibility of producing a pure product in a single stage. In addition, crystals produced with uniform sizes are desirable for good handling, packaging, storage and marketing.

Techniques of growing crystals have been known to humankind for centuries. However, the technology of designing a crystallizer and operating it still remains in the state of more of an art than a science, owing to incomplete understanding of the fundamental aspects of crystallization phenomena. Despite the many advances which have been made in recent years the crystal grower today still relies to a large extent on his past experiences; often he modifies empirical methods that have worked in the past.

The demand for ultrapure crystals in the solid-state industry has stimulated extensive studies of crystallization from melts. Among them zone refining has been demonstrated to be a promising method. Purifying chemicals from melts has many advantages. Rates of crystal growth are often high and use of a solvent is not required. Crystals produced from melts usually have better qualities.

Recently continuous fractional solidification for the purification of organic materials from melts has received considerable attention (Powers, 1966). To design a continuous fractional crystallization process properly one must have adequate knowledge about interfacial rate processes which govern both the growth rate and the purity of the crystals which are formed. This information is extremely scarce and is not likely to be found in the literature.

In designing crystallizers, either instant equilibrium or empirical rate expressions are often assumed to apply at the solid-liquid interface.

The equilibrium relationship is taken from the phase diagram. Particularly in zone refining studies or in fractional crystallization calculations the assumption of interfacial equilibrium is commonly used to relate the interfacial solid and liquid compositions. However, the departure of the interface conditions from equilibrium may be significant, owing to the interfacial kinetic resistance. Clarification of the interface phenomena is urgently needed if unsafe assumptions are to be avoided and operation of crystallizers improved.

The purpose of this study is to investigate the departure from equilibrium during the crystallization of mixed crystals grown in the binary organic liquid mixtures. The purity of such crystals is examined quantitatively in terms of growth rate and interface conditions. Two binary systems were used. The first, consisting of salol and thymol, forms a solid eutectic; at equilibrium either the one pure solid or the other solidifies. The other system was bibenzyl and trans-stilbene, which form a mixture with nearly complete solid solubility. Thus, two extremes of a class of phase diagrams were represented.

The proper interpretation of the results obtained from measurements of the rates of crystals in organic molten mixtures can not be accomplished unless the interfacial compositions and temperature are known. In Chapter II a new temperature-gradient microscope stage with facilities for the optical determination of interfacial liquid and solid compositions and temperature is described. This apparatus is suitable for the study of crystal growth from liquid mixtures of organic compounds with reasonable ranges of freezing points, because of its ability in stabilizing the crystal shape

at the interface owing to the imposed temperature gradient. The addition of facilities for quantitative determination of interface conditions to the apparatus previously used by Jackson et. al. (1966) makes it possible for the first time for interfacial rate phenomena to be studied successfully for organic substances.

It is known that crystal growth takes place by the attachment of atoms or molecules to the crystal surface. Before molecules can attach to the solid they have to diffuse to the interface and to be oriented in the right direction in order to be accepted into vacant sites in the crystal lattice. Although several quantitative models have been developed for mechanisms of molecular attachment none appears as promising as the application of a kinetic theory proposed by Eyring (1941) with the assumption of screw dislocation defects on the crystal surface according to Frank (1951). Such analyses have been made by Hillig and Turnbull (1956) and by Kirwan and Pigford (1969). Results have been encouraging but the expressions for growth rates obtained from such analyses have not yet been tested thoroughly.

In Chapter III the Eyring-type theory is reviewed critically, expecially the adaptation of it by Kirwan and Pigford (1956), and its application to data on the more complex organic molecules, such as polyphenyls, is discussed. The purpose is to test certain hypotheses concerning the estimation of the thermodynamic properties of the crystallization activated state, such as activation enthalpy and activation entropy for crystallization, suggested by Kirwan and Pigford.

In the past very little study has been conducted about the rates of growth of mixed crystals. With the help of the newly designed

temperature-gradient microscope stage described in Chapter II it is possible for the first time to determine the magnitude of the departure from equilibrium for the growth of mixed crystals from the binary mixtures. The experimentally determined liquid and solid compositions at the interface of a growing mixed crystal have shown to considerably deviate from their respective equilibrium values.

A new theory is also developed in Chapter IV by modifying the Eyring concept to interpret the experimental results for the growth of mixed crystals in terms of a separation factor. This factor is commonly applied in such separation process as fractional distillation. This factor, representing the deviation from equilibrium, is found to depend on the growth rate and interface conditions.

At least three objectives are accomplished from the work described in this thesis. One, the success in using the new temperature-gradient microscope stage, opens up a promising future for the study of interfacial rate phenomena of crystal growth for organic compounds. Secondly, the adaptation of Eyring-type theory in the prediction of rates of crystal growth by Kirwan and Pigford has been further tested and its application to crystal growth for various molecules of different structural complexity has been found to be good for an order-of-magnitude estimate. Finally, the experimental results have shown that considerable deviations of interfacial compositions and temperatures from the phase diagram can occur. The results suggest that the assumption of instantaneous phase equilibrium usually should not be used in design calculations for crystallization equipment. It is hoped that the results of these studies will contribute to the understanding of the interfacial rate process of crystallization.

CHAPTER II

EXPERIMENTAL STUDY OF RATES OF CRYSTAL GROWTH FROM ORGANIC MELTS

ABSTRACT

A new temperature-gradient microscope stage, suitable for the study of crystal growth from liquid mixtures of organic compounds, is described. The apparatus incorporates facilities for the optical determination of interfacial liquid and solid compositions and temperature through the use of light diffraction by a thin wedge of liquid. The imposed temperature gradient causes the profile of the solid-liquid interface to be more stable than in an isothermal liquid, despite compositional undercooling. Some results are presented for a binary system which forms a eutectic solution.

INTRODUCTION

Measurements of the rates of growth of crystals in molten mixtures of organic compounds can not be interpreted properly unless the composition and the temperature of the interface are known. Since the flux of material needed to form new solid phase sets up a diffusion gradient in the liquid and since the heat of fusion, released at the interface, has to be dissipated by heat conduction, use of bulk temperature and composition in the study of interface kinetic phenomena may lead to error. Consequently, Kirwan and Pigford (1969) and Berg (1938), Bunn (1949), Humphreys (1948), have employed optical interference methods for the observation of concentration patterns around crystals as they grow in supersaturated

solutions under microscopes. Similar methods have been used (Nishijima and Oster, 1956, and Secor, 1965) for the determination of diffusion coefficients from the shapes of interference fringes observed during the mixing of two liquids.

In most such work the liquid within which the crystals grow has been kept at a uniform temperature, except for the usually small temperature rise at the interface. By setting the temperature of the solution at a value beneath the equilibrium liquidus temperature the growth rate can be uniquely determined. Such measurements are very suitable for the study of crystal nucleation rates but they have an important handicap when growth of crystals, already present in the solution, is being observed. This is for the reason that the profile of a crystal interface as it advances into the adjacent liquid is often unstable at finite rates of growth. An interface which may be flat initially may project sharp points or "dendrites" into the undercooled liquid ahead, especially when that liquid is undercooled more than the interface liquid is. Thus, the shape of the liquid-solid interface may change as growth proceeds, especially when the system tends to grow rapidly even with small amounts of undercooling. In such a situation, as with the components salol and thymol, the freezing interface acts as a strong source of heat and the interface temperature rise, ΔT_i, may be as much as 2 to 3 deg. C. above the temperature, T_s, of the presumably isothermal microscope stage. A sharp pointed crystal, projecting itself into the adjacent liquid, will find even colder and more concentrated liquid a short distance from the interface than it feels at the interface itself.

To avoid such experimental problems during crystal growth studies Hunt, Jackson, and Brown (1966) introduced a temperature-gradient microscope stage (hereafter called TGMS) to study the growth behavior of certain pure organic substances, especially those for which the molecules are nearly spherical so that the freezing phenomena are like those for metals. By providing a flux of heat through the liquid within which the crystals were growing, the direction of the temperature gradient being normal to the interface, the shape of the interface was much more regular and more easily controlled. No provisions were made in their apparatus, however, for the measurement of bulk liquid or interfacial temperature. Furthermore, it is not easy to use their apparatus for observing the growth of crystals from solution because no means is provided for the determination of concentration patterns.

In the present work a new TGMS has been designed which provides not only a temperature gradient for the control of interface shape but also optical interference patterns for the calculation of temperature and concentration profiles near the crystal faces. The purpose of this paper is to describe this new equipment and to report a few results obtained with it using the binary systems salol-thymol. The bibenzyl-stilbene system is one in which undercooling is extremely slight, even at large rates of growth. Measurements for it were extremely difficult using an isothermal stage (Kirwan, 1967) and have been made possible with the aid of interface shape control. Details of the studies for this system will be reported in the future article.

DESCRIPTION OF TEMPERATURE-GRADIENT MICROSCOPE STAGE

The new TGMS, shown in Fig. 1, is suitable for growth rate studies using not only pure materials but also binary mixtures. The main features of this apparatus include hot and cold stages made from aluminum blocks 3/8 in. thick. These are placed at the left and right of a stationary mount which can be adjusted in position with the microscope's mechanical stage. The liquid is placed inside an optical wedge formed by two half-aluminized glass slides, as in the previous microscope optical interference apparatus (Kirwan and Pigford, 1969, and Kirwan, 1967). The opposite ends of the lower microscope slide rest on the hot and cold stages, respectively, and the temperature of the glass and of the liquid contained in the wedge varies nearly linearly with position in the space above the gap between the two stages. The glass slides are held in position relative to each other by a Teflon boat which is connected to a lead screw turned by a variable speed motor. As the screw advances the boat is moved horizontally under the microscope objective, the boat advancing toward the cold stage. Thus, a point in the wedge encounters progressively lower temperatures and increasing undercooling is experienced by the liquid at that point. The growth rate is determined by the setting of the motor which drives the lead screw.

In Fig. 2, the picture at the left shows the Teflon boat, used to move the diffraction assembly slowly toward the cold stage. The lead screw from the drive motor fits into the yoke at the left. The partially aluminized slides are at the right. The larger slide fits into the boat from below and forms the bottom of the wedge. The smaller slide is held at an angle to the longer slide by the adjustable lever on the boat.

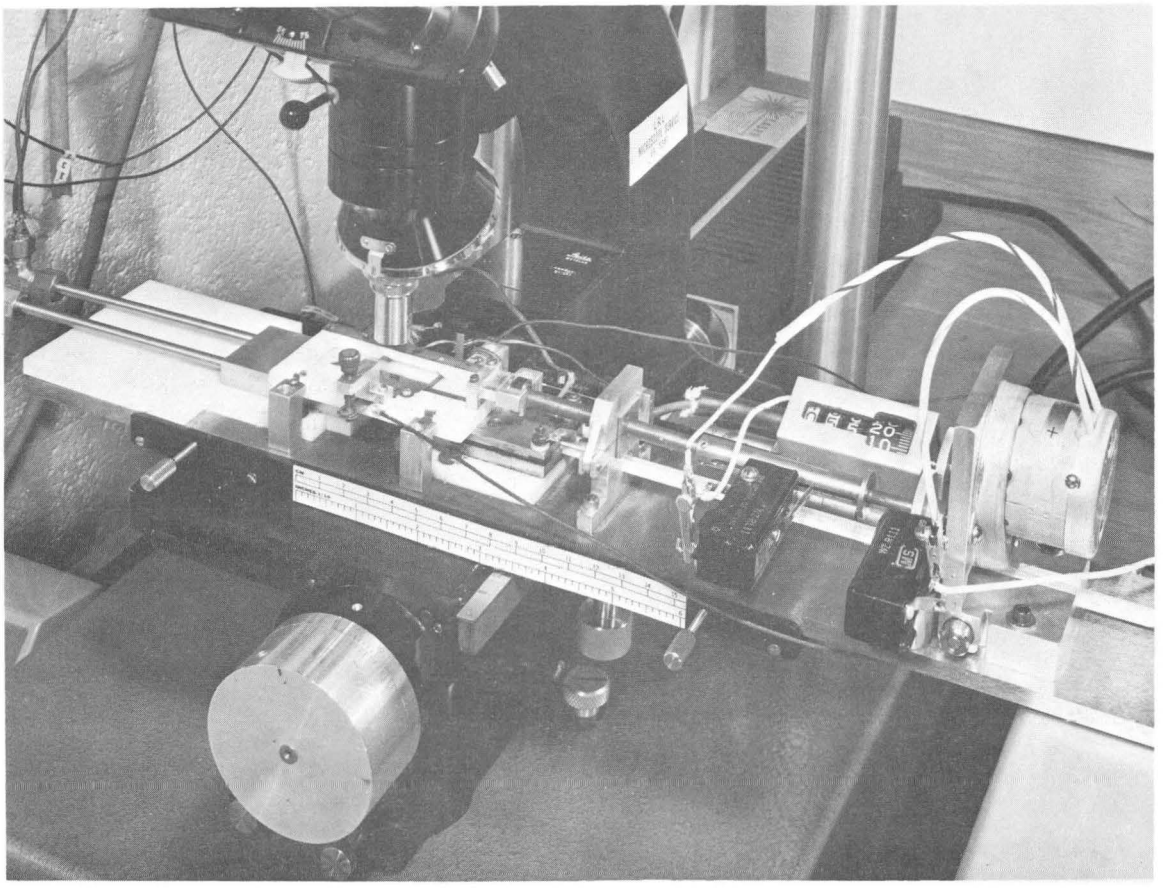

XBB 693-1781

Fig. 1. Temperature-gradient microscope stage.

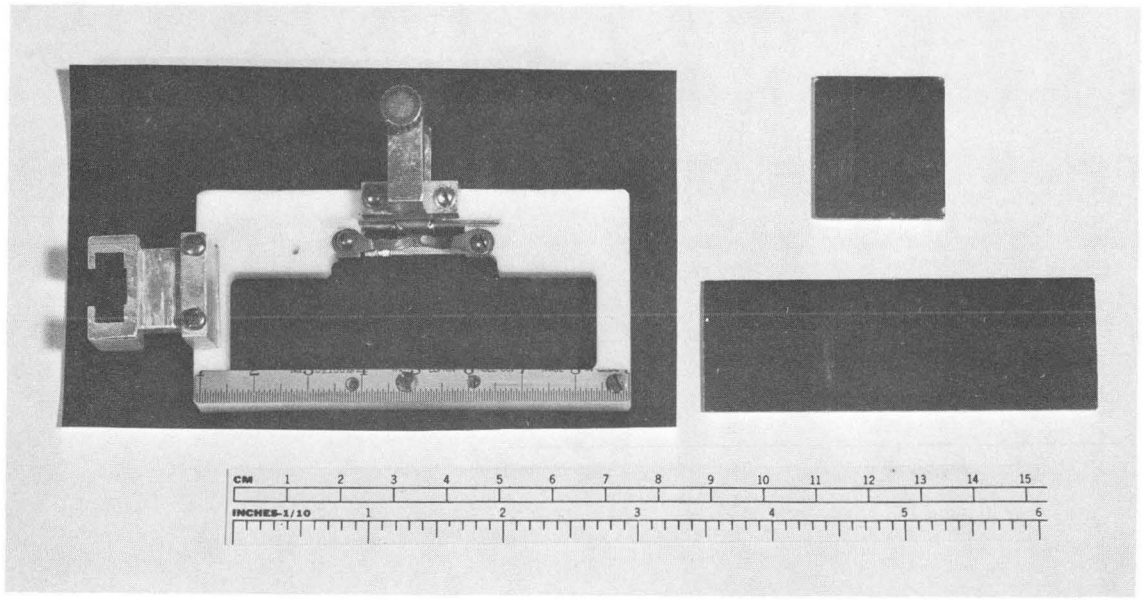

XBB 693-1782

Fig. 2. Optical wedge for crystal growth measurements.

Light for the diffraction patterns was provided by a helium-neon gas laser. The spacing between adjacent interference fringes and their sharpness are governed by the angle of the optical wedge, by the reflectivity of the metallic coating on the slides, and by the refractive index of the liquid in the wedge. The quantitative measurements depend on knowing the value of the wedge thickness corresponding to each position on the plan view of the slide. Thus, it is necessary to have some way for setting the wedge angle at a desired value and of adjusting it slightly. For this purpose a lever mechanism with a thumb screw was attached to the Teflon boat.

In most of the work done with this apparatus the gap between the opposed aluminum coatings varied from zero at the thinner edge of the wedge, where the edges of the slides touched, to about 0.25 mm. at the thicker edge some 2.5 cm. away. In some measurements involving thicker cyrstals, however, a modification was made to increase the gap while using the same wedge angle. In every case, however, the thickness values were checked by observing scratches in the upper and lower coatings and reading the corresponding positions of the vertical fine adjustment scale of the Leitz Ortholux microscope.

Liquid temperatures near the advancing crystal faces were observed with a very fine, calibrated copper-constantan thermocouple made from wire only 0.004 in. in diameter. This was inserted into the optical wedge perpendicular to the direction of motion. Since the thermocouple junction moves with the wedge while, at steady state, the crystal interface was fixed relative to the microscope objective temperature measurements at

different times corresponded to different distances from the interface. A last measurement of the thermocouple's position was made just as the junction touched the crystal itself. By using a linear least-squares fit of the observations the interface temperature could be computed accurately and its standard error estimated. The temperature gradient through the bulk of the liquid could also be determined. Fig. 3 shows the typical temperature distribution.

In some measurements trouble was encountered owing to the volatility of both solid and liquid components. When the hot stage had to be very hot and when the composition of the high-melting component was large it was not possible to complete measurements with the open-sided optical wedge just described. In these situations an optical wedge having a fixed angle was employed. This was prepared by closing all four sides of the wedge, except for small holes for injection of the sample and for the thermocouple. The loss of liquid was reduced to tolerable levels.

EXPERIMENTAL PROCEDURE

1. Sample Preparation: Salol (phenyl salicylate) and thymol (3-p-cymenol) system, which forms a single eutectic system for which the phase diagram is given by Timmermans (1959), was selected for the growth rate experiments. All the chemicals were obtained from the Eastman Kodak Company as "Reagent Grade." Salol was used as received after it had been degassed. Thymol was sublimed several times. The melting points of the purified samples were: salol, 42.14°C.; thymol, 49.60°C. These values compare favorable with the higher values accepted in the literature.

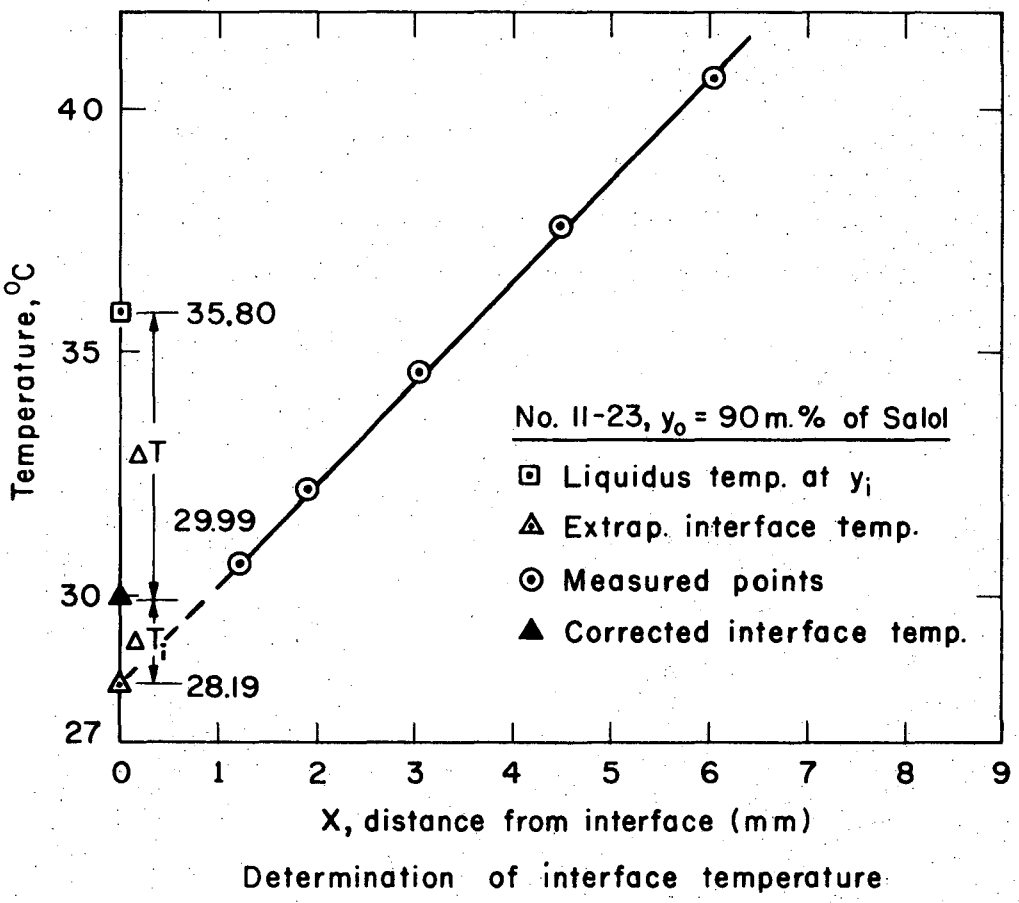

Determination of interface temperature

XBL 6910-3997

Fig. 3

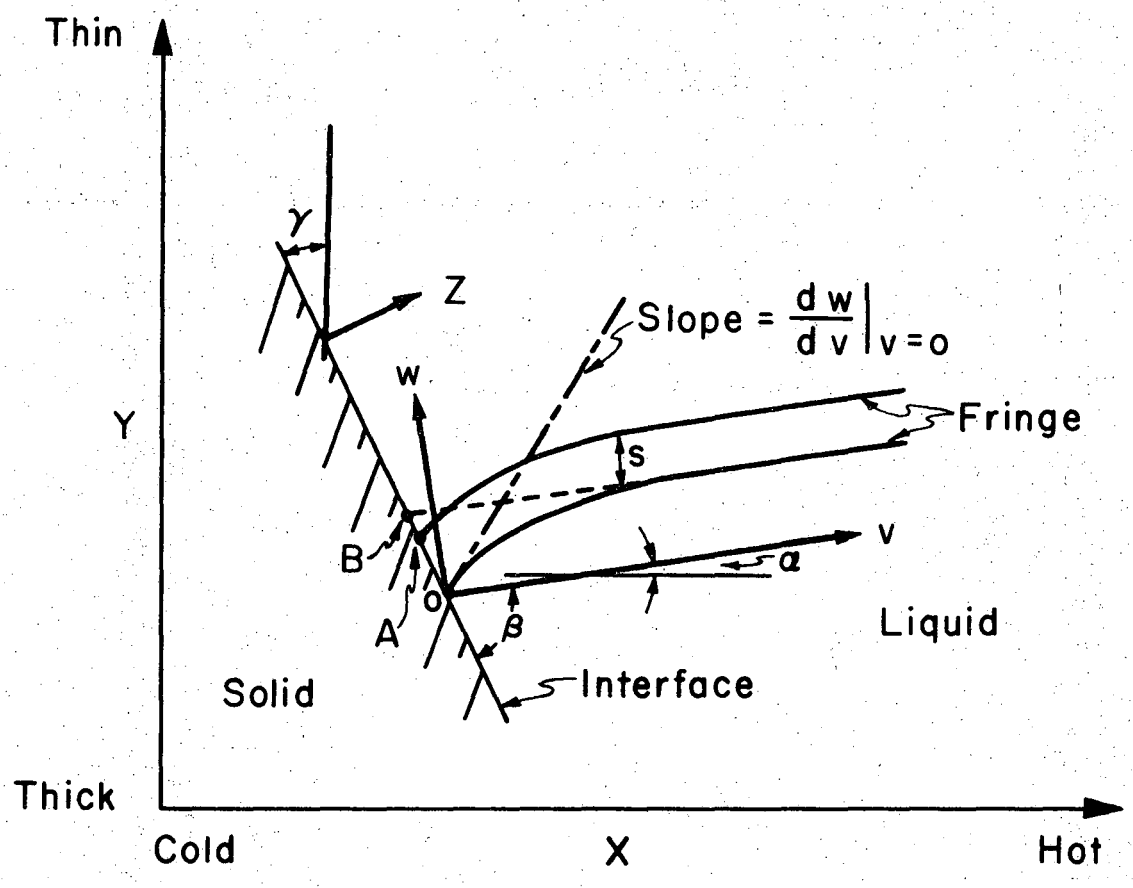

Fringe pattern at interface
during crystal growth

XBL6910-3998

Fig. 4

2. Experimental Method: After the temperatures of the hot and cold stages had become steady, crystallization was started by introducing a small seed crystal into the opening at the colder side of the optical wedge, in which the solution had been injected earlier. Then the drive motor was turned on to push the Teflon boat farther toward the cold stage. Eventually the crystal interface assumed a position that was apparently steady as viewed through the microscope such that the growth rate was equal to the velocity of the boat. If the crystal interface being observed through the microscope was not perpendicular to the direction of movement of the boat the velocity of the interface was computed from the motor speed by multiplying the boat's velocity by cos γ, where γ is the appropriate angle.

Thermocouple readings were recorded for the junction immersed in the liquid within the wedge and Polaroid pictures were taken to record the interference patterns. Figure 5 shows a typical photograph of such fringe patterns. A small correction was applied to the computed temperature of the interface, extrapolated from measurements in the adjacent liquid, owing to the heat release there caused by freezing. The corrections were based on measurements of temperature rise using the interference method to observe diffraction with the pure substances on the isothermal stage. The diffraction effects corresponded to temperature rises of 1.5 deg. C. for thymol at a growth rate of 1.0×10^{-3} cm./sec. and 2.0 deg. C. for salol at 1.5×10^{-3} cm./sec. At other growth rates the temperature rise at the interface above the straight line through the points observed a few mm. away in the liquid was assumed to be proportional to the growth rate.

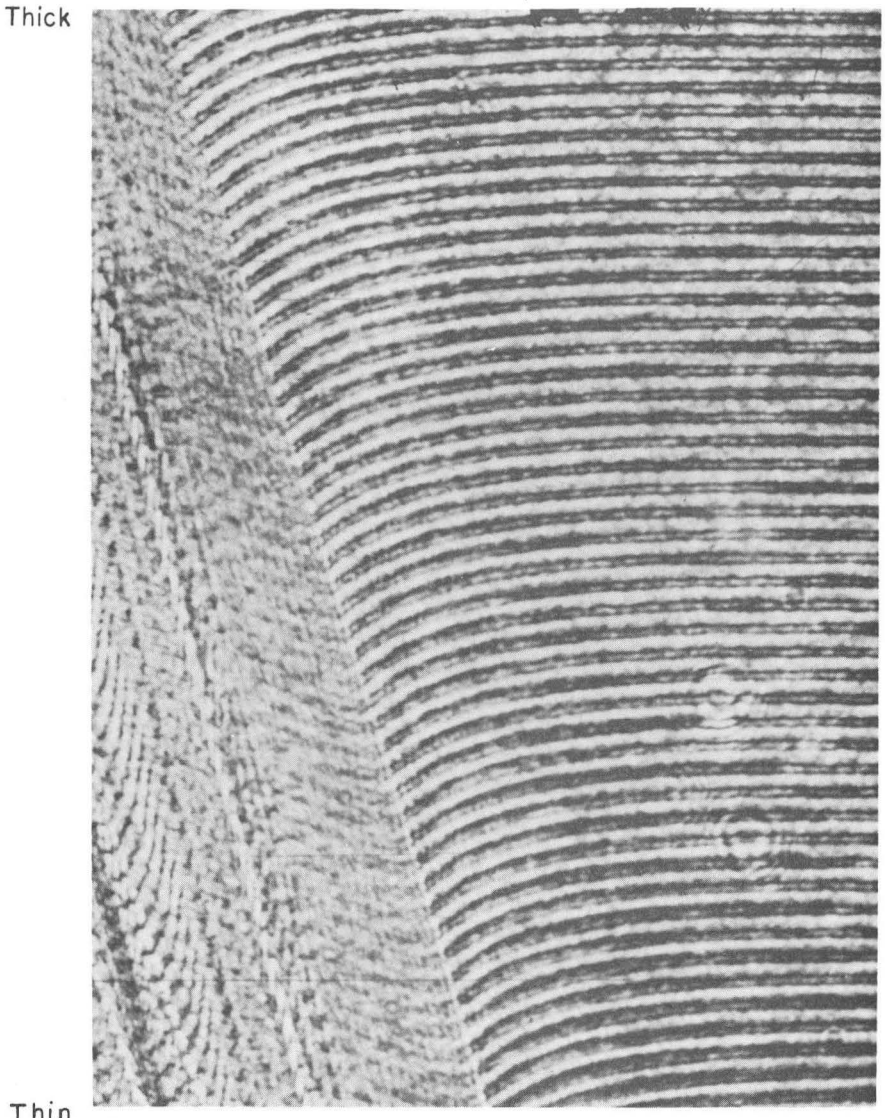

XBB 6910-6867

Fig. 5a. Fringe pattern at interface during crystal growth of thymol in 10 mole % salol solution.

RESULTS

Measurement of the Growth Rates of Pure Substances: The observed growth velocities of salol and thymol using the TGMS are shown in Figs. 6 and 7, along with similar data reported by Kirwan and Pigford (1969). The new data appear to be in good agreement with the previous results, and also with the results obtained in this work on isothermal stage, despite the presence of the thermal gradient in the new measurements. Although the points on the figures are scattered the growth rates are seen to follow the empirical formula

$$V = K(\Delta T)^2 , \qquad (1)$$

indicating, as suggested previously (Hillig and Turnbull, 1956), that the growth mechanism involves the presence of spiral screw dislocations on the advancing interface. The lines shown on Figs. 6 and 7 are based on this equation.

Growth from Binary Mixtures: Salol and thymol form a eutectic system with the equilibrium phase diagram shown in Fig. 8. On the assumptions that equilibrium is established instantly between the interfacial liquid and the solid, and that diffusion in a binary melt having the bulk composition, y_0 will deposit pure solid thymol when cooled to the liquidus temperature, T_0. If cooling continues until the temperature falls to T_i the liquid composition should move to point F. However, owing to the finite rates of diffusion and of interfacial kinetic reaction for the phase transformation the interfacial composition will shift from y_0 to y_i. The finite thermal driving force, $T_e - T_i = \Delta T$, is needed to

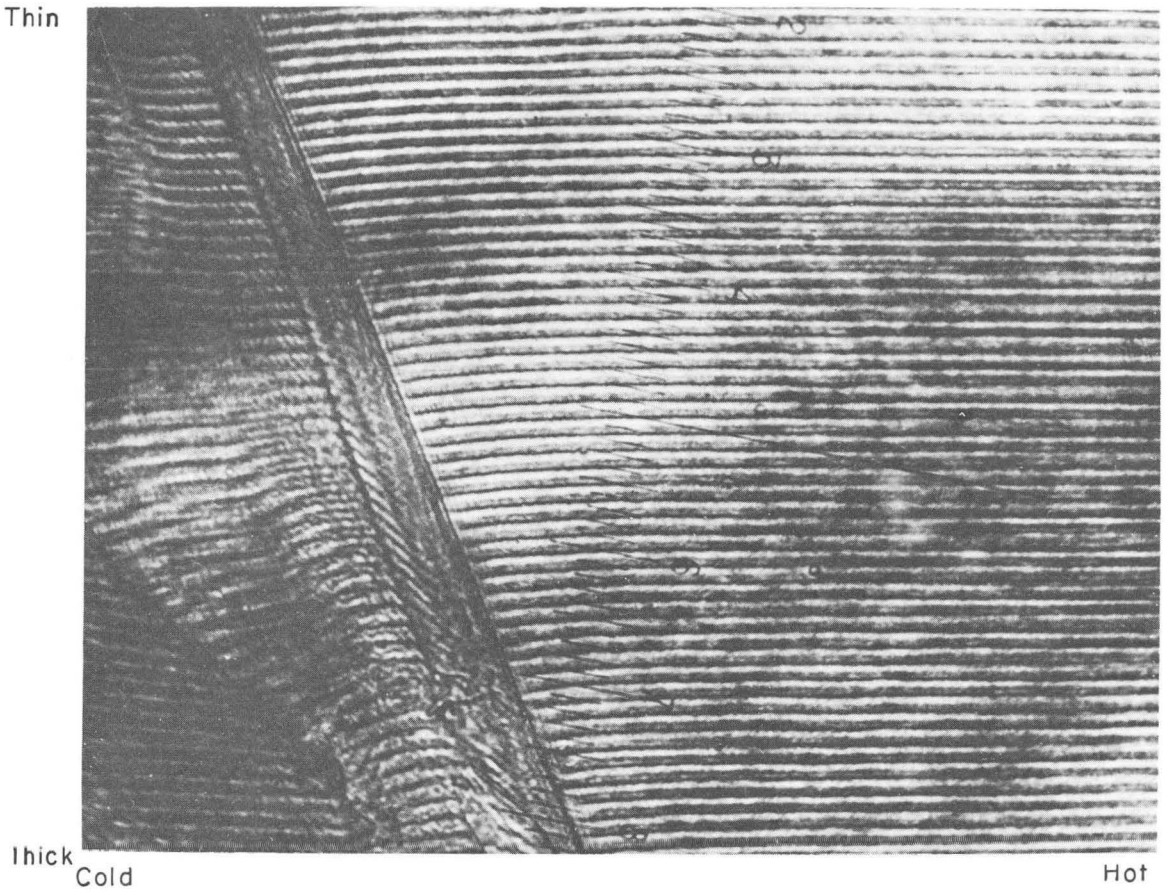

XBB 6910-6868

Fig. 5b. Fringe pattern at interface during growth of mixed crystal in 15 mole % stilbene solution.

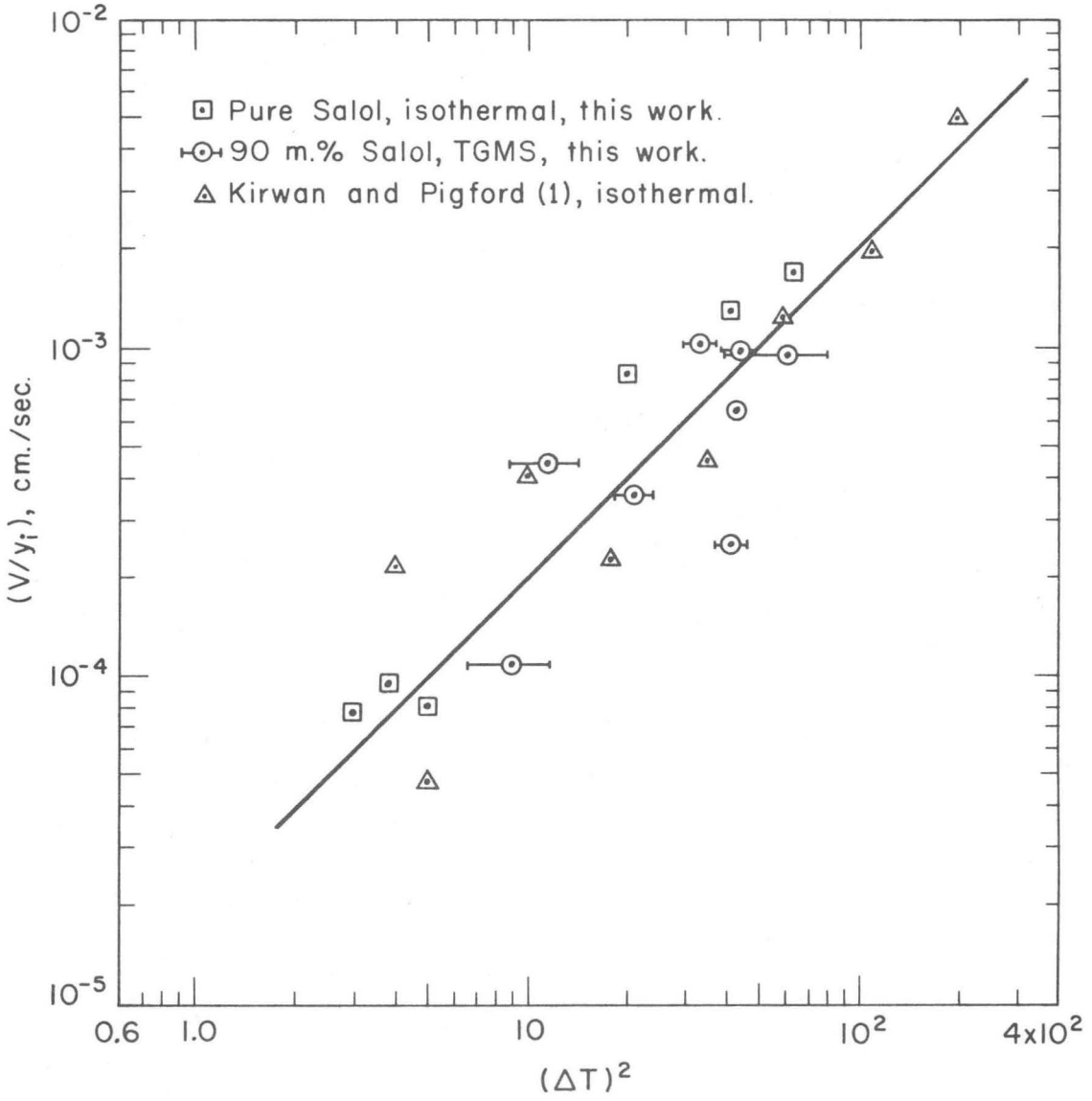

Growth rates of Salol crystals in undercooled liquids

XBL6910-3999

Fig. 6

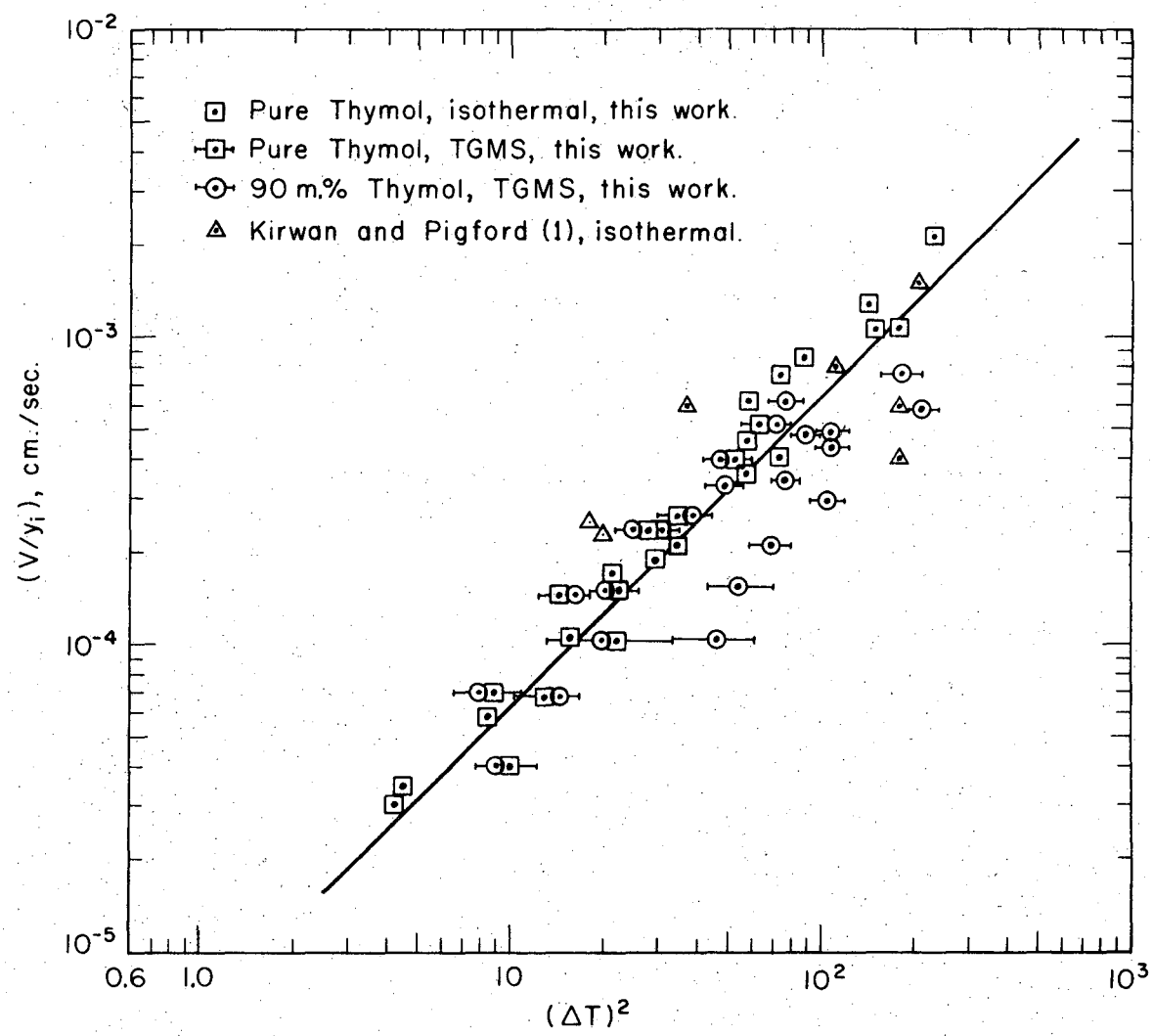

Growth rates of Thymol crystals in undercooled liquids

XBL6910-4000

Fig. 7

force the solid to form at the prescribed rate. Furthermore, the solid which forms may not be the pure thymol phase which is expected at equilibrium from the phase diagram instead, it may have a mole fraction, x_i, greater than zero. The interferometric apparatus makes it possible to determine the quantities y_i, x_i and T_i.

The interference fringes pattern is characterized by the equation

$$\frac{2nt}{\lambda_0} = N , \tag{2}$$

where N is an integer and is constant along each line in the pattern. In this equation $n = n(T,y)$ is the composition of temperature-dependent refractive index of the liquid, t is the local thickness of the liquid in the wedge, and λ_0 is the wavelength of the monochromatic light source used. The determination of y_i is based on the fact that the displacement of the fringes from their straight-line projections from the unaffected liquid to the interface implies a certain change in n. Part of this may be owing to the interfacial temperature rise; the residual part is owing to the difference in composition, $y_0 - y_i$.

The solid composition, x_i, is harder to find but can be computed from the same interference pattern. This is based on an interfacial diffusion flux balance. This leads to the equation

$$x_i = y_i + \frac{D}{V(\rho_s/\rho_L)} \left(\frac{dy}{dz}\right)_{z=0} \tag{3}$$

where D is the binary liquid diffusion coefficient, V is the measured growth velocity, z is the coordinate perpendicular to the interface, and

the ρ's are densities of liquid and solid phases. The computation of the composition derivative depends on the geometry of the fringe pattern and upon Eq. (2). In Fig. 4 the X-axis is drawn parallel to the vertex of the optical wedge. The thickness, t, is assumed to vary linearly in the Y direction. Far away from the interface the fringes are straight but are at the angle α from the X-axis, owing to the temperature gradient. The v-w coordinate system has its origin in the interface and the v-axis is parallel to the distant fringes. Coordinates of several fringe lines were measured in the v-w system using a precise instrument designed originally for locating particle tracks in photographic negatives. By considering the geometry involved it can be shown that the interfacial composition gradient is given by

$$\left(\frac{dy}{dz}\right)_{z=0} = \frac{\lambda_0 (dw/dv)_{v=0}}{2\, s\, t_i \cos\alpha \left[\sin\beta + (dw/dv)_{v=0} \cos\beta\right] (\partial n/\partial y)_T}, \quad (4)$$

where s is the fringe spacing measuring in Y direction. A detailed derivation of Eq. (4) can be found elsewhere (Cheng, 1969).

Equations (2), (3), and (4) were used to compute the interfacial compositions and temperatures for the salol-thymol system. Some of the results have been included in Figs. 6, and 7, where growth rates of the salol phase and the thymol phase from the solution are shown. Figure 9 shows the computed solid compositions of the thymol phase and indicates that the solid phase which grew at a finite velocity apparently contained as much as 10 mole percent salol. The interfacial liquid contained about 85 mole percent thymol in the same experiments.

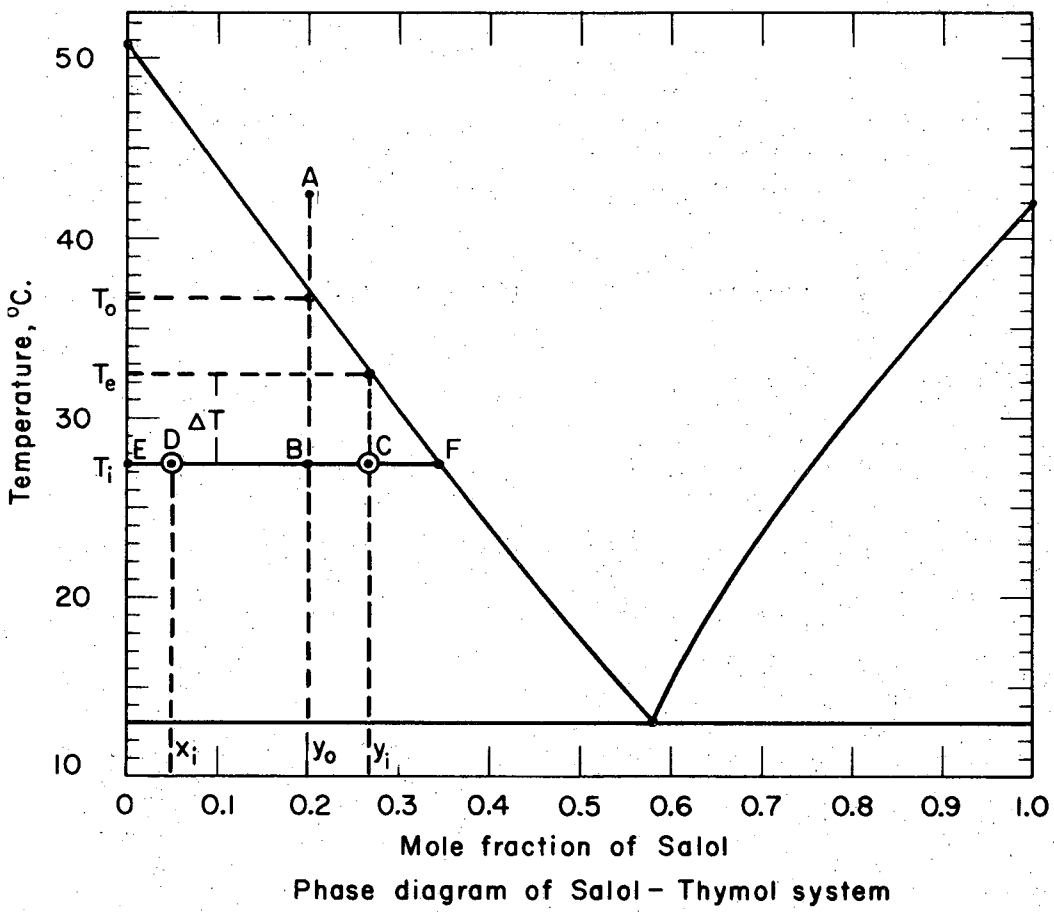

Phase diagram of Salol – Thymol system

XBL6910-3995

Fig. 8

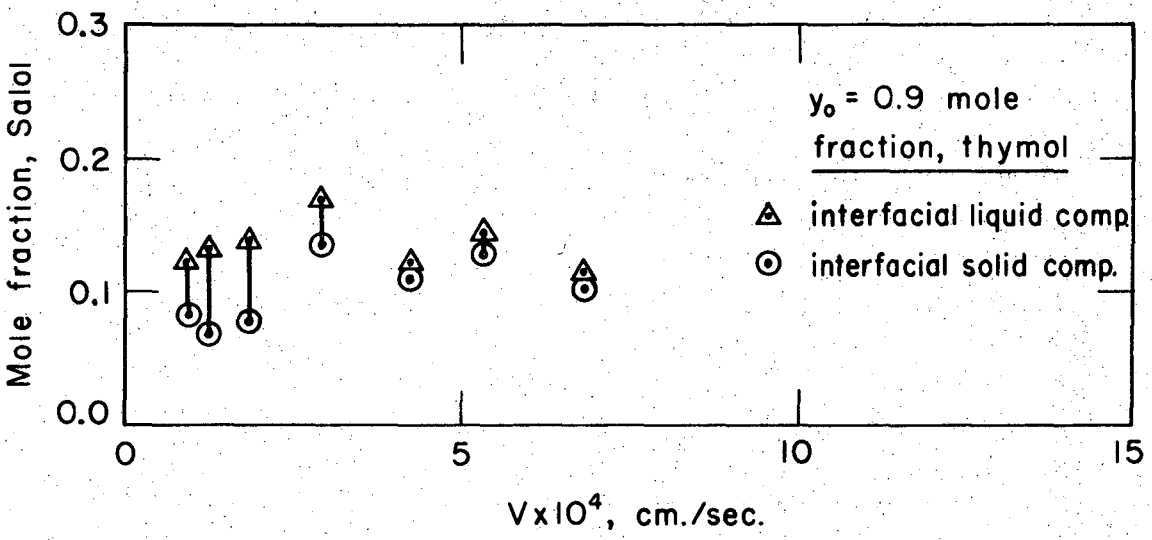

Compositions of Salol-thymol crystals growing in thymol-rich liquid mixtures

XBL6910-3996

Fig. 9

The accuracy of the computed interface solid composition depends not only on the accuracy of the fringe measurements and on the composition-derivative of the refractive index. It depends also on the liquid diffusion coefficient, which was not measured directly in this work and may be in error. The value used 0.74×10^{-6} sq. cm./sec. at 29.5°C, based on a few measurements by Kirwan (1967) and on the empirical correlation of Wilke and Chang (1955). It is believed that the probable error in this coefficient may account for the 10 percent deviation of x_i from the expected value.

For solutions, as for pure compounds, the growth velocity is approximately proportional to the square of the temperature driving force, indicating that the same spiral growth mechanism applies as before. The growth velocity on the ordinate of Figs. 6 and 7 is divided by the interfacial liquid mole fraction of the substance which is being deposited. Although it is not possible to prove that the velocity is proportional to the interface composition because of the scatter of the data, and because of the small variation of y_i, this quantity is included on the basis of a theory of crystal growth from solution which forms a eutectic system (Kirwan and Pigford, 1969).

CONCLUSIONS

The presence of an imposed constant temperature gradient is a decided advantage in measurements of the rate of growth of crystals in undercooled melts of organic substances, especially when mixtures are used and constitutional undercooling can occur. This is owing to the improvement in the stability of the interface as it advances, permitting

measurements of temperature and diffraction to be carried out long enough for repeat observations to be taken during periods of nearly steady state. The addition of facilities for quantitative measurement to the apparatus previously used by Jackson et. al. (1966) makes it possible for the first time for interfacial rate phenomena to be studied successfully for organic substances.

The results indicate that deviations of interfacial compositions and temperatures from the phase diagram values can be considerable, even at small growth rates and suggests that designs of crystallization equipment which are based on the assumption of instantaneous phase equilibrium may be considerably in error.

NOTATION

D = liquid phase diffusion coefficient, sq. cm./sec.

K = constant

n = refractive index of liquid

N = integer

s = fringe spacing, mm.

t = thickness of optical wedge, mm.

T = temperature, °C.

V = freezing velocity, cm./sec.

v,w = coordinates for interference fringe

x = mole fraction in solid phase

y = mole fraction in liquid phase

X,Y = coordinates for optical wedge

z = distance perpendicular to growing crystal face

GREEK LETTERS

α = angle, degree

β = angle, degree

γ = angle, degree

λ_0 = wave length of monochromatic light, 6328 Å for He-Ne gas laser

ρ = molar density, g mole/cc

SUBSCRIPTS

e = equilibrium condition

i = interfacial condition

L = liquid phase

s = stage condition, or solid phase

0 = initial condition

CHAPTER III

AN APPLICATION OF EYRING'S THEORY TO CRYSTALLIZATION KINETICS OF POLYPHENYLS

ABSTRACT

The Eyring-type theory developed by Kirwan and Pigford for the interfacial kinetics of crystal growth was applied to predict the rate of crystal growth for o- and m-terphenyls, and 1:3:5:-Tri-α-naphthylbenzene (TαNB). The predicted values agree well with experimentally measured data for m-terphenyl. The agreement between the computed values and reported literature data was good for o-terphenyl for undercooling below 12° C. An order of magnitude prediction was obtained for TαNB at undercooling below 40° C.

INTRODUCTION

Growth of crystals from their melts and from solutions continues to be more of an art than a science, even though crystalline products have been prepared for centuries. This is expecially true for organic substances because nowhere have their structures in the liquid and solid states received as much attention as the comparatively simpler metals. Yet the advance of methods for using crystallization phenomena in the purification of organic compounds requires that an understanding be developed for the rate processes which govern both the velocity of growth and the purity of the crystals which are formed.

It is known that crystal growth occurs by the attachment of molecules to the crystal surface. Furthermore it is intuitively obvious that such attachment will require that the approaching molecules be oriented in the right direction if they are to fit into vacant sites in the crystal lattice. Moreover, the molecules which are ready to attach themselves must break their bonds with their neighbors in the liquid. Finally, the concentration on the crystal face of vacancies suitable for the attachment of new molecules may be low, the more perfect surfaces offering fewer sites for attack.

Although several proposals have been made for the quantitative analysis of these factors none has seemed as promising as the combination of a kinetic theory which follows the ideas of Eyring (1941) with an estimate of surface defect structures according to Frank (1948, 1951). Such analyses have been made by Hillig and Turnbull (1956) and by Kirwan and Pigford (1969). Results have been somewhat promising but the expressions for growth rates obtained along such lines have not yet been tested in a definitive way.

A few more complicated organic compounds, such as polyphenyls, become very viscous when their melts are cooled. In fact, cooling may easily occur many degrees below the equilibrium freezing points of these substances because nucleation and growth of the solid phase are so slow.

Such substances apparently form highly oriented, multiple links between neighboring molecules, even in the liquid state, such temperature-dependent structures resulting in high liquid viscosity.

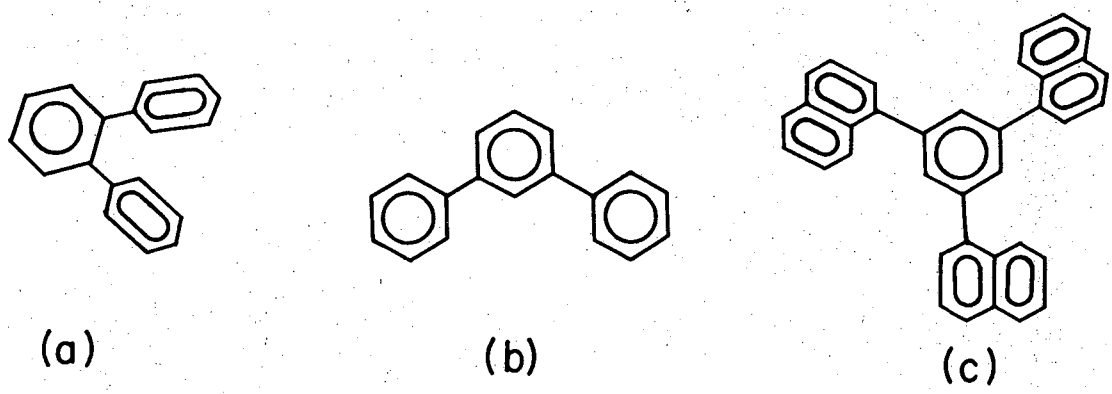

XBL6911-6203

Fig. 1. Units of molecular structure of polyphenyls
(a) o-terphenyl, M.W. = 230.31, (b) m-terphenyl, M.W. = 230.31
(c) 1:3:5-tri-α-naphthylbenzene, M.W. = 456.

Recently, growth rates and liquid viscosities for o-terphenyl have been reported by Greet (1967). This compound has a large, positive entropy of activation for viscous flow, indicating the presence of entangled structures in the liquid. It should be useful to compare predicted and observed growth rates for this substance to test the theories. Also, new data are reported here on the growth rates of an isomeric substance, m-terphenyl, which does not form so viscous a liquid and which, if the theories are right, should crystallize more quickly. In addition, data are available from Magill and Plazek (1967) on the growth rates of a still more complex structure, 1:3:5:-Tri-α-naphthylbenzene, providing a third set of data for which the rate theory comparison should be significant. Figure 1 shows the structures of the three compounds.

In the following the Eyring-type theory will be reviewed, especially the adaptation of it by Kirwan and Pigford (1969), and its application to data on the more complex organic molecules will be made. The aim is to test certain hypotheses concerning the estimation of the thermodynamic properties of the crystallization activated state, especially the suggestion of Kirwan and Pigford (1969) that the molecule which is ready to attach itself to the crystal lattice has less entropy than the molecule which is ready to flow, the difference being about equal to the entropy of fusion.

AN ABSOLUTE RATE THEORY OF CRYSTAL GROWTH

Following the developments of Hillig and Turnbull (1956) and of Clifton (1957), the net molar flux of material onto the crystal interface is given by

$$N = f\,(\lambda_L \rho_L k^F - \lambda_S \rho_S k^R) = f\,\lambda_S \rho_S (k^F - k^R)\,, \qquad (1)$$

where the terms in the parentheses represent the forward rate owing to the liquid molar concentration ρ_L and the reverse rate at which the solid dissolves owing to the concentration ρ_S. Each process shifts the interface by a small molecular spacing λ. The second equality follows from the assumption that the molecular spacings are inversely proportional to the densities. The fraction f represents the small fractional part of the surface to which arriving molecules can attach themselves. The complete theory comprises estimates of both the rate coefficients and the surface fraction in terms of thermodynamic and other pure component properties.

Following Eyring (1941) the forward rate constant becomes

$$k^F = \chi \left(\frac{kT}{h}\right) \exp\left(-\frac{\Delta H_C^{\ddagger}}{RT}\right) \exp\left(\frac{\Delta S_C^{\ddagger}}{R}\right) , \qquad (2)$$

where the quantities in the "frequency factor", kT/h have their usual meaning and where $\Delta S_C^{\ddagger} = S_C^{\ddagger} - S_L$ and $\Delta H_C^{\ddagger} = H_C^{\ddagger} - H_L$ represent the excess of the standard entropy and standard enthalpy of the molecule which is activated for attachment to the crystal over the standard state values for the liquid. χ is the transmission coefficient to allow for the possibility that not every activated complex is converted into one of the reaction products in which one is interested. A similar equation, based on the same activated standard state, applies to the reverse coefficient, k^R. It is simply related to Eq. (2) by

$$k^R = k^F \exp\left(\frac{-\Delta\mu^0}{RT}\right) , \qquad (3)$$

where $\Delta\mu^0 = \mu_L^0 - \mu_S^0$ is the difference between the standard-state chemical potentials of the phases. At the melting point of the pure substance, T_m, the chemical potentials are equal; their rate of change with respect to temperature depends on the entropy, so that $\Delta\mu^0 \sim \Delta S_f(T_m - T) = \Delta S_f \cdot \Delta T$ where ΔS_f is the entropy of fusion.

Estimation of f depends on the surface mechanism for attachment of molecules to the solid. Here we follow the proposal of Frank (1948, 1951) that many crystals grow by attachment of molecules to the spiral steps of screw-shaped dislocations on the surface. The value of f then is equal to the distance on the surface between adjacent arms of the spiral divided into the width on the surface of a single molecule. Assuming that the spiral is Archmidean in shape we obtain

$$f = \frac{\lambda_S}{4\pi r_c} \quad , \tag{4}$$

where r_c is the radius of curvature of the tip of the spiral. If we assume that this tip is of such size that is just neutrally stable, we may equate r_c to the thermodynamically calculated size of the critical two-dimensional nucleus,

$$r_c = \frac{\sigma}{\rho_S \Delta\mu^0} \sim \frac{\sigma}{\rho_S \Delta S_f \Delta T} \quad , \tag{5}$$

where σ is the excess surface free energy in the interface per unit of surface area. We obtain this value from the correlation of Turnbull (1958), according to whom, for non-metals and organic compounds,

$$\sigma = 0.3 \left(\frac{\Delta H_f}{N^{1/3} V_S^{2/3}}\right) , \qquad (6)$$

where ΔH_f is the enthalpy of fusion, N is Avogadro's number, and $V_S = \rho_S^{-1}$ is the molar volume of the solid.

Combining Eqs. (1) through (6) we develop the equation from which we intend to predict the crystal growth rate,

$$V = \left(\frac{\Delta T}{1.2\pi T_m}\right)\left(\chi \frac{kT}{h}\right) \lambda_S \left[1-\exp\left(\frac{-\Delta\mu^0}{RT}\right)\right] \exp\left(-\frac{\Delta H_C^{\ddagger}}{RT}\right) \exp\left(\frac{\Delta S_C^{\ddagger}}{R}\right) , \qquad (7)$$

where we have introduced the growth velocity, $V = N/\rho_S$, and $\lambda_S = (V_S/N)^{1/3}$. The first factor on the right of Eq. (7) is the surface fraction, f. Note that V depends on the amount of undercooling of the melt through the effect of ΔT both on f and on $\Delta\mu^0$. Thus, for this particular mechanism, the growth velocity varies more rapidly than in proportion to the undercooling. For many conditions $\Delta\mu^0$ is much smaller than RT for the third parenthesis in Eq. (7) to be approximated by the first term in its Taylor series, giving

$$V = \left(\frac{1}{1.2\pi}\right)\left(\frac{kT}{h}\right)\left(\frac{\lambda_S}{R}\right)\left(\frac{\Delta T}{T_m}\right)^2 \exp\left(-\frac{\Delta H_C^{\ddagger}}{RT}\right) \exp\left(\frac{\Delta S_C^{\ddagger}}{R}\right) , \qquad (7a)$$

showing that V is approximately proportional to the square of the undercooling. Comparison of the exponent on ΔT, determined from experimentally observed growth velocities, with the expected value according to Eq. (7a) has often been interpreted as a test of the postulate that growth occurs

by the screw dislocation mechanism (Hillig and Turnbull, 1956). Obviously, however, the equation will be of little use generally unless ways are found for the estimation of the entropy and enthalpy of the crystallization-activated state.

A plausible guess of the activation quantities was made by Hillig and Turnbull (1956) who suggested that the values appropriate for crystallization be assumed equal to those for viscous flow. The latter are likely to be available or, if not, they can be measured rather easily. Following this line of thought one may multiply Eq. (7) by the similar Eyring equation for the viscosity of the liquid (Glasstone, Laidler and Eyring, 1941),

$$\eta = \left(\frac{Nh}{V_L}\right) \exp\left(\frac{\Delta H_V^{\ddagger}}{RT}\right) \exp\left(-\frac{\Delta S_V^{\ddagger}}{R}\right) , \tag{8}$$

where the subscript V now refers to the activation quantities for viscous flow. From Eqs. (7) and (8), the product of the growth velocity and the liquid viscosity is given by

$$V\eta = \left(\frac{1}{1.2\pi}\right)\left(\frac{\Delta T}{T_m}\right)\left(\chi \frac{NkT}{V_L}\right) \lambda_S \left[1-\exp\left(-\frac{\Delta\mu^0}{RT}\right)\right] \exp\left(\frac{\Delta H_V^{\ddagger} - \Delta H_C^{\ddagger}}{RT}\right)$$

$$\exp\left(\frac{\Delta S_C^{\ddagger} - \Delta S_V^{\ddagger}}{R}\right) , \tag{9}$$

or, for small undercooling, ΔT, Eq. (9) can be further simplified to

$$V\eta = \left(\frac{1}{1.2\pi}\right)\left(\frac{\chi\lambda_S\Delta H_f}{V_L}\right)\left(\frac{\Delta T}{T_m}\right)^2 \exp\left(\frac{\Delta H_V^{\ddagger} - \Delta H_C^{\ddagger}}{RT}\right) \exp\left(\frac{\Delta S_C^{\ddagger} - \Delta S_V^{\ddagger}}{R}\right) , \tag{9a}$$

where ΔH_f will be expressed in erg/mole °K if poise units are used for η. Furthermore, if one would assume that the activated state is the same for the two processes the two exponential factors would vanish. Then, at fixed thermal driving force and temperature, the growth velocity would vary from one substance to another in inverse proportion to the liquid viscosity. For some substances, especially those with rather complex molecular structure, the viscosity can become very large at low temperatures. If such substances can be cooled far below their freezing points the rates at which they freeze may be small in spite of the very large ΔT.

Kirwan and Pigford (1969) suggested, however, that this simplest assumption about the properties of the molecule which is ready to attach itself to a crystal lattice may be too crude. After all, many molecules require very specific orientation if they are to fit into steps in the crystal. Some orientation may be needed for viscous flow but it seems very likely that the requirements are not nearly so stringent as for crystal growth. As an estimate of the difference of the entropies of the two standard states it was suggested that

$$\Delta S_C^{\ddagger} = \Delta S_V^{\ddagger} - (\Delta S_f - R) \ . \qquad (10)$$

This assumes that the entropy of the crystallization-activated molecule falls about as far below the entropy of the flow-activated molecule as the solid entropy falls below that of the liquid. The extra term, R, is an estimate of the entropy of fusion of a spherical molecule, which requires no orientation.

There appears to be no comparable way of guessing at the enthalpy of the activated state, just as there is seldom a way to estimate the activation energy of an ordinary chemical reaction. It seems very possible that $\Delta H_V^{\ddagger}$ could differ appreciably from $\Delta H_C^{\ddagger}$ because a somewhat different sequence of events is required for attachment to the solid and for flow. For the latter, not only must the molecule become so energetic that it is able to "jump", i.e. to break the bonds by which it is attached to its neighbors in the liquid but, in addition, a hole must occur in the liquid nearby. For crystallization, however, there is no energy requirement to "make a hole" for the crystal face itself offers a site for completion of the attachment reaction. Thus, the energy of activation for viscous flow can be subdivided into two different parts:

$$\Delta H_V^{\ddagger} = \Delta H_{V,j}^{\ddagger} + \Delta H_{V,h}^{\ddagger} \ , \tag{11}$$

or, to indicate the corresponding quantities which can be measured experimentally,

$$\Delta H_V^{\ddagger} = \left.\frac{\partial \ln(V_L \eta)}{\partial (1/T)}\right|_P = \left.\frac{\partial \ln(V_L \eta)}{\partial (1/T)}\right|_{V_L} + \left.\frac{\partial V_L}{\partial (1/T)}\right|_P \cdot \left.\frac{\partial \ln(V_L \eta)}{\partial V_L}\right|_T \ . \tag{12}$$

Thus, when in a very few cases the isothermal dependence of liquid viscosity on liquid density is known, the two parts of the right side of Eq. (11) can be found separately. It seems very likely that only the activation enthalpy needed to cause a molecule to jump away from its surroundings is sufficient for the cyrstallization rate equation, i.e., the first term

on the right of Eq. (12)--a number which may be smaller than the total activation energy for viscosity.

In a few cases where data were available it was possible for Whitaker and Pigford (1958) to compute $\Delta H^{\ddagger}_{V,j}$, and to compare it with $\Delta H^{\ddagger}_{V}$. They found that the ratio of the quantities depends on the nature of the molecule involved, including its tendency to form a hydrogen-bonded structure in the liquid. Thus for alcohols they found $(\Delta H^{\ddagger}_{V,j} / \Delta H^{\ddagger}_{V}) \sim 0.6$; for hydrocarbons like benzene and carbon tetrachloride the value was about 0.3. Thus it is difficult to estimate the term involving $\Delta H^{\ddagger}_{C}$ in Eq. (7) or (9), except for the simplest substances. In most cases it will be necessary to find the difference between the two activation enthalpies from one measured growth rate. Afterwards, other growth rates can be estimated from Eqs. (7), (9) and (10).

The final equation, based on introducing the assumption about entropy expressed in Eq. (10) into Eq. (9), is

$$V\eta = \left(\frac{e}{1.2\pi}\right) \lambda_s \left(\chi \frac{NkT}{V_L T_m}\right)(\Delta T)\left[1-\exp\left(-\frac{\Delta\mu^0}{RT}\right)\right] \exp\left(-\frac{\Delta S_f}{R}\right) \exp\left(\frac{\Delta H^{\ddagger}_{V} - \Delta H^{\ddagger}_{C}}{RT}\right). \quad (13)$$

The first purely numerical factor in Eq. (13) is equal to 0.72. For many conditions the first exponential factor can be approximated by $(\Delta S_f \Delta T/RT)$, as noted earlier. Since for most organic substances $\Delta H^{\ddagger}_{V} > \Delta H^{\ddagger}_{C}$, the last exponential factor usually exceeds unity.

Table I. Growth Rate Data and Physical Properties of Polyphenyls and Phosphorus

Compound	Equilibrium Thermodynamic Properties			Derived Properties from Viscosity				Rate-Derived Properties from Crystal Growth Rate				
	T_m	ΔS_f	ΔH_{vap}	T	η	$\Delta S_V^{\ddagger}$	$\Delta H_V^{\ddagger}$	V	$\Delta S_C^{\ddagger}$	$\Delta H_C^{\ddagger}$	$\Delta H_C^{\ddagger} / \Delta H_V^{\ddagger}$	
	°C	cal/mole°K	kcal/m	°C	poise	cal/m°K	kcal/m	cm/sec	cal/m°K	kcal/m		
o-terphenyl[g]	55.5	13.4 ±0.2	14.84[a]	50	0.50	24.0	14.0	3.3×10^{-4}	-260.0	-71.0	-5.1	
			15.77[b]	40	1.30	48.0	22.0	2.3×10^{-3}	26.0	17.0	0.77	
				30	5.42	77.0	31.0	1.6×10^{-3}	51.0	26.0	0.84	ave. = 0.82
				20	40.50	108.0	40.0	5.2×10^{-4}	79.3	34.0	0.85	
				10	6.1×10^{2}	142.0	50.0	1.0×10^{-4}	114.0	42.0	0.84	
m-terphenyl	85.61[c]	12.3	15.97[d]	84	0.057	5.0	7.5	2.5×10^{-4}	-5.3[i]	6.0	0.80	
	87.0 ±0.1		16.84[e]									
TαNB[h]	199.0	21.2	27.90[f]	195	0.48	14.92	17.09	1.7×10^{-7}	-627.3	-274.5	-16.10	
				190	0.63	21.65	20.22	1.6×10^{-5}	-355.9	-148.6	-7.33	
				185	0.83	28.60	23.42	4.4×10^{-5}	-78.3	-20.0	-0.85	

(continued)

Table I. continued

Compound	Equilibrium Thermodynamic Properties			Derived Properties from Viscosity				Rate-Derived Properties from Crystal Growth Rate				
	T_m	ΔS_f	ΔH_{vap}	T	η	$\Delta S_V^{\ddagger}$	$\Delta H_V^{\ddagger}$	V	$\Delta S_C^{\ddagger}$	$\Delta H_C^{\ddagger}$	$\Delta H_C^{\ddagger} / \Delta H_V^{\ddagger}$	
	°C	cal/mole°K	kcal/m	°C	poise	cal/m°K	kcal/m	cm/sec	cal/m°K	kcal/m		
				160	6.45	67.06	40.55	4.5×10^{-5}	47.45	37.1	0.92	ave. = 0.81
				140	222.0	103.0	55.74	8.2×10^{-6}	68.5	46.0	0.83	
				120	5.3×10^{3}	144.5	72.48	5.8×10^{-7}	93.0	55.7	0.77	
				100	1.5×10^{6}	192.9	91.02	1.1×10^{-8}	121.2	66.6	0.73	
phosphorus[j]	44.3	1.984		37.9	1.84	-2.6	2.62	23.4	9.1	3.06		
				35.1	1.90	-2.7	2.60	45.5	9.7	3.24		
				33.4	1.95	-2.8	2.59	63.0	10.1	3.36		
				33.2	1.99	-2.9	2.57	79.0	10.5	3.44		
				29.8	2.05	-3.0	2.55	102.0	10.9	3.61		
				29.3	2.06	-3.1	2.55	108.0	11.1	3.64		
				25.8	2.16	-3.3	2.51	153.0	11.9	3.89		
				25.0	2.26	-3.4	2.50	161.0	12.1	3.95		
				23.0	2.19	-3.4	2.49	181.0	12.5	4.07		

(continued)

Table I. continued

Compound	Equilibrium Thermodynamic Properties			Derived Properties from Viscosity				Rate-Derived Properties from Crystal Growth Rate			
	T_m	ΔS_f	ΔH_{vap}	T	η	ΔS_V	ΔH_V	V	$\Delta S_C^{\ddagger}$	$\Delta H_C^{\ddagger}$	$\Delta H_C^{\ddagger}/\Delta H_V^{\ddagger}$
	°C	cal/mole°K	kcal/m	°C	poise	cal/m°K	kcal/m	cm/sec	cal/m°K	kcal/m	
phosphorus[j]				22.0	2.30	-3.5	2.47	210.0	12.9	4.17	
				21.4	2.32	-3.6	2.47	210.0	13.0	4.21	

Note: m-terphenyl data, except for viscosity, obtained from this work.

[a]For temperature range from 280 to 340° C.

[b]For temperature range from 220 to 280° C.

[c]Measured value, this work.

[d]For temperature range from 330 to 380° C.

[e]For temperature range from 260 to 330° C.

[f]For temperature range from 430 to 530° C.

[g]Data of Greet (1967).

[h]Data of Magill and Plazek (1967).

[i]Computed from Eq. (10).

[j]Data of Hildebrand and Rotariu (1951).

EXPERIMENTAL DATA FOR m-TERPHENYL

For m-terphenyl the viscosity data and the melt specific volume via Batshinski relationship are measured by Andrew and Ubbelohde (1955). The molar volume of solid is taken as 200.4 cc/g mole (Andrew and Ubbelohde, 1955). The latent heat of fusion is taken to be as equal to that of o-terphenyl. The sample of m-terphenyl was obtained from Eastman Kodak Co. and used for the growth experiment after it was purified by zone refiner. The melting point was measured to be 85.61° C. The measurement by Andrew and Ubbelohde was 87.0 ± 0.1° C (1955). Experimental procedures are described in detail elsewhere (Cheng and Pigford, 1969).

The experimentally measured rates of growth are plotted in terms of $(\Delta T)^2$ in Fig. 3. The predicted values of growth rate at various undercoolings, using Eq. (9) with the assumption of $\Delta H_C^{\ddagger} = 0.76\ \Delta H_V^{\ddagger}$ and $\Delta S_C^{\ddagger}$ calculated from Eq. (10), are also plotted in Fig. 3. It appears that Eq. (9) does result in a reasonable prediction of the growth rate for m-terphenyl for a limited temperature range of experiment.

DISCUSSION

In Table I all the pertinent physical properties of the pure substances are listed, along with the calculated values of the two enthalpies and the two entropies of activation for each compound. At the higher temperatures for o-terphenyl and TαNB the values derived from crystal growth rates differ sharply from those from viscosity, and correspondingly, the lines shown on Fig. 2 change their courses sharply except for phosphorus. This suggests that in the range of small undercooling these polyphenyl compounds crystallize by a different mechanism than at lower

temperatures, where the lines are nearly striaght. At the lower temperatures the ratio $\Delta H_C^{\ddagger} / \Delta H_V^{\ddagger}$, is smaller than unity, as expected. Over most of the temperature ranges the ratio is about 0.81, which agrees with the value 0.80 found from the new m-terphenyl data after assuming that Eq. (10) gives the right entropy of activation. For the other three compounds the entropy of activation can be computed directly from the observed growth rates using Eq. (7), i.e. based on slopes of the curves in Fig. 2. Inspection of the table shows that the difference between $\Delta S_V^{\ddagger}$ and $\Delta S_C^{\ddagger}$ is greater than the entropy of fusion for o-terphenyl and TαNB, in contrast with Eq. (10). In fact, the difference is occasionally about twice the entropy of fusion. For phosphorus (Hildebrand and Rotariu, 1951) not only $\Delta H_C^{\ddagger}$ is larger than $\Delta H_V^{\ddagger}$ but also the large positive values of $\Delta S_C^{\ddagger}$ are to compare with the negative values of $\Delta S_V^{\ddagger}$. Apparently Eq. (10) does not hold for these three compounds.

In order to test the theory further, we have arbitrary taken $\Delta H_C^{\ddagger} = 0.89\ \Delta H_V^{\ddagger}$ and have $\Delta S_C^{\ddagger}$ computed from Eq. (10). Thus, the predicted values of growth rate, V, using Eq. (9) are plotted in Fig. 4 for o-terphenyl and in Fig. 5 for TαNB. For o-terphenyl it yields a reasonable agreement with the reported data at ΔT below 12° C. However the predicted values are higher than the literature values at ΔT greater than 12° C and ΔT below 3° C. For TαNB the agreement between the experimental data and the predicted values is rather poor. A larger value of $\Delta H_C^{\ddagger}$ for o-terphenyl than for m-terphenyl regardless the similarity of their molecular structures arises from the fact that the large interlocked molecules of o-terphenyl apparently require a larger activation enthalpy for jumping in viscous flow.

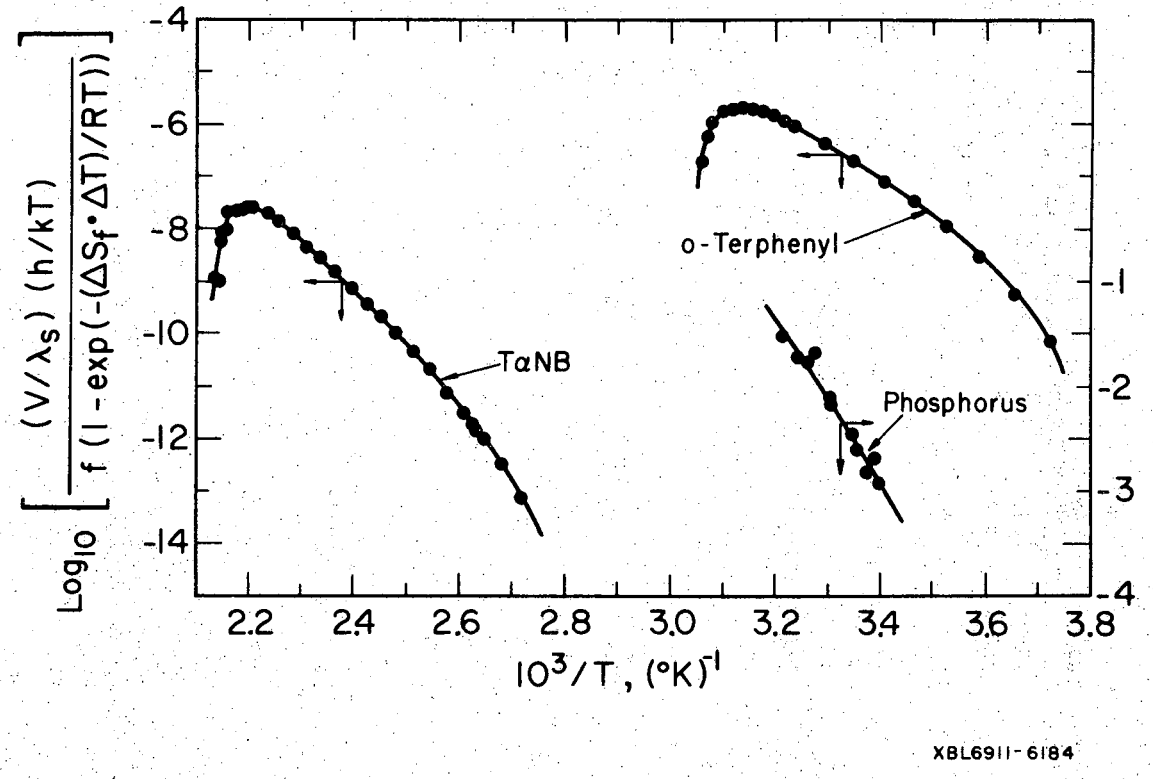

Fig. 2. Reduced growth rates of pure compounds in undercooled liquids.

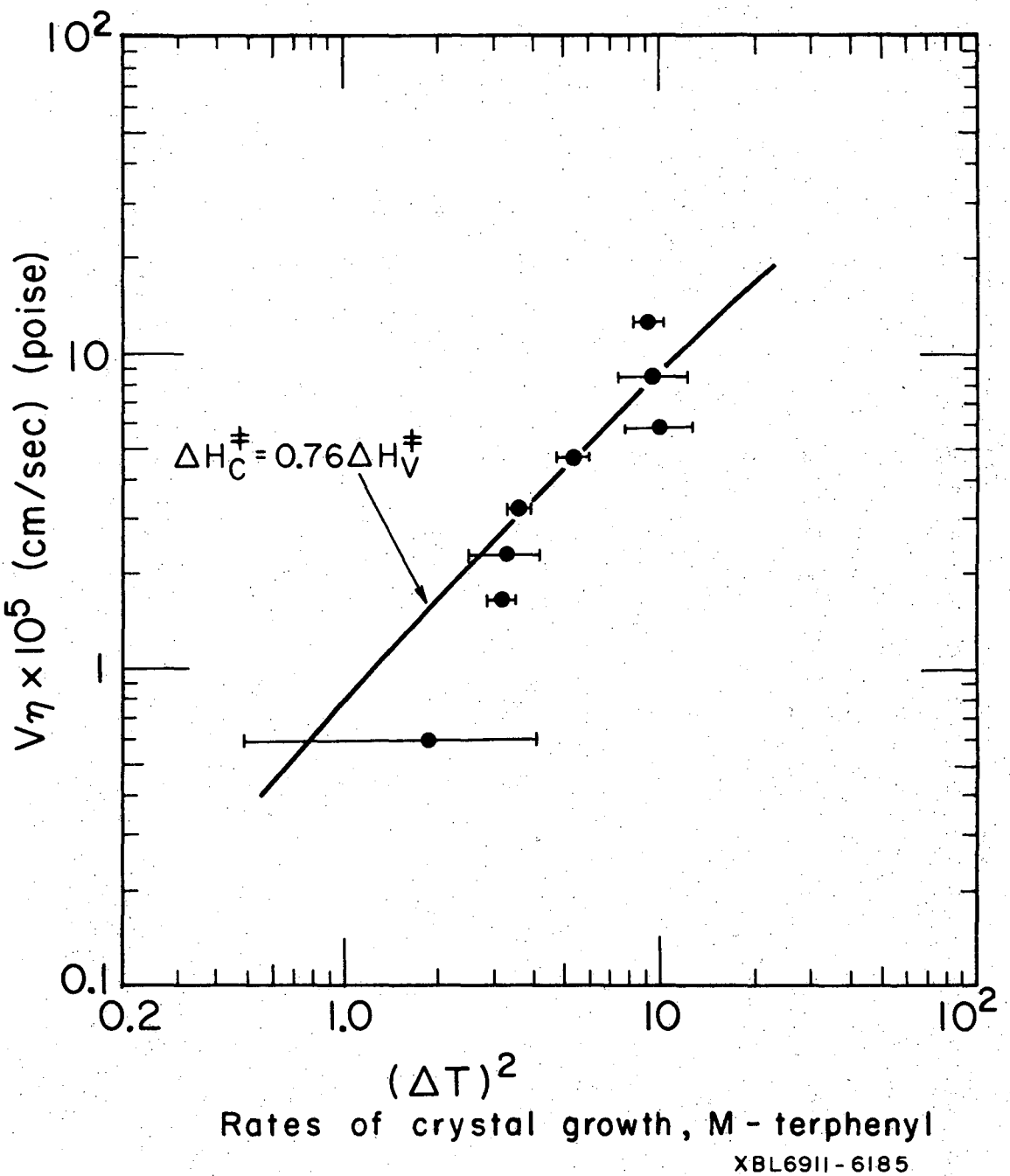
10^2
10
1
0.1
$V\eta \times 10^5$ (cm/sec) (poise)
$\Delta H_C^{\ddagger} = 0.76 \Delta H_V^{\ddagger}$
0.2
1.0
10
10^2
$(\Delta T)^2$
Rates of crystal growth, M - terphenyl
XBL6911-6185

Fig. 3

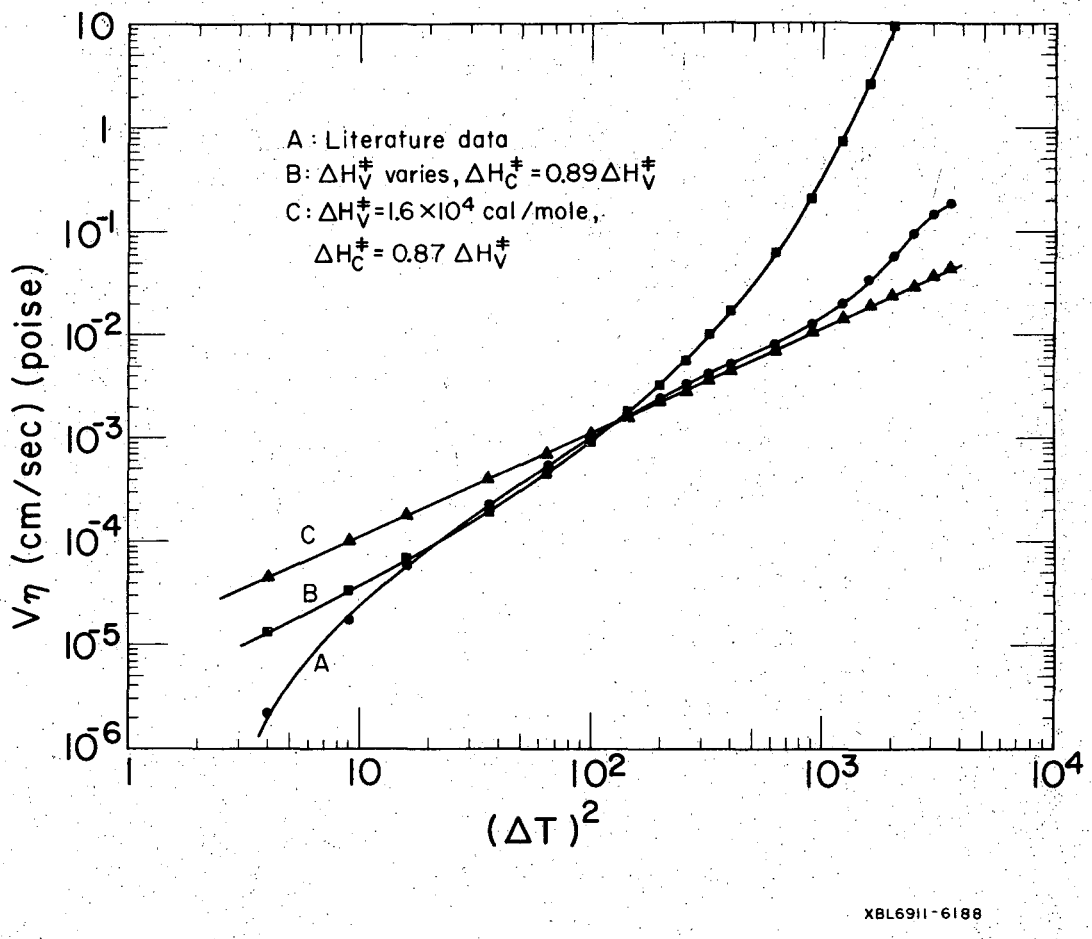

Fig. 4. Comparison of predicted growth rates and literature values, o-terphenyl.

A greater deviation occurs at lower temperature end (larger ΔT) is due to a large increase in the difference of $(\Delta H_V^{\ddagger} - \Delta H_C^{\ddagger})$. For most metals and substances whose molecular sturctures are simple the difference is constant under the assumption that $\Delta H_C^{\ddagger}$ can be approximated as equal to $\Delta H_{V,j}^{\ddagger}$, which is a fraction of $\Delta H_V^{\ddagger}$. Indeed this is the case for most of the experimental data used by Kirwan and Pigford (1969) for the test of the theory they developed. However this is not so for polyphenyls where the difference of two activation enthalpy varies approximately five times in the range of experimental data reported in the literature.

Curves C's in both Figs. 4 and 5 are the predicted growth rate, V, computed using Eq. (10) for $\Delta S_C^{\ddagger}$ and $\Delta H_V^{\ddagger}$ obtained from the slope of the best straight line fit of log η-vs-(1/T) at freezing point (Andrew and Ubbelohde, 1955). The deviation at lower ΔT are even greater while a reasonable agreement between the literature data and the predicted values at large undercooling may be fortuitous, because the screw dislocation mechanism may not be operable there due to the change of the morphology of the growing crystal.

Entropy effect may be a possible explanation to the deviations both at small and large undercoolings between the literature data and the computed values. Both the number of molecules present at the interface and their orientations in the right directions have significant effects on the kinetics of crystallization. For substances whose molecules interlock significantly in the melt such as o-terphenyl and TαNB the molecular orientation effect for the transformation from liquid to solid may be greater than $(\Delta S_f - R)$. If the predicted values of V would have to fit

the literature data with $\Delta H_C^{\ddagger} = 0.89\ \Delta H_V^{\ddagger}$, the $\Delta S_C^{\ddagger}$ should have values as plotted in Figs. 6 and 7 for both polyphenyl compounds. The deviation of this $\Delta S_C^{\ddagger}$ from that of estimated with Eq. (10) is considerable at large undercooling.

Both literature data for growth rates pass through a maximum value at temperature, T_{max} about 175° C for TαNB and around 40° C for o-terphenyl. Analysis done by Greet (1967) for o-terphenyl and by Magill and Plazek (1967) for TαNB indicated that the exponential relationship equivalent to growth by surface nucleation described their experimental results best for the temperature above T_{max}. This is in accord with what we had suggested earlier that apparently these polyphenyl compounds crystallize by a different growth mechanism in the range of small undercooling.

Although the hypothesis concerning the estimation of activation entropy for crystallization, $\Delta S_C^{\ddagger}$ by Eq. (10) has failed to hold for three compounds, except for m-terphenyl, tested here, there is no reason to doubt that Eq. (9) has its practical use in predicting the rates of crystal growth for a wider range of undercooling from one measured growth rate. In spite of the questionable model built in terms of macroscopic activated-state properties to represent the molecular transport phenomena and an idealized surface structure of the solid-liquid interface which is derived from the screw dislocation concept, thus, we have seen that Eq. (9), with some knowledge about transport process in the melt, appears to be capable in predicting the growth rate within an order of magnitude.

The kinetic rate formula expressed in terms of ART in the functional relationship as shown in Eq. (1) has an advantage in separating the surface

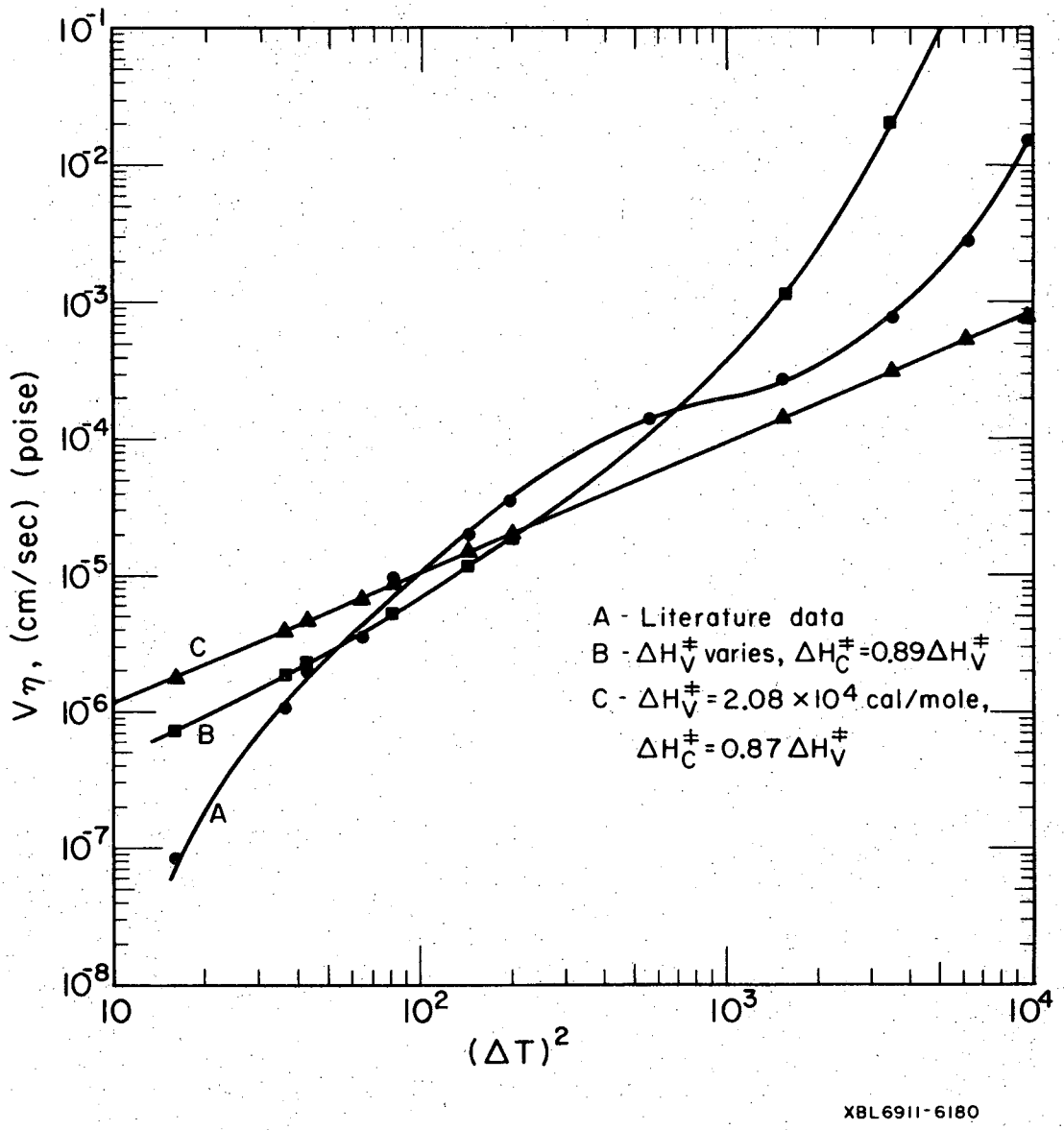

Fig. 5. Comparison of predicted growth rates and literature values, TaNB.

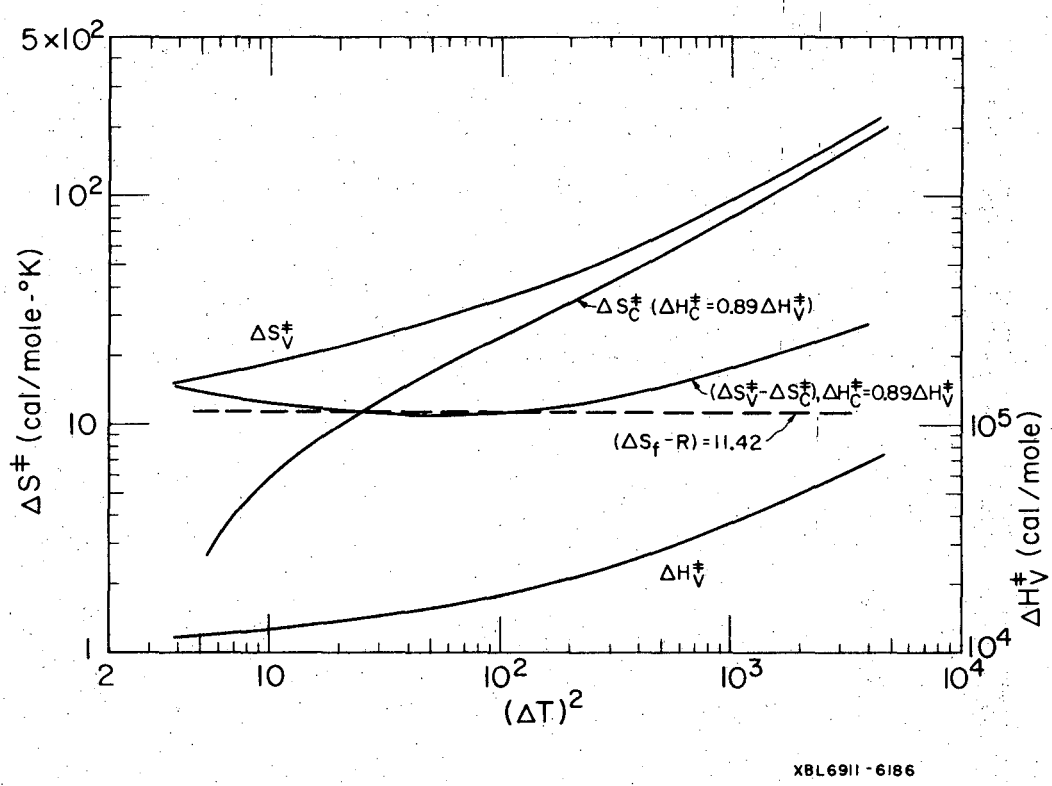

Fig. 6. Derived activated-state properties from viscosity and from crystal growth rate, o-terphenyl.

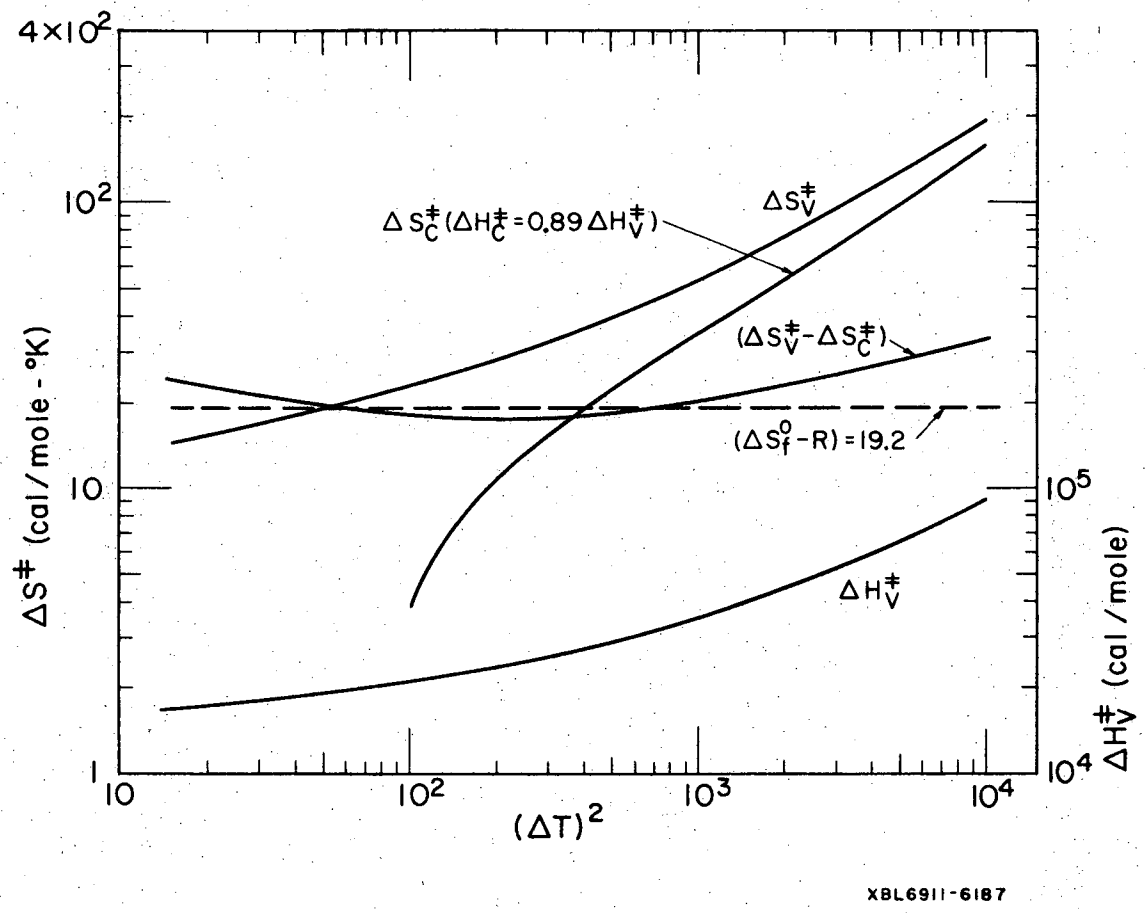

Fig. 7. Derived activated-state properties from viscosity and from crystal growth rate, TαNB.

condition and the transport terms which include the activation energy of jumping molecules and the free energy for the phase transformation. It is hoped in the future that better understanding on the liquid structure and possibility in predicting the surface structure in contact with the melt quantitatively will greatly improve the technology of crystallization and increase the knowledge in science of crystal growth so that the best condition in growing a specific crystal can be determined from the physical properties of the substances.

CONCLUSIONS

The Eyring-type of kinetic rate expression developed by Kirwan and Pigford, using screw dislocation concept for surface step density and the knowledge of the difference in the activated states for crystallization and that for viscous flow, is applied in predicting the growth rate of polyphenyls-o- and m-terphenyls and TαNB.

The predicted values of growth rate agree well with the experimental data for m-terphenyl when $\Delta H_C^{\ddagger} = 0.76\ \Delta H_V^{\ddagger}$ is used. For o-terphenyl the agreement between the computed values and the literature data is good for undercooling below 12° C but deviations magnify at larger undercooling when $\Delta H_C^{\ddagger} = 0.89\ \Delta H_V^{\ddagger}$ is used. The predicted values do not fit as well with the reported data for TαNB but an order of magnitude estimate is obtained for undercooling below 20° C. Values of $\Delta S_C^{\ddagger}$ estimated from Eq. (10) are used for these predictions although Eq. (10) itself does not seem to hold for three compounds tested here.

Until the quantitative knowledge about the crystal morphology in relation to the surface step density and about the liquid structure are

further advanced the present Eyring-type theories based on the macroscopic properties provide simple models for practical purposes.

NOTATION

f = surface step density

h = Planck's constant, 6.6252×10^{-27} erg/sec

H = molar enthalpy, cal/g mole

k = interfacial rate constant, sec^{-1}, or Boltzmann's constant, 1.38045×10^{-16} erg/°K

N = crystallization flux, mole/sq cm-sec, or Avogadro's number, 6.0232×10^{23} $mole^{-1}$

r_c = critical radius of two-dimensional nucleus, cm

R = gas constant, cal/g mole °K

S = molar entropy, cal/g mole °K

T = temperature, °C or °K

V = freezing velocity, cm/sec, or molar volume, cc/g mole

GREEK LETTERS

η = viscosity, poise

λ = interatomic spacing, cm

μ = chemical potential, cal/g mole

ρ = molar density, g mole/cc

σ = interfacial surface free energy, cal/sq cm

χ = transmission coefficient

SUPERSCRIPTS

F = forward process

0 = standard state property

R = reverse process

$\ddagger$ = activated state property

SUBSCRIPTS

C = crystallization activated state property

f = fusion process

h = hole formation process

j = jumping process

L = liquid state property

m = melting process

P = constant pressure condition

S = solid state property

T = constant temperature condition

V = viscous flow activated state property, or constant volume condition

vap = vaporization process

CHAPTER IV

PURITY OF CRYSTALS GROWN FROM BINARY ORGANIC MELTS

ABSTRACT

Binary liquid mixtures of stilbene and bibenzyl form mixed crystals which, according to the phase diagram, should be considerably richer in stilbene than the liquid in which they grow. By watching the growth under a microscope using interference fringes to follow concentration changes, the solid phase composition can be determined as a function of growth rate and interface subcooling. The deviations from equilibrium are considerable. They are found to depend on the growth mechanism in accord with a theory following Eyring and Frank

INTRODUCTION

The demand for ultrapure crystals in the solid state industry has stimulated extensive study of the processes by which crystals grow from the melt. The zone refining process, for example, has been very successful for producing pure metals but evidently has not yet been applied on a large scale in the organic chemical industry. The obvious need for improved continuous processes for the purification of high-melting organic compounds suggests that better understanding of the interface kinetic process itself--a key piece of information for rational design--is required.

The process of crystal growth includes the diffusive transport of molecules from the bulk liquid to the interface, orientation of the molecules for attachment to the solid surface, and conduction of the latent heat of fusion from the interface. The resistance to diffusion and to heat conduction can be minimized easily by mechanical stirring but if the major resistance is in the interface itself stirring is of no help.

In zone refining studies the assumption of interfacial equilibrium has been used frequently as a boundary condition to solve the liquid phase mass transfer equation in order to obtain the distribution of the minor component. The slowness of the process may make this assumption acceptable in many cases. However, when the impurity content is large or when the process is to operate rapidly and especially when the phase diagram exhibits solid solution behavior the equilibrium assumption can hardly be justified. Under these conditions the separation effect owing to crystallization may be severly reduced owing to interface kinetics.

Most of the previous work on crystal growth rate phenomena has been confined to pure substances, the key relationship being that between the growth rate and the thermal undercooling of the melt (Van Hook, 1963, and Chalmers, 1964). Cahn, Hillig, and Sears (1964) reviewed such information with particular emphasis on the distinction between theories involving attachment of molecules to the whole of a microscopically flat crystal surface and those involving attachment to a few surface sites connected with dislocations. The use of assumption that the whole surface is effective has been criticized by Jackson et. al. (1967), who concluded that such theories can only be applied to second-order phase transitions.

Among the theories which involve surface defects there are several possibilities but a suggestion made originally by Frank (1948) has appeared to be the most promising for many substances. According to Frank, the surface imperfection to which liquid molecules are able to attach themselves is a self perpetuating spiral defect consisting of a ledge step of molecular dimensions. Molecules can attach themselves in the corner of the step; as a result, the spiral winds around its center and eventually covers the whole crystal surface. Chernov (1961) has asserted that this screw dislocation mechanism, if it is not the only type of growth process, must be regarded as quite typical and universal.

THEORY OF THE GROWTH RATE OF A CRYSTAL FROM A SUBCOOLED BINARY MELTS

Following the usual assumption of Eyring (1941), the expression for the flux of component B toward the surface of a crystal to which both A and B molecules attach themselves is

$$N_B = f\,(\lambda_L k_B^F \rho_L y_B - \lambda_S k_B^R \rho_S x_B)\,, \qquad (1)$$

where the k's represent forward and reverse first-order rate coefficients, respectively, and where $\rho_L y_B$ and $\rho_S x_B$ are the molar concentrations of B in the interfacial liquid and solid, respectively. The fraction of the interface surface which is available for the attachment of molecules coming from the liquid is f, which may be a small number if the interface structure contains very few vacancies. The λ's represent the increments of distance accompanying the removal of one molecular spacing in the liquid or the addition of one layer of solid, respectively. If we assume that the lattice dimensions are inversely proportional to the molar densities we

may write Eq. (1) alternatively as

$$N_B = f\ \lambda_S \rho_S k_B^F \left(y_B - \frac{k_B^R}{k_B^F} x_B\right) . \qquad (2)$$

Since at equilibrium between the phases the flux must be zero we identify the ratio of the rate coefficients with the equilibrium phase compositions by

$$k_B^F/k_B^R = x_{Be}/y_{Be} , \qquad (3)$$

which, in a binary system at constant pressure, is a function of the interface temperature only.

Completion of the theory requires that expressions be developed for one of the rate coefficients, following Eyring, and for the surface fraction, based on some assumption about the geometry of lattice imperfections at the interface. Before going into these steps, however, we first call attention to some aspects of the theory which appear to have escaped attention in the past.

If we define u_A as the average of the velocities of the A molecules as they move toward the surface we obtain

$$u_A = N_A/\rho_L y_A = f\ \lambda_L k_A^F \left(1 - \frac{y_{Ae} x_A}{x_{Ae} y_A}\right) . \qquad (4)$$

Similarly,

$$u_B = N_B/\rho_L y_B = f\ \lambda_L k_B^F \left(1 - \frac{y_{Be} x_B}{x_{Be} y_B}\right) , \qquad (5)$$

and in a binary system the two velocities are obviously related to each other. In fact, since each of the coefficients in front of the parenthesis is positive and since the parenthetical expressions in Eq. (4) and (5) must be of opposite sign, u_A and u_B can not both be positive. If B-molecules move toward the surface then A-molecules must move away from it, according to the equations.

This anomolous situation is easily resolved if one notes that each of the equations so far developed is true in a coordinate system which moves toward the interface at a velocity given by

$$u^* = y_A u_A + y_B u_B = f \lambda_L (k_A^F \Delta_A + k_B^F \Delta_B) . \qquad (6)$$

In Eq. (6) the symbols Δ_A and Δ_B have been introduced as abbreviations for the driving forces,

$$\Delta_A = y_A - (y_{Ae}/x_{Ae})x_A \qquad (7a)$$

$$\Delta_B = y_B - (y_{Be}/x_{Be})x_B . \qquad (7b)$$

Obviously u^* can be positive, zero, or negative, depending on the ratio of the two forward rate constants.

Experimentally, it is difficult if not impossible to adjust the fluid velocity at the interface to the value u^*. In our experiments and in most others we have held the liquid-solid interface stationary and have measured the velocity, V, of the whole mass of liquid and solid needed to accomplish this. Thus, V is the velocity of propagation of the interface and the growth velocity of the crystal. The velocity of the liquid as it

approaches the stationary solid surface is not zero. A mass balance shows that the liquid moves at the velocity $V(\frac{\rho_S}{\rho_L})$ toward the interface, a value which can easily differ from u^*. Therefore, in order to obtain equations for the flux of each component in the laboratory coordinate system we must modify Eq. (1) by adding terms representing the convective transport of the components.

$$N_A = f\,\lambda_S \rho_S k_A^F \Delta_A + [V(\rho_S/\rho_L) - u^*]\rho_L y_A \,, \tag{8}$$

and a similar equation for N_B. By substituting u^* from Eq. (6) we obtain

$$N_A = f\,\lambda_S \rho_S\,(k_A^F \Delta_A\, y_B - k_B^F \Delta_B\, y_A) + V\,\rho_S y_A \,, \tag{9}$$

and

$$N_B = f\,\lambda_S \rho_S\,(k_B^F \Delta_B\, y_A - k_A^F \Delta_A\, y_B) + V\,\rho_S y_B \,. \tag{10}$$

It is not difficult now to obtain an equation for the composition of the solid which forms, for diffusion rates in the solid phase are so slow that the ratio of the mole fractions of the components is equal to the ratio of the molar fluxes onto the interface, i.e. $x_B = N_B/V\,\rho_S$, and Eq. (9) and (10) give

$$x_B = y_B + \frac{f\lambda_S}{V}\,(k_B^F \Delta_B\, y_A - k_A^F \Delta_A\, y_B) \,, \tag{11}$$

and a similar equation for x_A. It is clear now that the difference in composition between solid and interfacial liquid depends on the growth rate

parameter, $g_B = f\lambda_S k_B^F/V$, and on the ratio of the two first-order coefficients. When the values of k^F are very large the parenthetical expression in Eq. (11) must be zero, which will require that both the Δ's must be zero. Thus, phase equilibrium will be achieved. On the other hand, when the growth rate parameter is small the second term on the right will be negligible, despite a finite value for each of the Δ's. Then $x_B = y_B$ and no enrichment of the crystal occurs as it grows, the composition of the solid being the same as that of the contiguous liquid.

An alternative method for expressing the result given in Eq. (11) has come into popular use in metallurgy and in zone refining technology. It is to define an "effective distribution coefficient" for each component as the ratio of the actual solid mole fraction to the mole fraction in the interface liquid: $K_B^* = x_B/y_B$ and $K_A^* = x_A/y_A$. These values may differ from the values based on the equilibrium phase diagram, $K_A = x_{Ae}/y_{Ae}$ and $K_B = x_{Be}/y_{Be}$, owing to the rate effects we have been discussing. From Eq. (11) we obtain

$$K_B^* = \frac{1 + (f\lambda_S k_B^F/V)\,\{[1 - (k_A^F/k_B^F)]\,y_A + (k_A^F/k_B^F)(1/K_A)\}}{1 + (f\lambda_S k_B^F/V)\,\{(y_A/K_B) + (k_A^F/k_B^F)(y_B/K_A)\}} \quad . \qquad (12)$$

The equation for K_A^* is similar and can be obtained by exchanging subscripts in Eq. (12). According to Eq. (12), K_B^* approaches unity as the growth velocity increases or the forward rate constant decreases. As Eq. (12) indicates, the effective distribution coefficient, K^*, is not a constant, as has often been assumed; it depends on the temperature, the interfacial liquid composition and on the growth velocity. Its numerical value always lies between unity and the equilibrium value, K.

The result given by Eq. (11) can also be expressed in terms of the effective separation factor, defined by $\beta = (x_B/x_A)(y_A/y_B)$. This factor can be expected to be more nearly independent of composition than either K_A^* or K_B^*, at least for thermodynamically ideal systems. It is given by

$$\beta = \left(\frac{x_B}{x_A}\right)\left(\frac{y_A}{y_B}\right) = \frac{1 + (f\lambda_S k_B^F/V)\ \{[1 - (k_A^F/k_B^F)]\cdot y_A + (k_A^F/k_B^F)(1/K_A)\}}{1 + (f\lambda_S k_B^F/V)\ \{[(k_A^F/k_B^F) - 1]\cdot y_B + (1/K_B)\}} . \qquad (13)$$

In the limit of very large V, β approaches unity; there is no separation effect when the solid forms instantly in the liquid. At very small values of V, β approaches the value K_B/K_A.

ESTIMATION OF THE SURFACE STEP DENSITY, f

The surface step density, f, represents the fraction of the surface of the crystal which is available for attachment of individual molecules arriving from the liquid. For a surface that is sufficiently rough on a molecular scale, f is unity. According to Jackson (1967), many metals and some organic compounds which have very low values of the entropy of fusion are able to accept new atoms or molecules over their whole surfaces. For most substances, however, and particularly for more complex organic molecules only a very few positions on the crystal surface are available. The acceptable sites are in the corners of dislocation imperfections on the surface.

When a dislocation line intersects the crystal interface the dislocation winds itself into a screw as growth proceeds and provides a self perpetuating spiral step into the corner of which new molecules can become

attached. According to Frank (1948) the spiral structure is approximately the shape of an Archimedean spiral having a constant spacing between adjacent branches that depends on the radius of curvature at the center of the spiral, r_c. Thus, the surface fraction for such a structure is equal to the ratio of the width of one molecule to the distance between branches of the spiral, or

$$f = \lambda/4\pi r_c \ . \tag{14}$$

Furthermore, if we assume that the size of the spiral at its center, where it has the smallest radius of curvature and the greatest ratio of surface to volume of any point along the spiral, is equal to the size of a two-dimensional nucleus which is just critically stable thermodynamically, we can equate r_c to $\sigma/\rho_S\Delta G$ where ΔG represents the difference of the Gibbs free energy of a mole of solid and a mole of liquid of the same composition and σ is the excess Gibbs free energy per unit of surface in the interface. Then the equation for f becomes

$$f = \lambda\rho_S\Delta G/4\pi\sigma \ . \tag{15}$$

Using Turnbull's (1958) empirical expression for the surface energy,

$$\sigma = 0.3 \frac{\Delta H_f}{N^{1/3} V_S^{2/3}} \ , \tag{16}$$

where ΔH_f is the enthalpy of fusion and N is the Avagadro number, we get

$$f = \frac{1}{1.2\pi} \left(\frac{\Delta G}{\Delta H_f}\right) = \frac{1}{1.2\pi} \left(\frac{\Delta G}{T_m \Delta S_f}\right) . \qquad (17)$$

Our expression for f must now be completed by an evaluation of the Gibbs free energy change, ΔG.

CHANGE IN GIBBS FREE ENERGY DURING SPONTANEOUS CRYSTAL GROWTH

If we have a pure melt from which the crystal is growing the free energy difference is very nearly equal to $\Delta S_f \Delta T$, where ΔT represents the difference between the equilibrium melting point and the interfacial temperature, i.e. the amount of subcooling. When the crystal is formed in a solution, however, the free energy change depends both on the composition of the liquid and on the interfacial temperature.

Consider first the formation of a pure crystal of compound B in a liquid mixture having interfacial mole fraction y_A of the "impurity" component, A. Then the chemical potential difference of B across the interface is given by Kirwan and Pigford (1969).

$$\Delta G = \mu_B^L - \mu_B^S = [\Delta S_f - \Delta C_{PB}(1 - \frac{T}{T_{Bm}}) - R \ln(\gamma_B y_B)]\Delta T , \qquad (18)$$

where γ_B represents the activity coefficient of B in the interface liquid. The second term in the brackets is often negligible. Under these conditions the surface fraction f is somewhat reduced as compared with the value expected for crystallization from the pure liquid.

Moreover, for a system which forms a solid solution crystal, the thermodynamic driving force for growth can not be expressed simply in terms

of the interface subcooling, ΔT. As can be anticipated from Eq. (18), ΔG now depends both on interfacial temperature and on the interface composition driving forces.

The free energy change owing to phase transformation of one mole of liquid into one mole of solid solution, both liquid and solid having the solid's composition, is

$$\Delta G = (\mu_A^L - \mu_A^S)x_A + (\mu_B^L - \mu_B^S)x_B \ , \tag{19}$$

and the chemical potentials can be expressed in terms of their equal values on the liquidus and solidus curves of the phase diagram by the equations

$$\mu_B^L(y_B,T) = \mu_B^L\,(y_{Be},T) + RT \ln\,(\gamma_B y_B/\gamma_{Be} y_{Be})$$

$$\mu_B^S(x_B,T) = \mu_B^S\,(x_{Be},T) + RT \ln\,(\Gamma_B x_B/\Gamma_{Be} x_{Be}) \ ,$$

and two similar equations for component A. The γ's represent activity coefficients in the liquid solution; Γ's, in the solid solution. Substituting these expressions into Eq. (19) we get

$$\Delta G/RT = x_A \ln(x_{Ae}y_A/y_{Ae}x_A) + x_B \ln(x_{Be}y_B/y_{Be}x_B) + x_A \ln(\gamma_A\Gamma_{Ae}/\gamma_{Ae}\Gamma_A)$$

$$+ x_B \ln(\gamma_B\Gamma_{Be}/\gamma_{Be}\Gamma_B) \ . \tag{20}$$

The first two terms represent the free energy changes if the liquid and solid solutions were ideal mixtures; the last two terms take care of

deviations from ideality. The activity coefficients can sometimes be obtained from the phase diagram without resorting to any assumptions about solution behavior. Note that temperature appears in this expression for ΔG through its effect upon the equilibrium mole fractions, y_{Be}, x_{Be}, etc. Note also that $\Delta G = 0$ when both the temperature and the compositions fall on the solidus and liquidus lines of the phase diagram. Presumably ΔG must be positive for the spontaneous growth process to occur. To bring these ideas out more clearly we refer to the hypothetical phase diagram in Fig. 1, which shows a possible location for the real and the equilibrium liquid and solid compositions at the observed interface temperature. Note that the liquid is cooled below its equilibrium freezing temperature on the liquidus curve and therefore has a greater free energy than at equilibrium; the solid, on the other hand, is at a temperature above its equilibrium melting point and is therefore superheated. It, too, has a greater free energy than it would have at equilibrium. The value of ΔG for the process of solidification is positive when the liquid is subcooled far enough and the solid is not superheated too far.

Some concern may be felt over the fact that the solid phase is indicated to be superheated, in view of the fact that all attempts to superheat solids above their melting points have proved fruitless. Note in connection with the present situation, however, that the solid is not only superheated but is also growing as a result of the continuous bombardment by molecules which come from the over-energetic liquid.

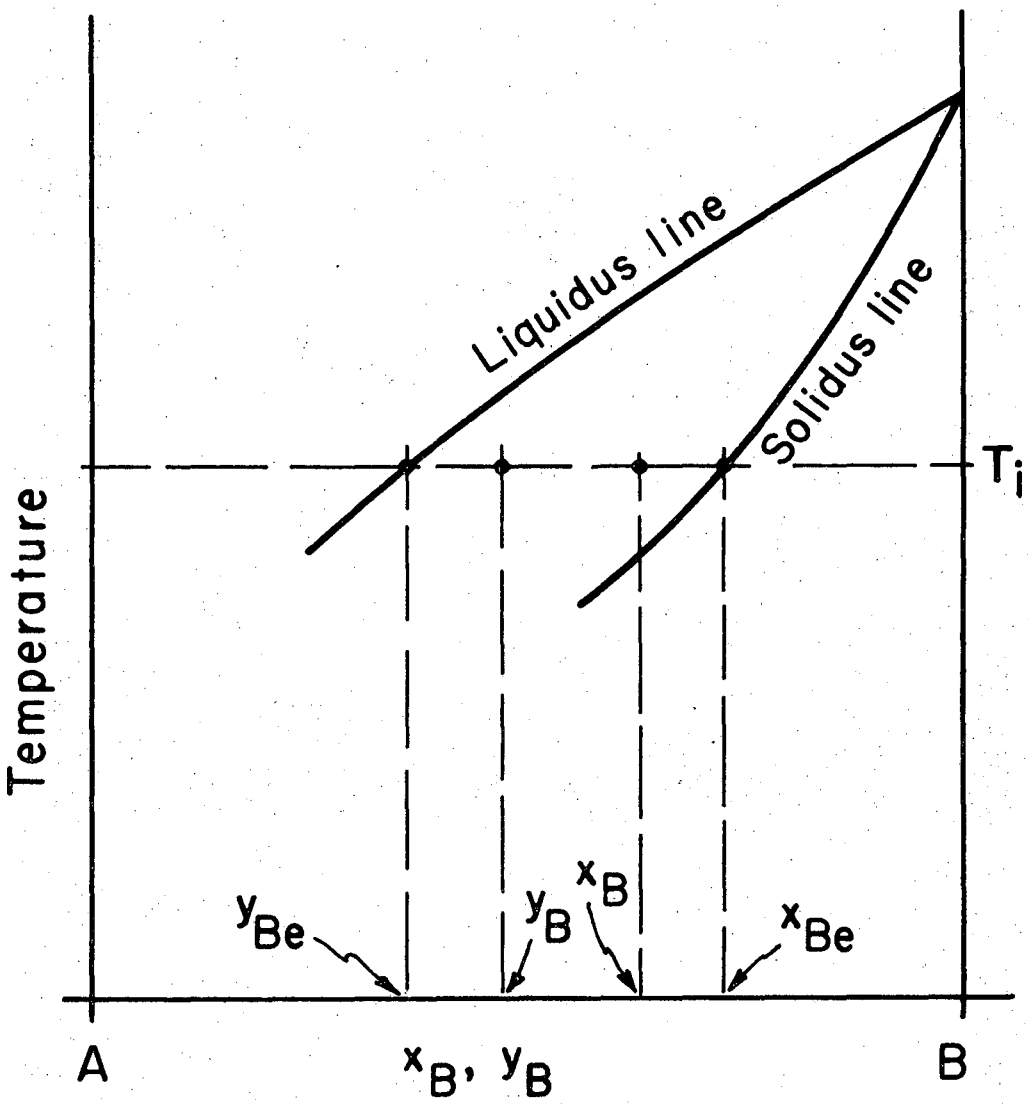

Fig. 1. Hypothetical phase diagram, bibenzyl and trans-stilbene system.

THE COMPUTATION OF THE CRYSTAL GROWTH VELOCITY, V

For a pure substance the crystal growth velocity is fixed when the temperature of the surrounding liquid is given; for growth from a binary solution fixing the interface temperature and the interface liquid composition are sufficient to determine V. How is such a relationship expressed by the equations given here?

From Eq. (12) one can compute the composition of the solid which forms in a liquid of fixed composition provided the ratio of the two forward rate constants (a function of temperature alone) is known and provided also that the group of variables, $f\lambda_S k_B^F/V$, is known. Thus for fixed T and y_B, x_B will be uniquely a function of $f\lambda_S k_B^F/V$. A typical relationship of this sort, computed for the binary system stilbene-bibenzyl, is shown in Fig. 2. As expected, the greater the value of the group the closer x_B approaches its equilibrium value at the assumed temperature.

Having found the solid composition it is now possible to compute ΔG and f, through Eq. (17). Furthermore, k_B^F is fixed by the temperature and is known. Thus, for each assumed value of the group, $f\lambda_S k_B^F/V$, all the quantities but V are determined, from which V follows by a simple computation. Fig. 2 also shows the relationship between ΔG and the dimensionless group for the illustrative example. By assuming $f\lambda_S k_B^F/V$ constant and varying y_B for fixed T it shows the values of $V/\lambda_S k_B^F$, which is proportional to f, is related to the undercooling, $\Delta T = T_e - T$, almost linearly as for pure compounds.

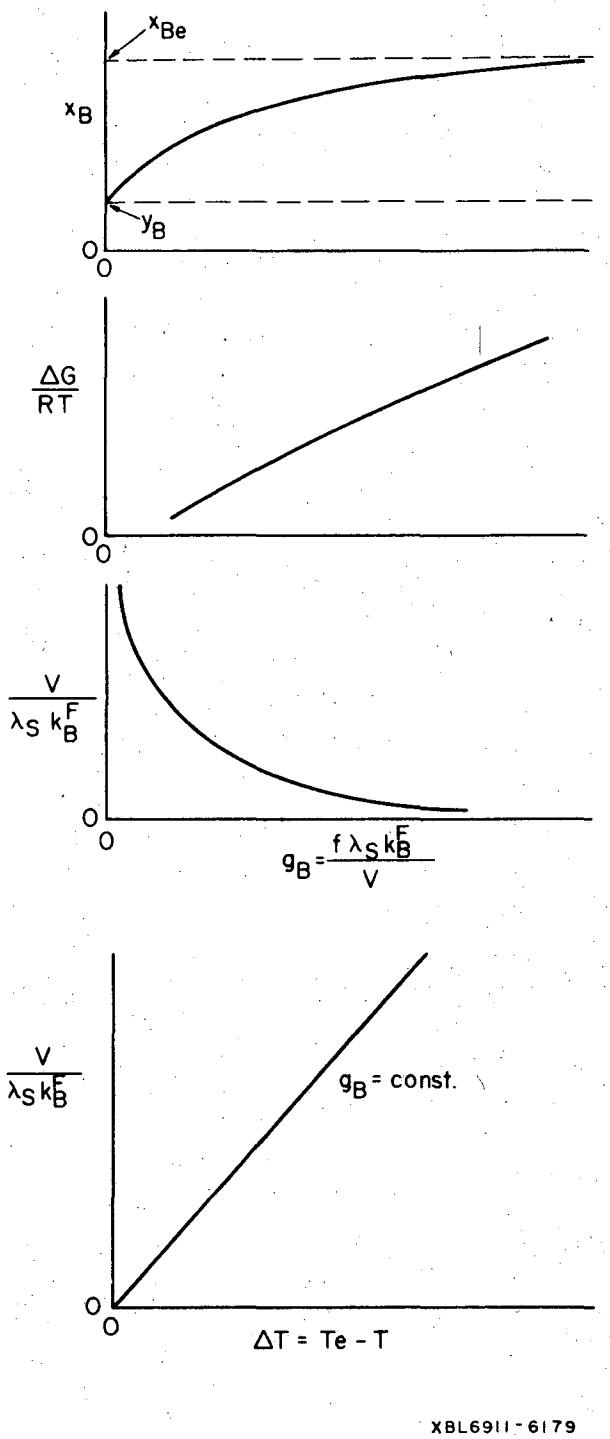

Fig. 2. Relationship for the determination of mixed crystal growth velocity.

DETERMINATION OF THE RATE COEFFICIENTS, k_A^F and k_B^F

Following the method of Eyring (1941), the expression for the first-order rate coefficient is

$$k_B^F = \chi\ (kT/h)\ \exp(-\Delta G_C^{\ddagger}/RT) = \chi\ (kT/h)\ \exp(\Delta S_C^{\ddagger}/R)\ \exp(-\Delta H_C^{\ddagger}/RT)\ , \qquad (21)$$

and a similar expression for k_A^F. In Eq. (21) χ represents the fraction of the activated molecules which pass over the activation barrier in the direction. $\Delta G_C^{\ddagger}$ is the excess of the standard free energy of the molecule which is activated for crystallization over the value in the liquid, and $\Delta S_C^{\ddagger}$ and $\Delta H_C^{\ddagger}$ are the related entropy and enthalpy differences, respectively. Use of such an expression required a knowledge of the numerical values of these thermodynamic properties of the activated state for each substance in the mixture.

There is some reason to believe that, even though numerical values of the activation properties may not be available from direct measurement of crystal growth rates, values can be estimated by using the corresponding values derived from viscosity. Viscosities of liquids are far easier to measure experimentally than are growth velocities and the molecular mechanisms involved may be similar.

On the other hand, as pointed out by Kirwan and Pigford (1969), there are some differences in the molecular processes involved in crystal growth and in viscous flow. For instance, the molecule which approaches the crystal and becomes attached has to have the orientation that is required in the crystal lattice. The molecule which is ready to undergo viscous flow displacement may need to be oriented too, but the requirement

is not likely to be as stringent. Thus, it may be possible to estimate $\Delta S_C^{\ddagger}$ from $\Delta S_V^{\ddagger}$ by subtracting the entropy of fusion, ΔS_f from the latter, plus a small correction of R entropy units to account for the observation that perfectly spherical molecules undergo an entropy increase of R units upon melting. Moreover, there is reason to believe that the enthalpy of activation for crystallization may be smaller than that for viscosity (Kirwan and Pigford, 1969). To detach itself from its neighbor molecules in the liquid is all that is needed for crystal growth, but flow of a molecule also requires that a vacancy or hole be formed in the liquid at an adjacent site. Thus it may be that

$$\Delta H_C^{\ddagger} = c\Delta H_V^{\ddagger} , \tag{22}$$

where c is a constant probably smaller than unity. The best course of action, however, is not to try to compute $\Delta H_C^{\ddagger}$ unless no experimental crystallization data are available; a better plan is to make at least one measurement of the growth velocity and to determine the enthalpy of activation from that value, using it in Eq. (21) for estimates at other temperatures. Determination of both $\Delta S_C^{\ddagger}$ and $\Delta H_C^{\ddagger}$ from experimental data is not likely to be possible because it is unusual to be able to cover a wide enough range of temperatures in experimental work to give a reliable value of the slope of the curve of log (V) versus 1/T.

EXPERIMENTAL RESULTS

Data were obtained for the binary system bibenzyl-stilbene, for which there is a wide range of solid compositions over which homogeneous

solid solutions are formed. The phase diagram for the system is shown in Fig. 3, based on the data of Kolosov (1958). The diagram shows that over most of the range of x the crystal structure resembles that of pure stilbene. At low mole fractions of stilbene there is a peritectic reaction but the compositions that were used in the experiments were all to the right of this range.

Crystallization rates and interfacial compositions and temperatures were observed with a temperature-gradient microscope stage, as described elsewhere (Cheng, 1969). The interface mole fraction of stilbene, y_B, was computed from the known composition of the liquid mixture introduced into the optical wedge of the apparatus and from the observed shift of the diffraction fringes owing to the concentration variation which accompanies the diffusion boundary layer in the liquid. The equation relating these quantities is

$$y_B = y_B(\infty) - \Delta N(\lambda_0/2t)(\partial n/\partial y)_T^{-1} , \qquad (23)$$

with ΔN = the number of fringe displacements at the interface, λ_0 = the wavelength of the laser light used, t = the wedge thickness at the observation point, and $(\partial n/\partial y)_T$ = the derivative of refractive index of the solution with respect to composition.

Compositions of the solid phase were determined in two ways. First, the same diffraction pattern was used in combination with a diffusion flux balance at the interface,

$$x_B = y_B + (\rho_L D/\rho_S V)(dy_B/dz)_{z=0} , \qquad (24)$$

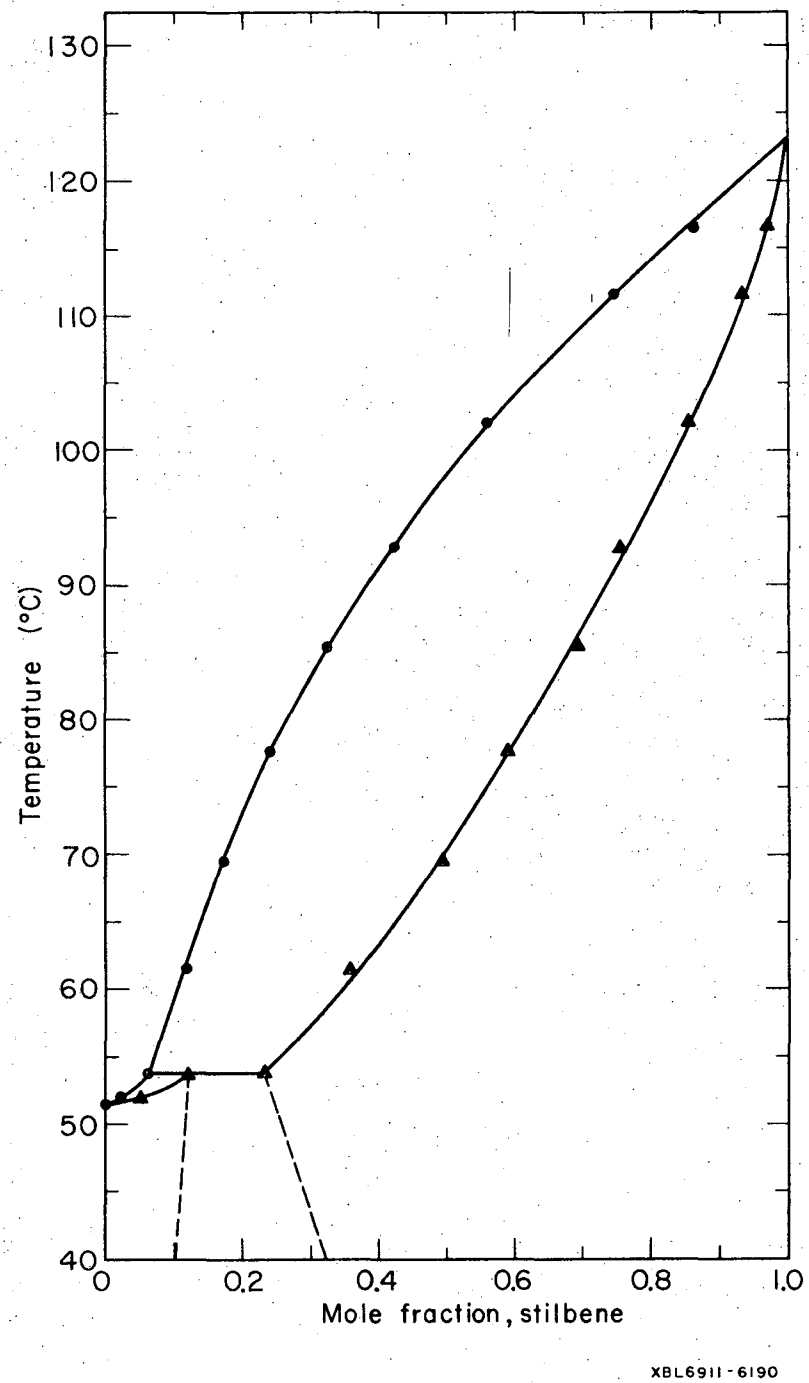

Fig. 3. Phase diagram, bibenzyl and trans-stilbene system.

in which D is the binary diffusion coefficient in the liquid and dy_B/dz is the normal gradient of mole fraction at the interface. The latter quantity could be computed from careful measurements of the slopes of several diffraction lines using the equation

$$dy_B/dz = \frac{\lambda_0 S}{2\ s\ t\ \cos\ \alpha(\sin\ \beta + S\ \cos\ \beta)(\partial n/\partial y)_T} \quad , \tag{25}$$

where S represents the measured slope of the diffraction fringes and s is their spacing. The angles α and β represent inclinations of the crystal face and of the distant straight diffraction lines, respectively. A detailed derivation of these equations is given elsewhere (Cheng, 1969).

In order to obtain an independent check of the computed solid compositions, a few measurements were obtained by taking small samples of the solid phase obtained from the diffraction wedge and subjecting these to ultra violet absorption analysis in ethanol. Such measurements were tedious and somewhat inaccurate but they agreed fairly well with the computed compositions using Eqs. (23) and (24), as will be seen shortly.

The pure materials were carefully purified by zone refining and sublimation. Measured melting points of the purified samples were 123.0° C for trans-stilbene (vs. 123.3° C reported (Kolosov, 1958)) and 52.03° C for bibenzyl (vs. 51.1° C reported (Kolosov, 1958)). Other properties of the pure components are shown in Table II.

The liquid diffusion coefficient was not measured directly. A value observed by Kirwan (1967) was combined with an estimate based on the empirical correlation of Wilke and Chang (1955); the value used was

7.6×10^{-6} sq. cm/sec at 63.3° C. It is believed to have a probable uncertainty of about ±20%. The intermolecular spacing for the solid, λ_S, was computed by taking the cube root of the column of the solid phase per molecule. Liquid viscosity data were determined by Kirwan (1967).

Table II. Physical Properties of Pure Materials[a]

Substance	M.W.	T_m	ΔH_f	ΔS_f	$\sigma x 10^7$	η	$\Delta H_V^{\ddagger}$	$\Delta S_V^{\ddagger}$
		°K	cal/g mole		(cal/cm^2)	c.p.	cal/g mole	
Bibenzyl	182.27	325.18	5580	17.18	4.76	2.0	3243	-3.709
t-stilbene	180.25	396.15	7080	17.87	8.70	1.0	3625	-3.083

[a]Dimensions see notation

DATA FOR PURE STILBENE

Figure 4 shows the experimentally observed growth velocities for pure trans-stilbene. The data are plotted in the form V vs. the square of the undercooling, ΔT. It can be shown that for the screw dislocation surface mechanism and for values of $\Delta S_f \Delta T / RT_m$ that are sufficiently small.

Equating the average velocity of movement toward the surface of the B molecules to the fluid velocity toward the same surface, $V(\rho_S/\rho_L)$, we get

$$V = f\, \lambda_S k_B^F \Delta_B = f\, \lambda_S k_B^F \left[1 - \exp\left(-\frac{\Delta S_f \Delta T}{RT}\right)\right]$$

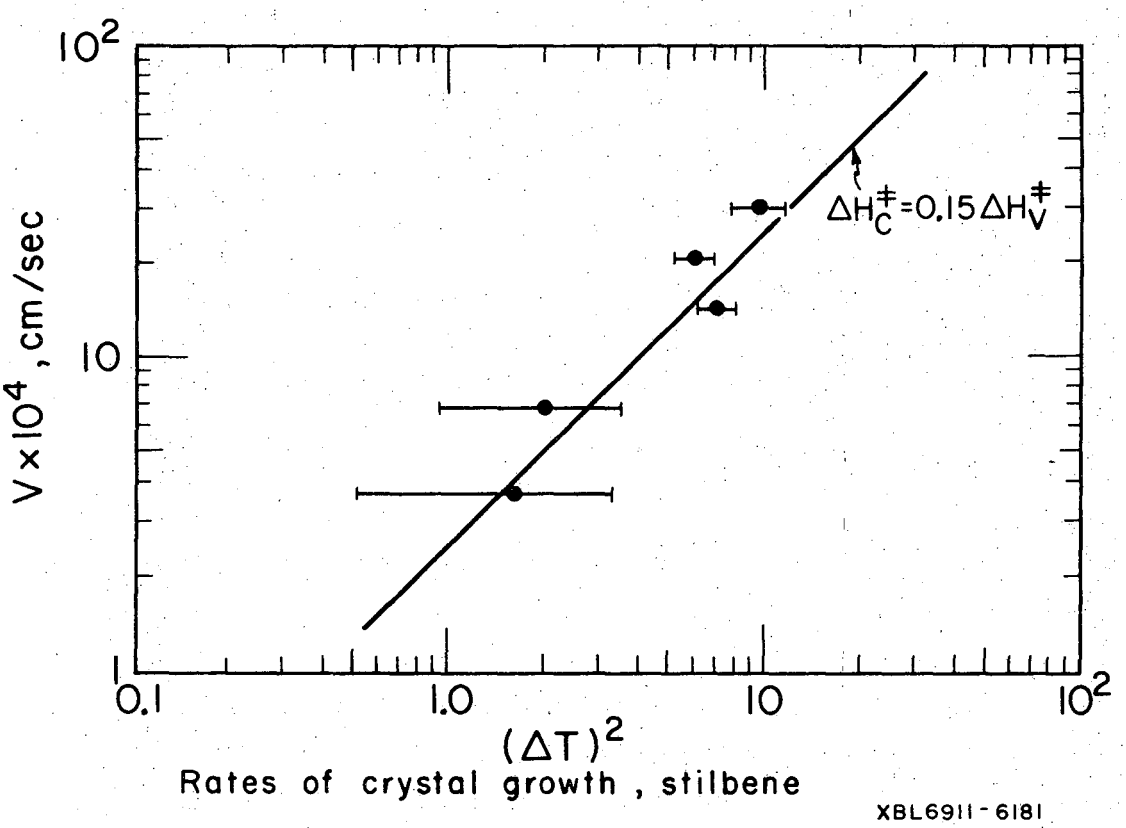
10^2
10
1
$V \times 10^4$, cm/sec
0.1
1.0
10
10^2
$(\Delta T)^2$
$\Delta H_c^{\ddagger} = 0.15 \Delta H_v^{\ddagger}$
Rates of crystal growth, stilbene
XBL6911-6181

Fig. 4

or

$$V \sim (1/1.2\pi)(\lambda_S k_B^F)(\Delta S_f \Delta T/\Delta H_f)(\Delta S_f \Delta T/RT_m)$$

$$= (1/1.2\pi)(\lambda_S k_B^F)(\Delta S_f/R)(\Delta T/T_m)^2 , \qquad (26)$$

in which the exponential term has been expanded in a series. The data on the figure are not sufficiently accurate, owing to uncertainties in the interface temperature, to test the hypothesis that V is proportional to the square of ΔT. However, if we evaluate the entropy of activation in k_B^F from the equation,

$$\Delta S_C^{\ddagger} = \Delta S_V^{\ddagger} - (\Delta S_f - R) , \qquad (27)$$

and approximate the enthalpy of activation by choosing $c = 0.15$ in Eq. (22) we obtain a line from Eq. (26) which passes through the data points. In view of the reasonable values of the activation quantities and the at least approximate agreement of the exponent on ΔT with the expected value, it seems likely that the pure stilbene crystals grew by the screw dislocation mechanism.

Evaluation of the surface fraction leads to $f \sim 6 \times 10^{-4}$ for stilbene at one degree of subcooling.

DATA FOR STILBENE-BIBENZYL SOLUTIONS

The experimental data for interface liquid and solid compositions and interfacial liquid temperatures are listed in Table III for three series of runs, each series corresponding to a constant value of the liquid mole

fraction of stilbene at a great distance from the crystal, y_{B0}. The observed liquid and solid compositions are plotted in Fig. 5. There one sees that, owing to the finite growth velocity, the interfacial liquid mole fraction of stilbene fell slightly below y_{B0} at finite values of V. The greatest deviation from equilibrium occurred in the solid composition, as shown by the upper lines in the figure. At very small values of V the values of x_B tended toward the equilibrium value but at most of the values of V used x_B fell considerably below its equilibrium value. At large values of V the crystal's composition differed only very slightly from that of the liquid from which it grew. The figure shows that the principal cause of the failure to reach equilibrium was not the diffusional resistance of the liquid but the slowness of phase growth.

Although the measurements were carried out with great care it is of course possible that the solid compositions which were obtained by calculation from the diffusion flux balance, Eq. (24), were in error. This could have occurred if any of the measurements were not precise, if the estimated diffusion coefficient was wrong, or if the growing crystals did not fill the optical wedge completely. By computation of the possible errors of measurement it was concluded that the true value of y_B might have been off by about 0.0042 mole fraction and that the derivative, dy_B/dz might be in error by about 0.0052 mole fraction units. The probable error of D was estimated to be about 20 percent. The other quantities in the equation were precise. Thus, the total probable error in x_B should have been about 0.01 mole fraction units, which is smaller than the vertical difference between the pairs of curves on Fig. 5.

Table III. Crystallization of Mixed Crystals from Binary Melts of Stilbene and Bibenzyl System

Run No.	V, (cm/sec)×10³	$y_B(0)$, mole fraction	$x_B(0)$, mole fraction	T(0), °C	T_e[a], °C	y_{Be}, mole fraction	x_{Be}, mole fraction	$x_{B,cal}$[b], mole fraction
$y_{BO} = y_B(\infty) = 0.15$ mole fraction, stilbene								
III- 72	0.68	0.1356	0.1498	63.53	64.22	0.131	0.397	0.150
III- 73	1.00	0.1319	0.1411	64.17	63.70	0.135	0.407	c
III- 75	1.92	0.1388	0.1437	62.11	64.67	0.120	0.374	0.157
III- 76	0.51	0.1263	0.1671	63.61	62.93	0.131	0.398	c
III- 77	0.50	0.1407	0.1585	63.08	64.97	0.127	0.390	0.189
III- 99	0.74	0.1273	0.1513	63.37	63.07	0.129	0.394	c
III-101	0.34	0.1295	0.1707	62.86	63.38	0.126	0.386	0.150
III-102	0.40	0.1370	0.1662	62.68	64.41	0.125	0.383	0.190
III-103	0.15	0.1365	0.2055	62.48	64.35	0.123	0.380	0.249
III-104	0.13	0.1397	0.2224	63.17	64.78	0.128	0.391	0.252
III-105	0.39	0.1415	0.1702	62.73	65.04	0.125	0.384	0.210
III-106	0.21	0.1452	0.1784	61.82	65.53	0.118	0.370	0.281
III-107	0.31	0.1436	0.1736	63.28	65.32	0.129	0.393	0.220
III-140	0.42	0.1436	0.1651	63.65	65.32	0.131	0.399	0.196
III-141	0.35	0.1358	0.1624	62.49	64.19	0.123	0.380	0.189
III-143	0.23	0.1401	0.1760	63.76	64.84	0.132	0.400	0.198
III-144	0.15	0.1410	0.2019	63.06	64.98	0.127	0.389	0.258
III-145	0.09	0.1461	0.1923	63.49	65.66	0.130	0.396	0.307
III-146	0.03	0.1445	0.3168	62.13	65.44	0.121	0.375	0.381

(continued)

Table III. continued

Run No.	V, (cm/sec)×10^3	$y_B(0)$, mole fraction	$x_B(0)$, mole fraction	T(0), °C	T_e[a], °C	y_{Be}, mole fraction	x_{Be}, mole fraction	$x_{B,cal}$[b], mole fraction
$y_{BO} = y_B(\infty)$ = 0.15 mole fraction, stilbene								
III-147	0.20	0.1371	0.1973	62.66	64.43	0.124	0.383	0.225
III-148	0.73	0.1466	0.1519	60.10	65.73	0.106	0.342	0.228
III-149	0.25	0.1398	0.1864	62.22	64.80	0.121	0.376	0.240
IV - 1	0.21	0.1428	0.1907	63.13	65.21	0.128	0.391	0.243
IV - 2	0.15	0.1425	0.2123	63.94	65.16	0.134	0.403	0.232
IV - 3	0.10	0.1431	0.2483	62.93	65.25	0.126	0.387	0.301
IV - 4	0.07	0.1424	0.2801	63.12	65.15	0.128	0.390	0.313
IV - 5	0.79	0.1429	0.1508	64.86	65.23	0.140	0.417	0.150
IV - 6	0.65	0.1404	0.1542	62.90	64.89	0.126	0.387	0.180
IV - 7	0.35	0.1381	0.1616	62.37	64.57	0.122	0.379	0.208
IV - 8	0.15	0.1417	0.2014	62.74	65.08	0.125	0.384	0.271
IV - 9	0.24	0.1459	0.1647	63.64	65.63	0.131	0.399	0.237
IV - 10	0.12	0.1416	0.2256	63.42	65.08	0.130	0.395	0.261
$y_{BO} = y_B(\infty)$ = 0.25 mole fraction, stilbene								
III- 78	0.48	0.2314	0.2623	74.04	76.33	0.212	0.548	0.333
III- 79	0.87	0.2307	0.2494	75.86	76.25	0.227	0.571	0.244
III- 80	1.33	0.2271	0.2364	74.77	76.84	0.218	0.557	0.269
III- 81	1.62	0.2353	0.2411	74.36	76.77	0.215	0.552	0.276

(continued)

Table III. continued

Run No.	V, (cm/sec)×10^3	$y_B(0)$, mole fraction	$x_B(0)$, mole fraction	T(0), °C	T_e[a], °C	y_{Be}, mole fraction	x_{Be}, mole fraction	$x_{B,cal}$[b], mole fraction
$y_{B0} = y_B(\infty) = 0.25$ mole fraction, stilbene								
III- 84	0.16	0.2327	0.3257	75.56	76.48	0.225	0.568	0.350
III- 85	0.52	0.2404	0.2574	75.03	77.42	0.220	0.561	0.344
III- 86	1.24	0.2357	0.2486	75.13	76.81	0.221	0.562	0.274
III- 89	0.89	0.2276	0.2452	74.83	75.89	0.219	0.558	0.260
III- 91	2.00	0.2392	0.2450	74.26	77.22	0.214	0.550	0.280
III- 92	0.71	0.2247	0.2474	74.80	75.56	0.218	0.558	0.254
III- 93	0.96	0.2297	0.2439	74.34	76.13	0.214	0.552	0.278
III- 94	0.57	0.2330	0.2505	74.26	76.51	0.214	0.550	0.323
III- 96	0.10	0.2345	0.3953	76.42	76.68	0.232	0.579	0.301
III- 97	0.06	0.2377	0.5202	76.42	77.04	0.232	0.579	0.411
III- 98	0.13	0.2368	0.3842	74.90	76.94	0.219	0.559	0.442
$y_{B0} = y_B(\infty) = 0.45$ mole fraction, stilbene								
III-108	0.83	0.4350	0.4546	92.74	93.88	0.419	0.762	0.506
III-109	0.58	0.4356	0.4685	93.88	93.93	0.435	0.774	0.441
III-110	0.39	0.4412	0.4790	92.59	94.33	0.417	0.761	0.597
III-113	0.16	0.4436	0.5000	91.37	94.50	0.401	0.749	0.707
III-115	0.76	0.4308	0.4646	91.17	93.58	0.399	0.746	0.556
III-116	0.34	0.4398	0.4934	92.75	94.23	0.420	0.763	0.594

(continued)

Table III. continued

Run No.	V, (cm/sec)×10³	$y_B(0)$, mole fraction	$x_B(0)$, mole fraction	T(0), °C	T_e^a, °C	y_{Be}, mole fraction	x_{Be}, mole fraction	$x_{B,cal}$[b], mole fraction
$y_{B0} = y_B(\infty) = 0.45$ mole fraction, stilbene								
III-117	0.29	0.4427	0.4946	93.00	94.44	0.423	0.765	0.609
III-118	0.15	0.440	0.5795	93.38	94.53	0.428	0.769	0.645
III-119	0.14	0.4309	0.5815	90.32	93.59	0.388	0.738	0.704
III-132	0.86	0.4318	0.4678	87.55[d]	93.65	0.353	0.708[d]	0.616[d]
III-133	0.47	0.4276	0.4784	95.63	93.34	0.460	0.791	c
III-134	0.72	0.4412	0.4648	93.23	94.33	0.426	0.767	0.519
III-135	2.08	0.4412	0.4470	92.96	94.33	0.422	0.765	0.480
III-136	2.99	0.4428	0.4471	91.19	94.45	0.399	0.747	0.500
III-137	1.49	0.4388	0.4485	92.39	94.16	0.415	0.759	0.502
III-138	2.06	0.4361	0.4443	91.90	93.97	0.408	0.754	0.490
III-139	0.45	0.4318	0.4704	95.62	93.65	0.459	0.791	c

[a] Equilibrium temperature based on interfacial composition, $y_B(0)$.

[b] With k_B^F calculated from Eq. (21) using $\chi = 0.01$, and $\Delta T = T_e - T(0)$ for computing step density f.

[c] Because of negative ΔT, this value is not computed.

[d] Measured interfacial temperature T(0) was in error.

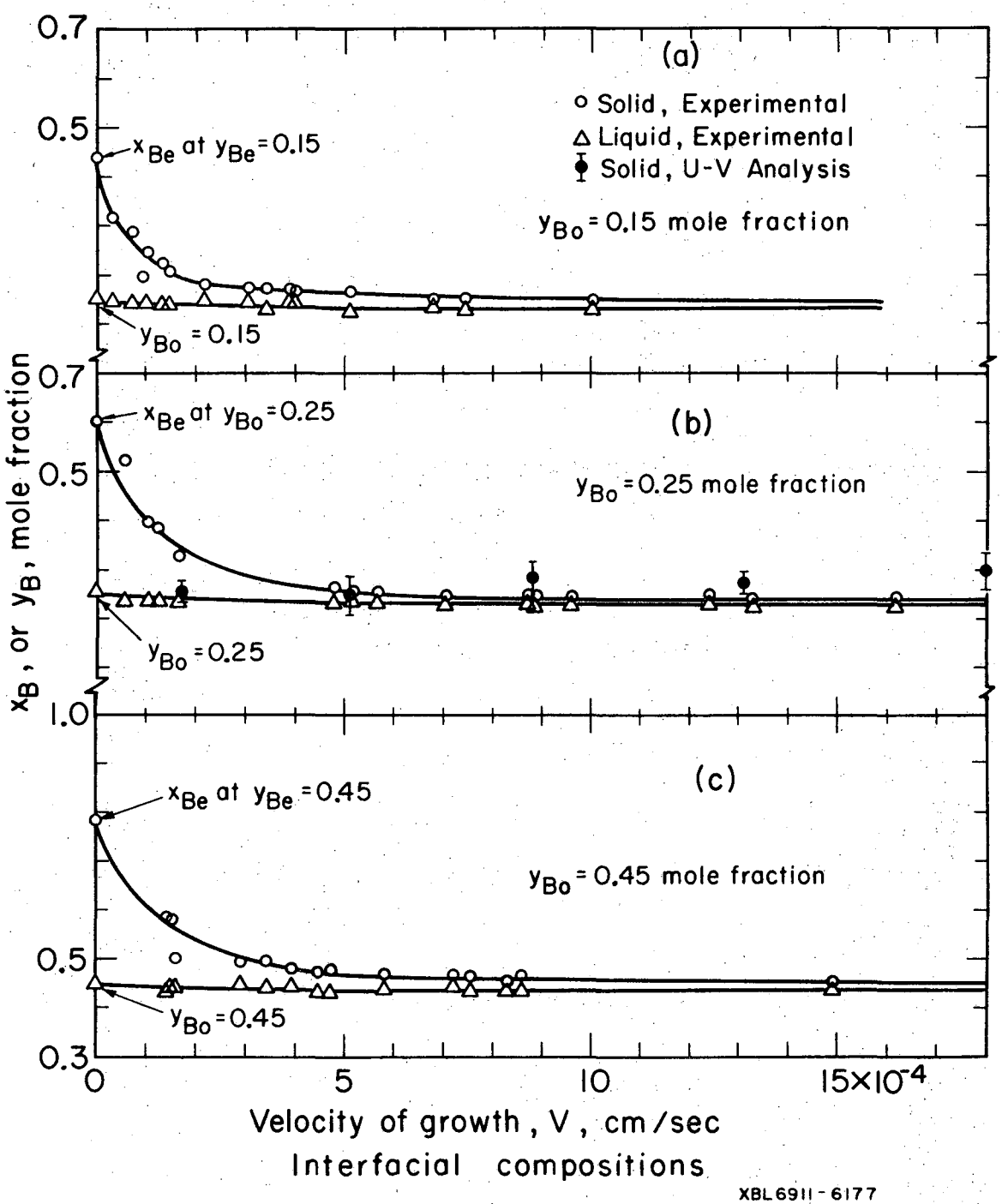

Fig. 5. Interfacial compositions, bibenzyl and trans-stilbene system.

An even stronger indication that the measured values of x_B are reliable was obtained when some of the crystallization runs were repeated and small samples of the solid were taken from the optical wedge and analyzed by ultra violet absorption. The following table summarized the values obtained and supports the use of Eq. (24) The results of such analyses are also shown in Fig. 5.

Table IV. Comparison of Solid Compositions Computed from Flux Balance with Values from Ultra Violet Absorption

Growth Velocity $V \times 10^3$, cm/sec	Mole Fraction Stilbene, x_B	
	From Eq. (24)	From Ultra Violet Analysis
1.85	0.240 ± 0.010	0.300 ± 0.031
1.31	0.243 ± 0.010	0.274 ± 0.019
0.88	0.251 ± 0.010	0.284 ± 0.033
0.51	0.260 ± 0.015	0.248 ± 0.039
0.17	0.340 ± 0.015	0.252 ± 0.017

One other piece of evidence is available to support the reported values of x_B. It consists of the measurements, also using Eq. (24), of the composition of the solid phase which grows at a finite rate in the system of salol-thymol. These compounds are completely insoluble in each other as solids, the phase diagram indicating that to the right of the eutectic point, $x_{Be} = 1$ and $x_{Ae} = 0$. Application of Eq. (11) shows that the rate theory is satisfied under these conditions only by the value $x_A = 0$ at finite V. Compute values of x_A based on the diffraction fringes, were not precisely zero but were close. The average value for several experiments

was about 0.1. Recognize, however, that the theory which we have used may be defective in such a situation for it assumes that the surface fraction for attachment of A molecules and that for B molecules is exactly the same. In fact, it may be possible that f_A is zero on a pure-B surface.

INTERPRETATION OF THE RESULTS

The Separation Factor, β: Figure 6 shows values of the separation factor based on Eq. (13) using the thermodynamic properties of the stilbene-bibenzyl system and assuming c = 0.15 in Eq. (22). The dimensionless quantity $g_B = f\lambda_S k_B^F/V$ is sufficient to determine β as a function of the interface composition and temperature. As g_B increases the equilibrium separation factor is approached. Figure 7 compares the separation factors computed from the observed compositions with values found from Fig. 6. Some of the data points are based on c = 1.0; others, on c = 0.15. The difference is small because only the ratio of the two forward coefficients, k_A^F/k_B^F, is affected in the rate theory. The agreement is satisfactory.

Determination of the Surface Step Density and the Rate Coefficient: Using the observed solid and interfacial liquid compositions and temperature and the crystal growth velocity it is possible to compute values of the product fk_B^F from Eq. (11). The determination of the separate values of f and k_B^F is not possible; one has to be found from the theory in order to determine the other from the data.

There are two ways in which the surface fraction, f, can be determined from the experimentally observed interface temperature, and the interface liquid and solid compositions. First, the values of V, T, y_B, and

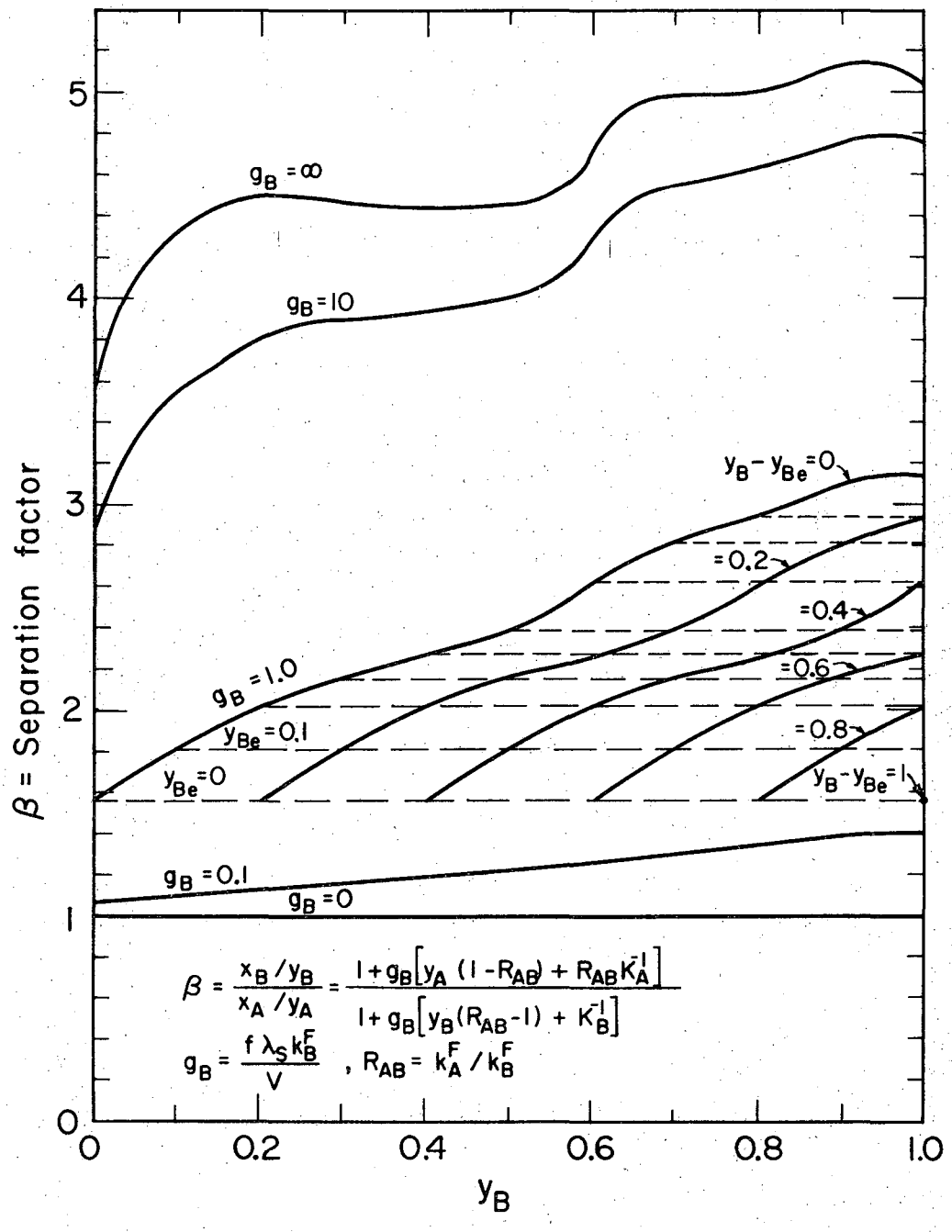

Fig. 6. Separation factor, bibenzyl and trans-stilbene system.

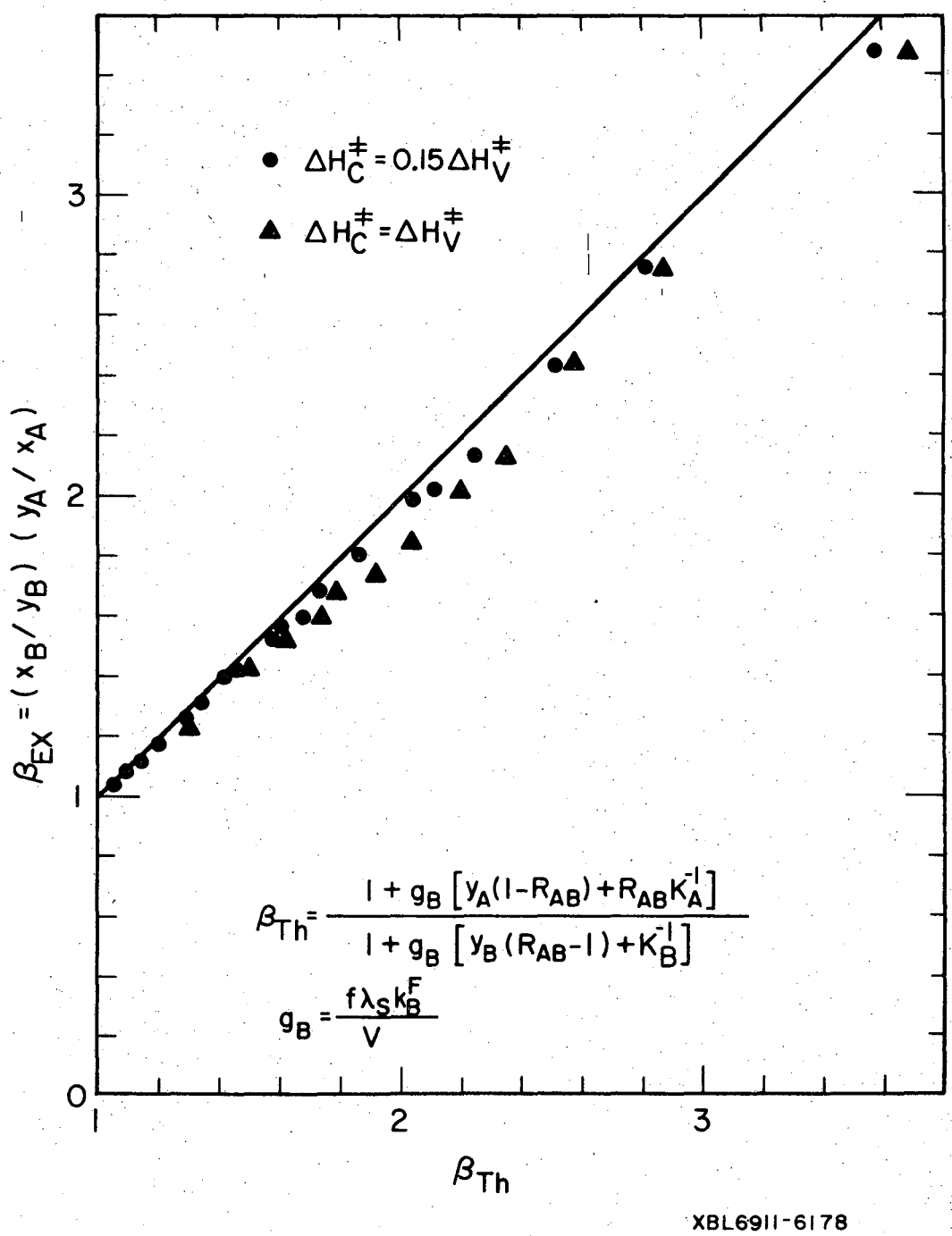

Fig. 7. Comparison of separation factors, bibenzyl and trans-stilbene system.

x_B can be substituted in Eq. (11) to obtain values of the group $f\lambda_S k_B^F$. Then with estimates of λ_S and of k_B^F and k_A^F (the latter from the Eyring theory, Eq. (21), and $\Delta S_C^{\ddagger}$ and $\Delta H_C^{\ddagger}$ from Eq. (27) and (22) with $c = 0.15$) f follows directly, provided χ is known. Assuming $\chi = 1$ yields $f \approx 10^{-5}$, which is about two orders of magnitude greater than the value obtained from the data for pure stilbene. Thus, in order to reconcile the data for the pure crystal with those for the solution one may assume $\chi \approx 10^{-2}$.

Alternatively, f can be computed from Eq. (17) using values of ΔG found from the compositions and temperatures using Eq. (20) and, in the absence of any data, assuming ideal solution behavior in both the solid and the liquid phases. According to such calculations, ΔG was negative for all but two of the experimental runs--a situation which is manifestly impossible since it implies that the spontaneous process of phase growth occurs with an increase in the Gibbs free energy of the material forming the crystal surface.

It seems very possible that in a system which exhibits peritectic phase behavior over some part of the composition range there will be deviations from ideal solution behavior throughout the phase diagram and that the values of chemical potential estimated by assuming that γ and Γ are both unity will be erroneous. No data are available to test this belief but, in order to determine how sensitive the computations might be to small deviations in ideality the regular-solution equation for activity coefficients was introduced:

$$\ln \gamma_B = (\omega^L/RT)\, y_A^2 \quad \text{(liquid phase)}$$

$$\ln \Gamma_B = (\omega^S/RT)\, x_A^2 \quad \text{(solid phase)}$$

The result of adding the non-ideal terms to Eq. (20) is to increase the value of $\Delta G/RT$ by the quantity

$$(\omega^S/RT)(x_{Be} - x_B)^2 - 2(\omega^L/RT)(y_B - y_{Be})\left(x_B - \frac{y_B + y_{Be}}{2}\right) .$$

The first term, reflecting the influence of non-ideal behavior in the solid phase, has a positive coefficient; the coefficient of the second term is negative. In a typical experiment, Run No. III-93 of Table III, the expression above is $-0.0007(\omega^L/RT) + 0.095(\omega^S/RT)$ and the uncorrected ideal value of $\Delta G/RT$ based on the observed liquid and solid compositions and the temperature was -0.359. The coefficient of (ω^L/RT) is small because the interface liquid composition was rather close to the equilibrium value; the coefficient of (ω^S/T) is larger because x_B was considerably less than x_{Be}. Since ω^L is likely to be smaller than ω^S it seems likely that the term representing the lack of ideality in the liquid can be neglected completely and that we can conclude that (ω^S/RT) must have been at least $0.359/0.095 = 3.78$ or $\omega^S = 2.5$ kcal/mole in order to force the change in Gibbs free energy negative for the transition from liquid to solid.

In the absence of reliable thermodynamic information for the solid solution we can only conclude that the experimentally observed compositions probably do not violate the Second Law. When the information is available it will be possible to recalculate the values of ΔG and to estimate the

surface fraction f from the assumption of growth by a screw dislocation mechanism. In the mean time we have no reason to doubt the validity of Eq. (11) for the solid composition or of Eq. (17) for the surface fraction.

Table III shows values of the solid composition, x_B, computed from the theory using $\chi = 0.01$ and taking the activation quantities from viscosity with modifications according to Eq. (21) and (22) with $c = 0.15$. The values are by no means in perfect agreement with those observed but the departure from equilibrium is of the right magnitude and the variation with the growth velocity is about right. When no experimental information whatever is available this procedure is suggested.

CONCLUSIONS

Use of the temperature-gradient microscope stage with provisions for determination of interface conditions by optical interference is a promising method for investigating the interfacial kinetic phenomena. For the binary system used here and probably for most other high-melting organic compounds which form solid solutions the interfacial rate of phase growth is the controlling factor in the determination of the solid composition; the diffusion process in the interfacial liquid is of minor importance.

A theory based on Eyring's theory for the first-order process of solid deposition and on a screw-dislocation mechanism for surface attachment accounts approximately for the observed phenomena, including the large departure of the solid composition from its equilibrium value according to the phase diagram. In the absence of any experimental rate data, estimates of the interfacial rate coefficients can be based on activation enthalpy and viscosity from viscosity data suitably adjusted to account for differences in the molecular phenomena accompanying crystal growth and viscous flow.

NOTATION

C_p = molar heat capacity, cal/g mole °C

D = diffusion coefficient, or interface transport coefficient, sq cm/sec

f = surface step density, dimensionless

g_B = dimensionless growth rate parameter, $\lambda_S f k_B^F / V$

G = molar gree energy, cal/g mole

h = Planck's constant

H = molar enthalpy, cal/g mole

k = interfacial rate constant, sec^{-1}, or Boltzmann's constant, erg/°K

K = equilibrium or effective distribution coefficient, a function of composition

M = molecular weight

n = refractive index of liquid

N = crystallization flux, g mole/sq cm sec, or Avogadro's number, or integer in Eq. (38)

r_c = critical radius of two-dimensional nucleus, cm

R = gas constant, cal/g mole °K, or ratio of interfacial rate constants for species A and B

s = interference fringe spacing, mm

S = molar entropy, cal/g mole °K

t = thickness of optical wedge at observation point, mm

T = temperature, °C or °K

u = average molecular velocity, cm/sec

v = specific volume, cc/g

V = freezing velocity, cm/sec, or molar volume, cc/g mole

x = mole fraction in solid phase

y = mole fraction in liquid phase

GREEK LETTERS

α = angle, degree

β = separation factor, or angle, degree

Γ = solid phase activity coefficient

γ = liquid phase activity coefficient

η = viscosity, poise

λ = interatomic spacing, cm

λ_0 = wavelength, 6328 Å, for He-Ne gas laser

μ = chemical potential, cal/g mole

ρ = molar density, g mole/cc

σ = interfacial surface free energy, cal/sq cm

χ = transmission coefficient

ω = excess free energy, cal/g mole

SUPERSCRIPTS

F = forward process

L = liquid state property

0 = standard state property

R = reverse process

S = solid state property

‡ = activated state property

* = equilibrium condition

SUBSCRIPTS

A = component A, minor component, bibenzyl

B = component B, major component, stilbene

C = crystallization activated state property

e = equilibrium condition

ex = experimental condition

f = fusion process

i = interfacial condition

L = liquid state property

m = melting process

0 = initial condition

S = solid state property

T = constant temperature condition

V = viscous flow activated state property

CHAPTER V

APPENDICES

I. Description of Experimental Equipment.

II. Physical Properties of Compounds.

III. Development of Equation for Calculating Interfacial Concentration Gradient Normal to the Growing Crystal Face.

IV. Estimate of Errors of Temperature Measurement with Thermocouple.

V. Liquid and Solid Phase Compositions by Normal Freezing of Binary Mixtures between Glass Slides.

VI. Experimental Results.

I. DESCRIPTION OF EXPERIMENTAL EQUIPMENT

An overall-view of the equipment used for the experiment is shown in the photograph of Fig. 1. The major items consist of:

1. Leitz Research Microscope Ortholux and Leitz Arisophot stand for photomicrography consisting of large base plate, vertical camera carrier on twin columns with adjustable prismatic bar, Leitz focusing attachment with horizontal telescope, Leitz holder for Bolex H-16 reflex movie camera, and polaroid camera back model CB 100.

2. Temperature gradient microscope stage. The detail description of this stage is given in Chapter II.

3. Quantum Physics Model LS-30 He-Ne gas laser with integral power supply unit provides a standard wavelength of 6328 Å coherent, monochromatic light.

4. Leeds and Northrup K-2 Potentiometer.

5. Batt-Sub constant voltage supply for K-2 potentiometer with output 3.0 VDC at 24.4 m.a. by Dynage, Inc. Hartford, Conn.

6. D.C. Power Supply for the adjustment of D.C. clock motor.

A fine thermocouple of copper-constantan having a wire diameter of 0.004 in. is used for the temperature measurement. The thermocouple calibration was performed against two standard reference points: one was for the transition point of amorphous sodium sulfate to its hydrate crystal at 32.384° C; the other was for the boiling point of water corrected with the atmospheric pressure, using a Cottrell apparatus. A Buchi apparatus purchased from Rinco Instrument Co., Inc., Greenville, Illinois was used for all the melting point determination.

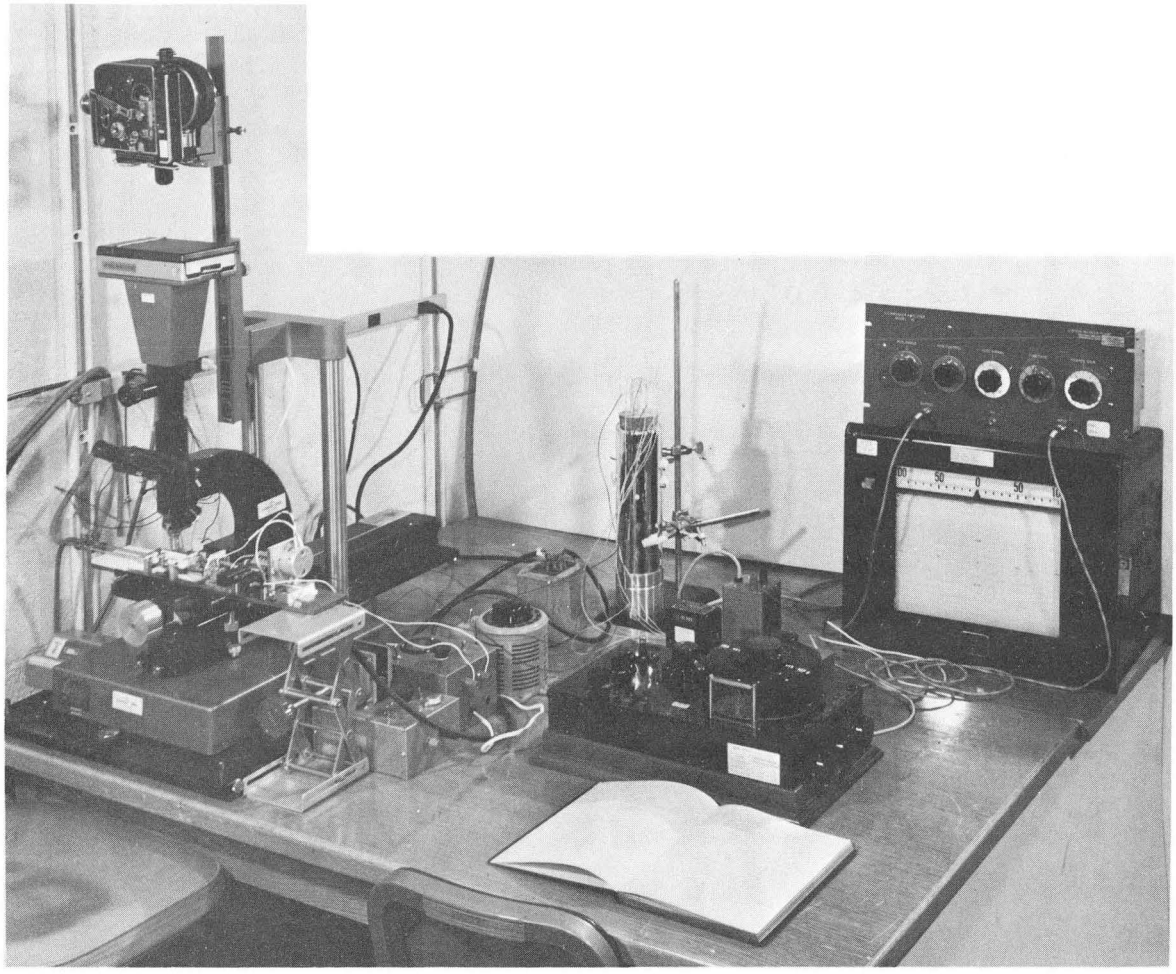

XBB 693-1783

Fig. 1. Overall-view of experimental apparatus.

A Fisher Zone Refiner was used to purify the following chemicals, which were received as "reagent grade": trans-stilbene, m-terphenyl, thymol. Slight purification was noticed for stilbene and m-terphenyl by measuring the melting points of the samples before and after the zone refining for at least 30 passes. As much as one deg C difference was observed for thymol but very little effect on salol was noticed by zone refining. This type of zone refiner did not appear to be very effective.

II. PHYSICAL PROPERTIES OF COMPOUNDS

A. Bibenzyl-Stilbene System

1. Phase Diagram. The phase diagram for this system is given by Kolosov (1958) as shown in Fig. 3 of Chapter IV. Owing to the peritectic nature of the system shown in the phase diagram, the mixed crystals grown at temperature above and compositions to the right of peritectic range have crystal structures like those of pure stilbene.

2. Refractive Index. The refractive index of the mixture at various concentration is required to evaluate $(\partial y/\partial n)_T$ for determination of the interfacial concentration gradient, as shown in Eq. (4) of Chapter II and Eq. (25) of Chapter IV.

a. Methods of Measurement. Two methods were used to determine the refractive index as a function of composition:

(1) The "Becke-Line" procedure: this method employs glass powders of known refractive index as standard. By raising or lowering the microscope focus on the organic solution containing one of these standard glass powders on the microscope hot stage, one notices that the bright halo moves toward the medium of higher refractive index, and toward the medium of lower

refractive index, respectively. The temperature of the melt is adjusted until there is no shift in the halo upon raising or lowering the focus. The refractive index of the liquid matches then the value for the standard glass powder at that temperature. A set of 24 standard glass powders having refractive indices in steps ranging from n_D = 1.3400 to 1.6877 was available from Arthur H. Thomas Co.

The light source used for the determination of the refractive index of organic mixture was laser light of 6328 Å wavelength while the sodium-D line was 5890 Å for D_2 and 5896 Å for D_1. Owing to the dispersion effect of the substance at different wavelengths the use of He-Ne gas laser light instead of the Na-D line will give wrong measurement using the standard glass powder, for which the refractive index value is given in Na-D line. It has been found that the refractive index of solids increase about 0.001 for every 10 ∿ 20 mμ decrease in wavelength; liquids exhibit about twice as much change. The measurements using laser light, therefore, yield lower values than the refractive indices of the mixtures based on Na light.

(2) Direct Measurement using Bausch and Lomb Precision Refractometer: measurements were made also directly in a modified Abbe-type refractometer by using both Na-D light and light from the He-Ne gas laser.

Results of measurements made by above two methods are listed in Table V.

3. Viscosity and Diffusivity. The viscosities of pure stilbene and bibenzyl were measured by Kirwan (1967). The Wilke-Chang correlation (1955) and the viscosity measured by Kirwan were used for the prediction of the diffusivities at infinite dilution of bibenzyl in stilbene and

Table V. Refractive Index Measurements

T,°C	50		60		70		80		85		90	
Melts	Na-D	Laser	Na-d	Laser	Na-D	Laser	Na-D	Laser	Na-D	Laser	Na-d	Laser
Pure T[b]	1.5090	1.5061	1.5049	1.5018	1.5007	1.4075						
Pure T[a]		1.5072		1.5031		1.4988						
10 m% S[b]	1.5172	1.5139	1.5128	1.5096	1.5086	1.5055						
10 m% S[a]		1.5152		1.5108		1.5065						
30 m% S[b]	1.5322	1.5286	1.5278	1.5243	1.5237	1.5204						
30 m% S[a]		1.5290		1.5247		1.5204						
90 m% S[b]	1.5709	1.5661	1.5666	1.5619	1.5627	1.5576						
90 m% S[a]		1.5687		1.5640		1.5593						
Pure S[b]	1.5765	1.5717	1.5723	1.5674	1.5684	1.5639						
Pure S[a]		1.5745		1.5700		1.5653						
Pure B[b]	1.5529	1.5490			1.5434	1.5398	1.5395	1.5359				
15 m% St.[b]					1.5584	1.5542	1.5541	1.5502	1.5516	1.5474		
25 m% St.[b]							1.5629	1.5584	1.5611	1.5565	1.5585	1.5542

T = thymol, S = Salol, B = bibenzyl, St. = stilbene, m% = mole %.

[a]Determined by the "Becke-Line" procedure, using standard glass powder of known refractive index.

[b]Determined with Bausch and Lomb Precision Refractometer.

stilbene in bibenzyl solutions. The results of such prediction with the measured viscosity by Kirwan were reproduced in Fig. 2. The correlation suggested by Vignes (1966) was applied to compute diffusivities of the mixtures:

$$D_{BS} = (D^{\circ}_{BS})^{y_S} (D^{\circ}_{SB})^{y_B} .$$

B. Salol-Thymol System

1. Phase Diagram. The phase diagram for this system is plotted from the data given by Timmermans (1959) as shown in Fig. 8 of Chapter II. The crystal structures of both species are given by Flachsbart (1957).

2. Refractive Index. The refractive index of binary mixtures as well as that of pure melts were measured by "Becke-Line" procedure and with a modified Abbe-type refractometer. The results of such measurements are listed in Table V.

3. Viscosity and Density. Kirwan (1967) had made several measurements of the viscosities of pure salol and thymol. It is believed that the literature values by Jantsch (1956) for salol and by Slavyanski (1948) for salol, and thymol, and its binary mixtures are more reliable. Therefore, the literature values were used for the necessary calculations. Density data were taken from Timmermans (1950). Values appropriate for the range of temperatures used in this study are listed in Table VII.

4. Diffusivity. The diffusivity of binary mixtures was measured by Kirwan (1967) and given as an average value of $(0.74\pm0.12)\times10^{-6}$ sq cm/sec at 29.5° C. Since this reported value is comparable to what is predicted

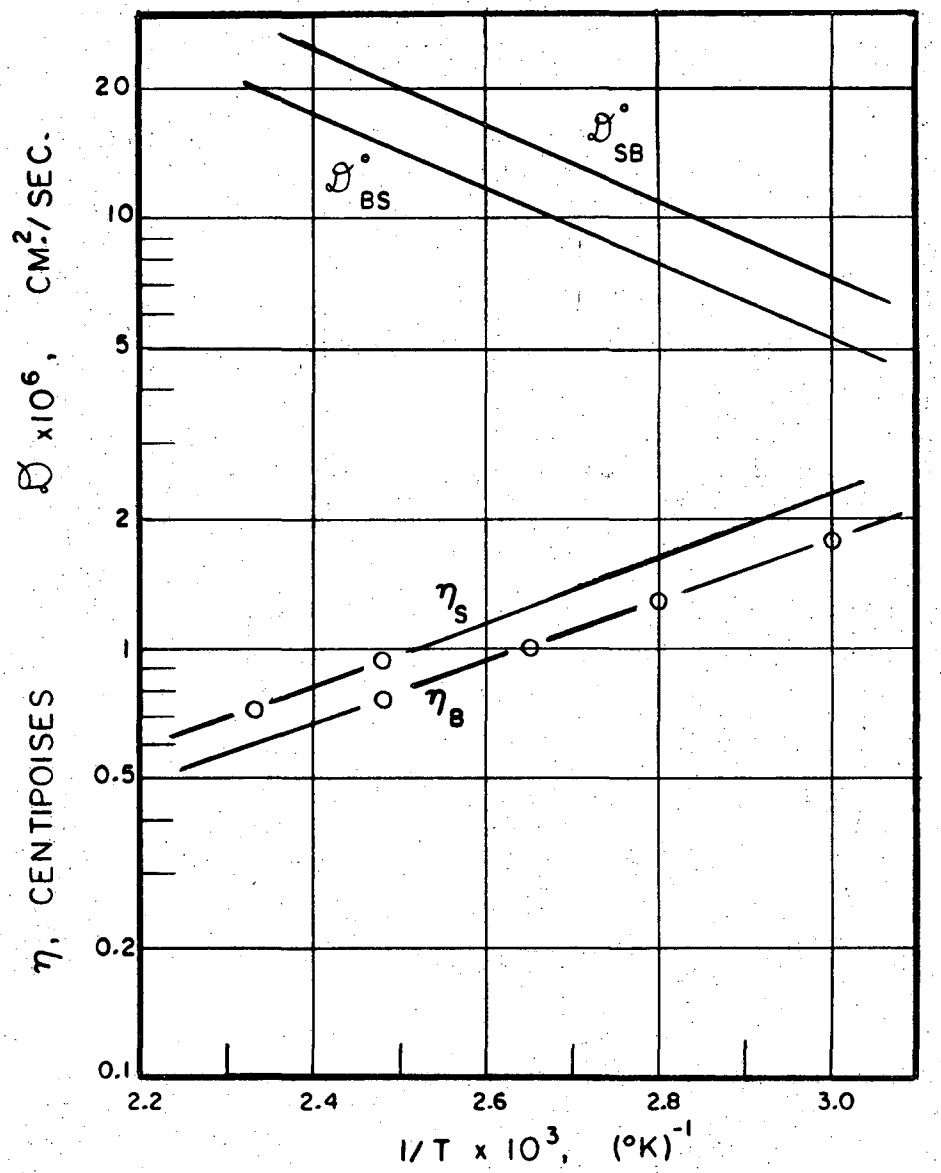

VISCOSITY AND DIFFUSIVITY OF THE BS SYSTEM

XBL 6911-6506

Fig. 2

by Wilke-Chang correlation and by the method of prediction proposed by Gainer and Metzner (1965), this value was used to compute the interfacial solid composition using the interfacial flux balance shown in Eq. (3) of Chapter II. The relationship (D/T) = constant was used to correct D_{ST} for other temperatures.

Table VI. Diffusivities in the Salol-Thymol System

Method	T °C	D_{ST} (sq cm/sec)×10^6	D_{TS}
Wilke-Chang	27	1.25	0.77
Gainer-Metzner	27	0.80	0.67

C. Polyphenyls

1. O-Terphenyl (1, 2-Diphenylbenzene. Rates of crystal growth and melt viscosity reported by Greet (1967) are listed in Table VIII. Listed are also values of computed thermodynamic properties for activated state.

Table VII. Viscosities and Densities of Pure Salol and Thymol

T	η_S [a]	η_S [b]	η_T [b]	d_S [c]	d_T [c]
°C	poise	poise	poise	g/cc	g/cc
9.6	--	--	--	--	0.9816
25.0	--	0.216	0.200	--	--
28.4	0.171	--	--	--	--
29.2	0.168	--	--	--	--
30.0		0.155	0.150	--	--
32.8	0.137	--	--	--	--
35.0	--	0.107	0.110	--	--
37.5	0.109	--	--	--	--
40.0	--	0.095	0.096	--	--
41.7	0.091	--	--	--	--
45.0	--	0.076	0.072	1.17858	--
45.10	0.079	--	--	--	--
50.0	--	--	0.058	--	--
51.4	--	--	--	--	0.9484
54.9	--	--	--	--	0.9461
55.0	--	--	0.049	1.16981	--

[a] Viscosity of salol melt by Jantsch (1956).

[b] Viscosities of pure salol and pure thymol by Slavyansky (1948).

[c] Densities of salol and thymol given by Timmermans (1950).

Table VIII. Rates of Crystal Growth and Melt Viscosity, and Thermodynamic Properties, o-Terphenyl

T	ΔT	$\log_{10} V$	$\log_{10} \eta$	$\Delta H_V^{\ddagger} \times 10^{-4a}$	$\Delta S_V^{\ddagger} \times 10^{-2a}$	$\Delta S_C^{\ddagger} \times 10^{-2b}$	$\Delta H_C^{\ddagger} \times 10^{-4c}$	$\Delta H_C^{\ddagger} \times 10^{-4d}$	$\Delta S_C^{\ddagger} \times 10^{-2d}$
°C	°C	(cm/sec)	(poise)	cal/mole	cal/mole-°K		cal/mole		cal/m °K
53.5	2.0	-5.26	-0.40	1.16	0.16	0.008	1.15	-17.5	-5.68
52.5	3.0	-4.39	-0.37	1.24	0.18	0.054	1.14	-14.6	-4.77
51.5	4.0	-3.88	-0.34	1.32	0.20	0.088	1.18	-11.7	-3.86
49.5	6.0	-3.35	-0.29	1.47	0.25	0.142	1.30	-5.7	-2.03
47.5	8.0	-3.04	-0.22	1.63	0.30	0.192	1.44	0.3	0.03
45.5	10.0	-2.85	-0.15	1.79	0.35	0.240	1.59	1.3	0.14
43.5	12.0	-2.73	-0.06	1.95	0.40	0.287	1.75	1.4	0.18
41.5	14.0	-2.66	0.04	2.12	0.46	0.333	1.91	1.6	0.23
39.5	16.0	-2.63	0.14	2.29	0.51	0.383	2.07	1.7	0.28
37.5	18.0	-2.62	0.25	2.46	0.56	0.432	2.24	1.9	0.33
35.5	20.0	-2.64	0.36	2.63	0.62	0.481	2.41	2.0	0.38
30.5	25.0	-2.78	0.70	3.06	0.76	0.608	2.85	2.4	0.50
25.5	30.0	-3.00	1.09	3.52	0.91	0.741	3.30	2.8	0.64
20.5	35.5	-3.26	1.56	3.99	1.07	0.884	3.76	3.2	0.78
15.5	40.0	-3.57	2.09	4.47	1.24	1.036	4.23	3.7	0.93
10.5	45.0	-3.96	2.72	4.97	1.41	1.196	4.71	4.1	1.10
5.5	50.0	-4.46	3.44	5.49	1.60	1.344	5.22	4.6	1.26
0.5	55.0	-5.11	4.27	6.03	1.79	1.539	5.75	5.1	1.44
-4.5	60.0	-6.00	5.26	6.59	2.00	1.718	6.30	5.6	1.62

(continued)

Table VIII. continued

[a]Computed from Eq. (8) of Chapter III using listed values of η.

[b]Computed from Eq. (9) of Chapter III using listed values of V and η, assuming $\Delta H_C = 0.89\ \Delta H_V$ and $\chi = 1$.

[c]Computed from Eq. (13) of Chapter III using listed values of V and η, assuming $\chi = 1$.

[d]Computed from Eq. (7) of Chapter III using listed values of V, assuming $\chi = 1$.

The specific volumes for the liquid and solid phases were satisfactorily fitted by the following equations (Greet and Turnbull, 1967)

$$v^L(cc/g) = 0.911 + 6.46 \times 10^{-4} T + 6.46 \times 10^{-7} T^2$$

$$v^S(cc/g) = 0.85791 + 2.7491 \times 10^{-4} T \ ,$$

where T is in deg C.

The activation enthalpy and activation entropy for viscous flow calculated from the slopes of the smoothed log η-vs-$(1/T)$ curve fitted by a least-squares second-order polynomial, are given in Fig. 6 for o-terphenyl and in Fig. 7 for TαNB in Chapter III.

2. M-Terphenyl (1,3-Diphenylbenzene). The viscosity and liquid specific volume data were calculated from the plot by Andrew and Ubbelohde with the aid of the Batshinski relationship for m-terphenyl (Andrews and Ubbelohde, 1955)

$$\frac{1}{\eta}(poise)^{-1} = \left(\frac{v^L - w}{C}\right) \ ,$$

where $C = 12.15 \times 10^{-4}$ and $w = 0.938$. Results of such calculations were tabulated below:

Table IX. Viscosity and Liquid Specific Volume, m-Terphenyl

T °C	74.76	77.73	80.83	83.99	87.21	90.49	93.82	97.22
η, cp	7.6914	6.9657	6.2517	5.6625	5.1881	4.7534	4.3152	3.9811
v^L, cc/g	0.9538	0.9554	0.9574	0.9595	0.9614	0.9636	0.9662	0.9685

The activation enthalpy and activation entropy for viscous flow were determined from the slope of the log η -vs- (1/T) curve. The curve was fitted by a least square second-order polynomial as follows:

$$\log(\eta v^L) = A + B(1/T) + C(1/T)^2 ,$$

and the activation enthalpy was obtained as the slope;

$$\Delta H_V^{\ddagger} = 2.3\ R\ (B + 2\ C(1/T)),$$

where A = 3.9659, B = -5.3718×10^3, C = 1.2516×10^6, T = °K and R is the gas constant in cal/g mole °K. The $\Delta S_V^{\ddagger}$ is then computed from Eyring's equation for the viscosity of liquid (see Eq. (8) of Chapter III) with known $\Delta H_V^{\ddagger}$.

Table X. Rates of Crystal Growth and Some Derived Physical Properties, m-terphenyl

Run No.	$V \times 10^4$ (cm/sec)	T_i °C	T_1 °C	T_2 °C	T_e °C	$\Delta H_V^{\ddagger} \times 10^{-3}$[a] cal/mole	$\Delta S_V^{\ddagger}$[a] cal/mole °K	$\Delta S_C^{\ddagger}$[a,b] cal/mole °K
IV - 38	9.81	83.46	82.83	92.10	85.61	7.62	5.35	-5.70
IV - 39	8.00	83.30	83.38	83.23	85.61	7.55	5.14	-5.09
IV - 40	5.68	83.72	83.75	83.69	85.61	7.51	5.03	-5.08
IV - 41	4.05	83.80	84.02	83.58	85.61	7.50	5.01	-5.60
IV - 42	2.91	83.82	83.90	83.74	85.61	7.50	5.01	-6.22
IV - 45	14.20	82.53	82.93	82.12	85.61	7.62	5.33	-4.90
IV - 47	1.06	84.25	84.91	83.60	85.61	7.46	4.90	-7.24
IV - 48	21.30	82.60	82.73	82.47	85.61	7.61	5.32	-4.02

(continued)

Table X. continued

[a] Computed based on T_i.

[b] Computed from Eq. (9) of Chapter III using measured V and η from the literature, assuming $\Delta H_C^{\ddagger} = 0.76\ \Delta H_V^{\ddagger}$ and $\chi = 1$.

3. 1:3:5:-Tri-α-Naphthylbenzene (TαNB). The viscosity data and the reported rates of growth of TαNB were given by Magill and Plazek (1967, 1966). Computed values of the thermodynamic properties for activated state are also listed in the Table XI.

The liquid density was reported to be:

$$\rho = 1.1348 - 6.06 \times 10^{-4}(T - 100),\ g/cc\ ,$$

where T is in deg C.

Table XI. Rates of Crystal Growth and Melt Viscosity, and Thermodynamic Properties, TαNB

T °C	ΔT °C	$\log_{10}V$ (cm/sec)	$\log_{10}\eta$ (poise)	$\Delta H_V^{\ddagger}\times10^{-4}$[a] cal/mole	$\Delta S_V^{\ddagger}\times10^{-2}$[a] cal/mole °K	$\Delta S_C^{\ddagger}\times10^{-2}$[b]	$\Delta H_C^{\ddagger}\times10^{-4}$[c] cal/mole	$\Delta H_C^{\ddagger}\times10^{-4}$[d]	$\Delta S_C^{\ddagger}\times10^{-2}$[d] cal/mole °K
195.0	4.0	-3.209	-0.315	1.71	0.15	-0.086	1.72	-27.5	-6.27
193.5	5.5	-2.983	-0.289	1.80	0.17	-0.069	--	-23.7	-5.49
193.0	6.0	-2.139	-0.281	1.83	0.18	-0.027	1.68	-22.4	-5.19
192.5	6.5	-1.893	-0.272	1.87	0.183	-0.013	1.67	-21.2	-4.92
191.0	8.0	-1.664	-0.233	1.96	0.203	0.009	1.75	-17.4	-4.12
190.0	9.0	-1.235	-0.201	2.02	0.217	0.037	1.74	-14.9	-3.56
187.0	12.0	-0.983	-0.125	2.21	0.258	0.078	1.92	-7.2	-1.91
185.0	14.0	-0.796	-0.080	2.34	0.286	0.108	2.02	-2.0	-0.78
160.0	39.0	-0.790	0.810	4.06	0.671	0.451	3.73	3.7	0.47
140.0	59.0	-1.529	2.346	5.57	1.030	0.773	5.23	4.6	0.68
120.0	79.0	-2.682	3.720	7.25	1.445	1.153	6.85	5.6	0.93
100.0	99.0	-4.395	6.143	9.10	1.929	2.600	8.61	6.7	1.21

[a] Computed from Eq. (8) of Chapter III using listed values of η.

[b] Computed from Eq. (9) of Chapter III using listed values of V and η, assuming $\Delta H_C^{\ddagger} = 0.89 \cdot \Delta H_V^{\ddagger}$ and $\chi = 1$.

[c] Computed from Eq. (13) of Chapter III using listed values of V and η assuming $\chi = 1$.

[d] Computed from Eq. (7) of Chapter III using listed values of V, assuming $\chi = 1$.

III. DEVELOPMENT OF EQUATION FOR CALCULATING INTERFACIAL CONCENTRATION GRADIENT NORMAL TO THE GROWING CRYSTAL FACE.

Referring to Fig. 4 of Chapter II, v-w represent the coordinates for interference fringe, X-Y for optical wedge in which the measured growth rate is -X direction. The actual growth rate normal to the crystal face is in z direction. If the measured growth rate in -X direction is V_X, then the actual crystal growth normal to the crystal face in z direction is $V_X \cos \gamma$.

Note that α is the angle between a fringe and the edge of photograph, which is assumed parallel to edge of optical slide; and β is the angle between the crystal face and the v axis. Along any single fringe there is a relationship between refractive index of the medium and wedge thickness as follows:

$$n\,t = (N/2)\lambda_0 = \text{constant} , \tag{1}$$

or after differentiation,

$$d\,n = -\frac{n}{t}\,d\,t . \tag{2}$$

Now assume that the thickness of the wedge is a linear function of X and Y as if the top and bottom surfaces were flat:

$$t = aY + bX, \text{ or } d\,t = a\,dY + b\,dX , \tag{3}$$

where a is a negative quantity. Assume also that the refractive index is a function of composition and temperature,

$$d\,n = \frac{\partial n}{\partial T})_y\,dT + \frac{\partial n}{\partial y})_T\,dy . \tag{4}$$

Thus, noticing that $T = T(X)$, the equation of a fringe line is,

$$\frac{\partial n}{\partial T})_y \, dT + \frac{\partial n}{\partial y})_T \, dy = - \frac{n}{t} (a \, dY + b \, dX) \, . \tag{5}$$

Rotation of axes from (X,Y) to (v,w) produces the transformation of coordinates,

$$dY = dv \sin \alpha + dw \cos \alpha \tag{6a}$$

$$dX = dv \cos \alpha - dw \sin \alpha \, , \tag{6b}$$

and these can be introduced into Eq. (5) with the relationship $dT = (dT/dX)dX$. First, however, note that v-axis is parallel to the fringe in the region far from the interface, where there is no concentration gradient, $dy = 0$ and $dw = 0$, then

$$dn = \frac{\partial n}{\partial T})_y \, dT = \frac{\partial n}{\partial T})_y \, (\frac{dT}{dX}) \, dX \, , \tag{7}$$

and from Eq. (5), after eliminating dT, dY and dX,

$$\frac{\partial n}{\partial T})_y (\frac{dT}{dX}) \, dv \cos \alpha = - \frac{n}{t} (a \sin \alpha + b \cos \alpha) \, dv \tag{8}$$

or

$$\frac{\partial n}{\partial T})_y (\frac{dT}{dX}) = - \frac{n}{t} (a \tan \alpha + b) \, . \tag{9}$$

Now at the vicinity of interface Eq. (5) holds, that is, after eliminating dT, dX and dY,

$$\frac{\partial n}{\partial T})_y (\frac{dT}{dX}) \ (dv \cos \alpha - dw \sin \alpha) + \frac{\partial n}{\partial y})_T \ dy =$$

$$- \frac{n}{t} \ [a(dv \sin \alpha + dw \cos \alpha) + b(dv \cos \alpha - dw \sin \alpha)] \ , \qquad (5a)$$

Substituting Eq. (9) into (5a) one then obtains

$$\frac{\partial n}{\partial y})_T \ dy = \frac{n}{t} \ [(a \tan \alpha + b)(dv \cos \alpha - dw \sin \alpha) - (a \sin \alpha + b \cos \alpha)dv$$

$$- (a \cos \alpha - b \sin \alpha)dw]$$

$$= - \frac{n}{t} \ \frac{adw}{\cos \alpha} \ . \qquad (10)$$

Here we need the normal derivative of concentration $(dy/dz)_{z=0}$. Since

$$dz = dv \sin \beta + dw \cos \beta \ , \qquad (11)$$

by dividing Eq. (10) by Eq. (11) we get

$$\frac{dy}{dz})_{z=0} = - \frac{anw_0'}{t \cos \alpha \ (\sin \beta + w_0' \cos \beta)(\partial n/\partial y)_T} \ , \qquad (12)$$

where $w_0' = (dw/dv)_{v=0}$.

If $\alpha = 0$, and $\beta = \pi/2$, which make the far fringes parallel to the side of the wedge (X-axis) and the crystal growing exactly across the direction of movement, then

$$\frac{dy}{dz})_{z=0} = -(\frac{n}{t})\ a\ w_0'\ (\frac{\partial y}{\partial n})_T \ . \tag{12a}$$

If the thickness t is a function of Y only then the fringe spacing s can be obtained from Eq. (1) by noticing

$$a = \frac{dt}{dY} \tag{13}$$

$$nt_N = \frac{N}{2}\lambda_0 \qquad \text{and} \qquad nt_{N+1} = \frac{N+1}{2}\lambda_0 \ . \tag{13a}$$

Thus

$$a = -(\frac{t_{N+1} - t_N}{s}) = -\frac{\lambda_0}{2ns} \ . \tag{14}$$

Substituting Eq. (14) into Eq. (12) for a one gets,

$$\frac{dy}{dz})_{z=0} = \frac{\lambda_0 w_0'}{2st\ \cos\alpha\ (\sin\beta + w_0'\cos\beta)(\partial n/\partial y)_T} \ . \tag{15}$$

Eq. (15) is used to calculate the concentration gradient normal to the crystal face at interface from the measured interfacial fringe gradient, w_0', and s, t, α, β, and $(\partial n/\partial y)_T$.

IV. ESTIMATE OF ERRORS OF TEMPERATURE MEASUREMENT WITH THERMOCOUPLE

Suppose that the final result y is related to the component x_i by the relation

$$y = F(x_1, x_2, \ldots\ldots x_n) \ , \tag{16}$$

where F is a known functional form. The small variations dx_i in x_i will alter y by the amount

$$dy = \sum_{i=1}^{n} \left(\frac{\partial F}{\partial x_i}\right) dx_i \ . \tag{17}$$

The square of the error will be

$$(dy)^2 = \sum_{i,j} \left(\frac{\partial F}{\partial x_i}\right)\left(\frac{\partial F}{\partial x_j}\right) dx_i dx_j \ . \tag{18}$$

If the components dx_i, $dx_2, \ldots . dx_n$, are independently distributed and symmetrical with respect to positive and negative values, then $dx_i dx_j$ $(i \neq j)$ will vanish, on the average, so that

$$\overline{(dy)^2} = \sum \left(\frac{\partial F}{\partial x_i}\right)^2 \overline{(dx_i)^2} \ . \tag{19}$$

Therefore

$$\sigma^2 = \sum \left(\frac{\partial F}{\partial x_i}\right)^2 \sigma_i^2 \ , \tag{20}$$

where

σ^2 is variance of y, and

σ_i^2 is variance of i^{th} component of x.

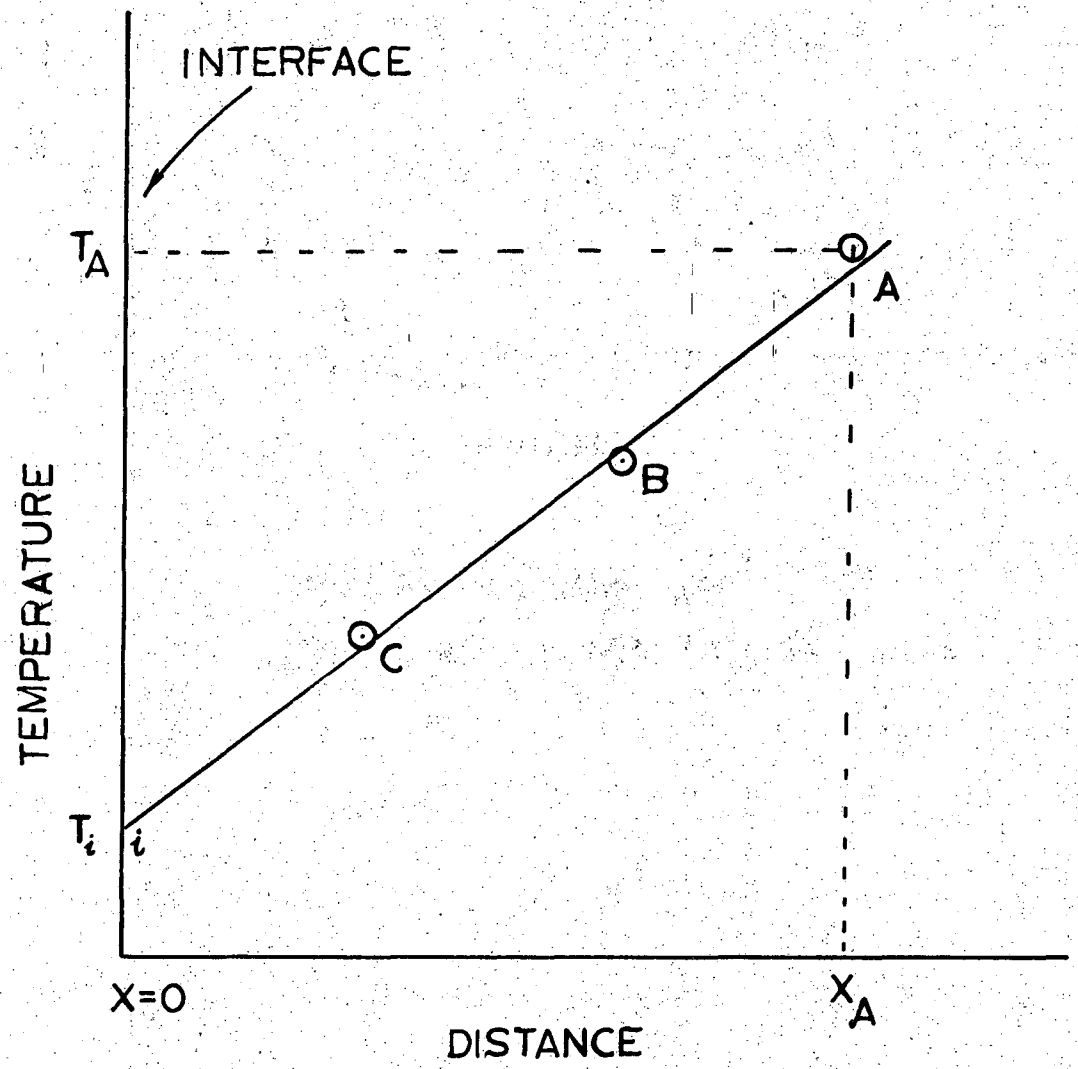

DETERMINATION OF
INTERFACE TEMPERATURE

XBL 6911-6501

Fig. 3

Refer to Fig. 3 where A, B, and C are locations where temperatures are measured. By a linear least-square fit the interfacial temperature T_i is obtained by extrapolation. Errors in T_i is expected due to the error in the slope of the fitted line.

Assume line $\overline{Ai}$ is fitted so that the sum of the square of deviation is minimum. The equation has a form $T = a\,x + b$. The sum of the squares of the deviation is

$$\sum_{i=1}^{n} (T_i - T)^2 = \sum_{i=1}^{n} (T_i - ax_i - b)^2 = \text{minimum} . \tag{21}$$

Assume also that the error is solely due to the temperature measurement (or no error in the measurement of distance x). Differentiate Eq. (21) with respect to a and b,

$$\frac{\partial}{\partial a} \sum (T_i - ax_i - b)^2 = -2 \sum (T_i - ax_i - b)\, x_i = 0$$

$$\frac{\partial}{\partial b} \sum (T_i - ax_i - b)^2 = -2 \sum (T_i - ax_i - b) = 0 ,$$

or

$$a \left(\sum x_i^2\right) + b \left(\sum x_i\right) = \sum T_i x_i \tag{22}$$

$$a \left(\sum x_i\right) + nb = \sum T_i . \tag{23}$$

Solving for a and b,

$$a = \frac{n \sum T_i x_i - \left(\sum x_i\right)\left(\sum T_i\right)}{n\left(\sum x_i^2\right) - \left(\sum x_i\right)^2} \tag{24}$$

$$b = \frac{(\sum T_i)(\sum x_i^2) - (\sum x_i)(\sum T_i x_i)}{n(\sum x_i^2) - (\sum x_i)^2} \quad . \tag{25}$$

The errors in a and b are assumed primarily due to the errors in temperature measurement T_i, so

$$\frac{\partial a}{\partial T_i} = \frac{n\, x_i - \sum x_i}{n(\sum x_i^2) - (\sum x_i)^2} \tag{26}$$

$$\frac{\partial b}{\partial T_i} = \frac{(\sum x_i^2) - x_i(\sum x_i)}{n(\sum x_i^2) - (\sum x_i)^2} \quad . \tag{27}$$

Similar to Eq. (20) one obtains the variance of a and b

$$\sigma_a^2 = \sum (\frac{\partial a}{\partial T_i})^2 \sigma_{T_i}^2 \tag{28}$$

$$\sigma_b^2 = \sum (\frac{\partial b}{\partial T_i})^2 \sigma_{T_i}^2 \quad . \tag{29}$$

Further assume that the σ_{T_i} is the same for component x_i and equal to the deviation between the standard EMF value of thermocouple and the value actually measured at the average of some calibrated points, σ_T, then

$$\sigma_a^2 = \sigma_T^2 \sum (\frac{\partial a}{\partial T_i})^2 = \sigma_T^2 \sum (\frac{n\, x_i - \sum x_i}{n(\sum x_i^2) - (\sum x_i)^2}) \tag{30}$$

$$\sigma_b^2 = \sigma_T^2 \sum (\frac{\partial b}{\partial T_i})^2 = \sigma_T^2 \sum (\frac{(\sum x_i^2) - x_i(\sum x_i)}{n(\sum x_i^2) - (\sum x_i)^2}) \quad . \tag{31}$$

If one places x_i at the origin ($x_i = 0$), then the measured interfacial temperature is

$$T_i = b \pm 2\sigma_b \quad . \tag{32}$$

V. LIQUID AND SOLID PHASE COMPOSITIONS BY NORMAL FREEZING OF BINARY MIXTURES BETWEEN GLASS SLIDES.

A. Unsteady State Solution

Mathematical formulations consider fluxes of the component in and out of a differential element Δz in the melt as shown in Fig. 4. Diffusive fluxes $-DA\rho_L(\partial y/\partial z)$ and convective fluxes $VA\rho_S x$ enter at one side of the element and leave at the other. The rate of accumulation of the component within the element $A\rho_L(\partial y/\partial t)\Delta z$ is the difference between fluxes in and out of the element.

$$DA\rho_L[(\frac{\partial y}{\partial z})_{z+\Delta z} - (\frac{\partial y}{\partial z})_z] + VA\rho_S(y_{z+\Delta z} - y_z) = A\rho_L(\frac{\partial y}{\partial t})\Delta z \quad . \tag{33}$$

Dividing by $A\rho_L\Delta z$ and letting $\Delta z \to 0$ as the limit, the following differential equation is the result by choosing the coordinates with respect to the freezing interface as stationary.

$$\frac{\partial y}{\partial t} = D\frac{\partial^2 y}{\partial z^2} + V(\frac{\rho_S}{\rho_L})\frac{\partial y}{\partial z} \quad , \tag{34}$$

with the following boundary conditions to be satisfied.

B.C. 1. $y(\infty,t) = y_0$ (initial liquid composition) (35)

2. $y(z,0) = y_0$ (36)

3. $D\left(\frac{\partial y}{\partial z}\right)_{z=0} = V\left(\frac{\rho_S}{\rho_L}\right)\left[x(0) - y(0)\right]$. (37)

B.C. 3 is the result of the interfacial flux balance shown in Fig. 5.

Let $\phi = \frac{y}{y_0}$, $\tau = \frac{t}{4D}\left(V\frac{\rho_S}{\rho_L}\right)^2$ and $\eta = \left(\frac{zV}{D}\right)\left(\frac{\rho_S}{\rho_L}\right)$, and

introduce these groups into Eq. (34) and all the boundary conditions.

$$\frac{\partial\phi}{\partial\tau} = \frac{\partial^2\phi}{\partial\eta^2} + \frac{\partial\phi}{\partial\eta} , \tag{38}$$

with the boundary conditions,

$\eta = \infty$, $\tau > 0$, $\phi = 1$ (35a)

$\tau = 0$, $\eta > 0$, $\phi = 1$ (36a)

$\eta = 0$, $\left(d\phi/d\eta\right)_{\eta=0} = \phi_s - \phi$, where $\phi_s = x(0)/y_0$. (37a)

If one assumes that an equilibrium condition prevails at any time at interface ($\eta = 0$) as in most zone refining literature, Eq. (37a) becomes

$$\left(\frac{d\phi}{d\eta}\right)_{\eta=0} = \phi(k - 1), \tag{37b}$$

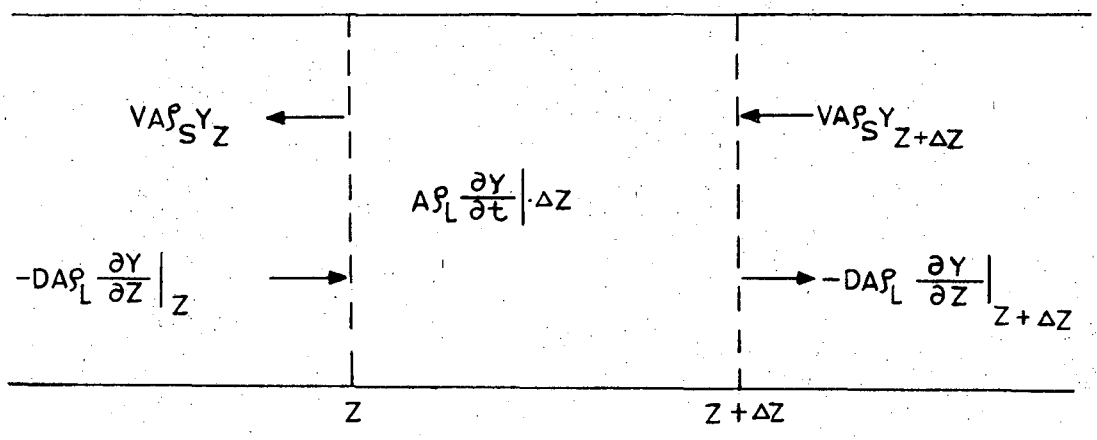

MATERIAL BALANCE IN MELT FOR PURE DIFFUSION

XBL 6911-6502

Fig. 4

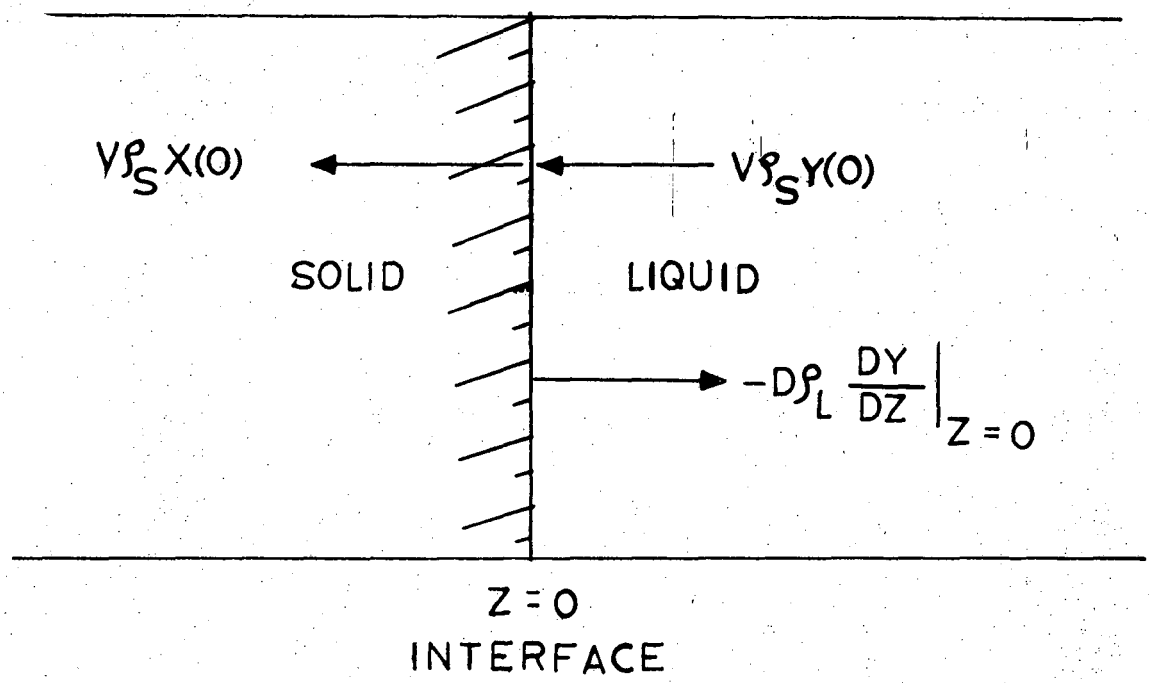

INTERFACIAL FLUX BALANCE

XBL 6911-6503

Fig. 5

where

$$k = x(0)/y(0) \ . \tag{39}$$

The analytical solution to Eq. (38) with boundary conditions of (35a), (36a) and (37b) is given for liquid as well as solid phase compositions. (Smith, Tiller and Rutter, 1955; Hulme, 1955; Memelink, 1956; and Pigford, 1969.)

$$\phi(0,\tau) = \frac{1}{2k}\left\{1 + \text{erf}(\sqrt{\tau}) + (2k-1)\ \exp\ [4k(k-1)\tau]\cdot\text{erfc}[(2k-1)\sqrt{\tau}]\right\} \tag{40}$$

$$\phi_s(0,\tau) = k\ \phi(0,\tau)$$

$$= \frac{1}{2}\left\{1 + \text{erf}(\sqrt{\tau}) + (2k-1)\ \exp\ [4k(k-1)]\ \text{erfc}[(2k-1)\sqrt{\tau}]\right\} . \tag{41}$$

Notice that ϕ or ϕ_s apply only to the minor component with k less than 1, and also that solutions such as Eqs. (40) and (41) only apply to the situation where there is no fluid mixing in the liquid phase.

For a binary mixture which yields mixed crystals the equilibrium at the interface does not hold. However one may propose an effective distribution coefficient which could depend on the liquid compostiion and interface temperature. As shown in Chapter IV, for minor component A, this effective distribution coefficient is found to be

$$K_A^* = \frac{1 + g_B[(R_{AB} + K_B^{-1} - 1) - y_A(R_{AB} - 1)]}{1 + g_B[R_{AB}K_A^{-1} + (K_B^{-1} - R_{AB}K_A^{-1})y_A]} . \tag{IV-14}$$

The experimental results indicated that y_A did not vary much at a constant initial liquid composition for freezing rates ranging from 5×10^{-5} to 2×10^{-3} cm/sec. However the experimentally determined values of K^* are much smaller than the equilibrium values and are strongly dependent on g_i. Experimentally measured and calculated values of K^* along with the equilibrium values K_i are listed in Tables XVIII, XIX, and XX.

B. Steady State Solution

For a steady state condition Eq. (34) becomes

$$\frac{\partial^2 \phi}{\partial \eta^2} + \frac{\partial \phi}{\partial \eta} = 0 \ , \tag{42}$$

with boundary conditions of Eqs. (35a) and (37a) to be satisfied.

Solution to Eq. (42) has a form of

$$\phi = A + B \exp(-\eta) \ . \tag{43}$$

By applying Eqs. (35a) and (37a) with the effective distribution coefficient K^* into Eq. (43) we get $A = 1$ and $B = (K^* - 1)/K^*$. Therefore,

$$\phi = 1 + \left(\frac{K^* - 1}{K^*}\right) \exp(-\eta) \ , \tag{44}$$

and

$$\phi_s = K^* \phi = K^* + (1-K^*) \exp(-\eta) \ . \tag{45}$$

If the steady state condition prevails the plot of log $[(1-K^*)/(\phi_s - K^*)]$ vs. V on semi-log coordinates should result in a straight line. The slope

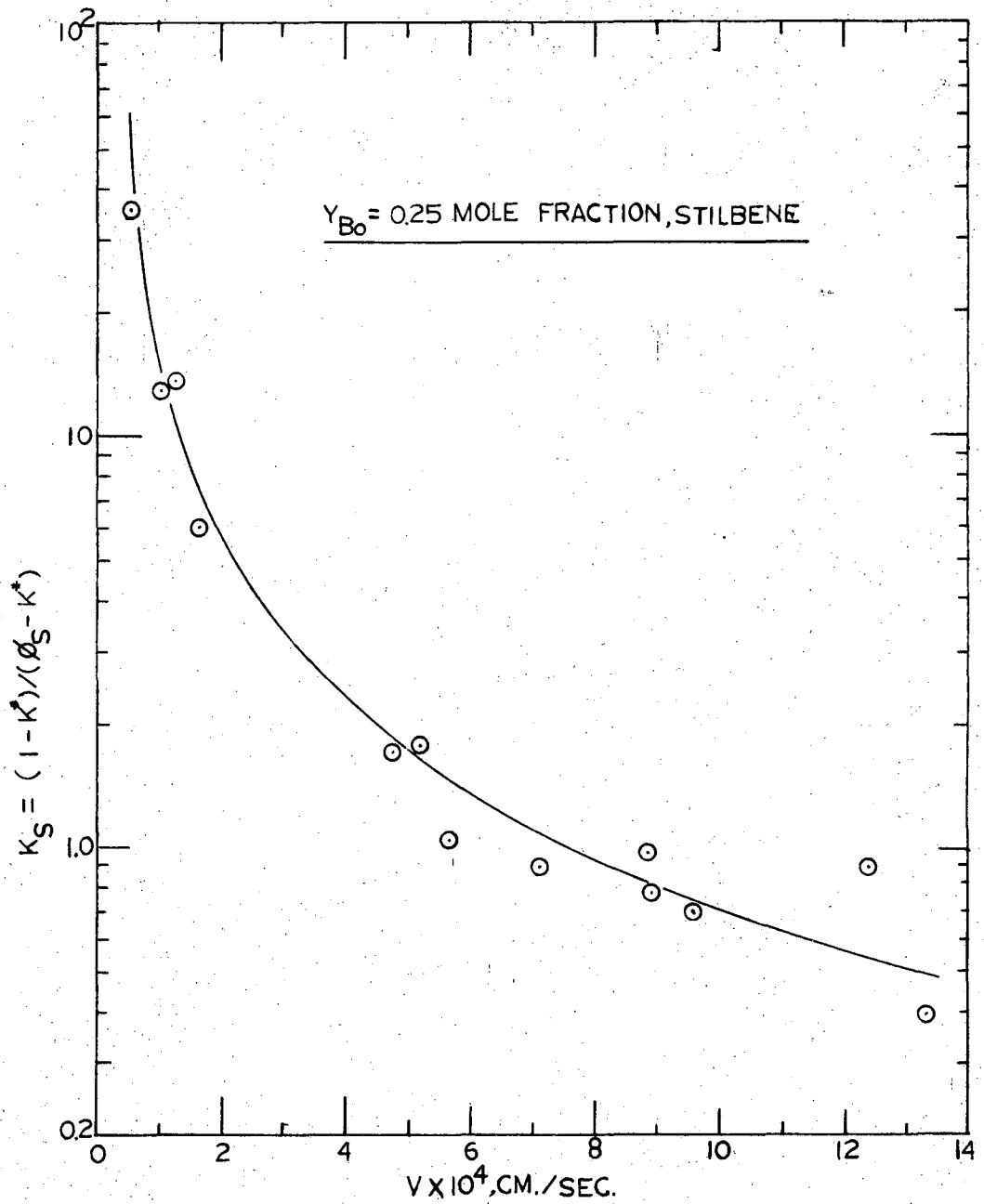

STEADY-STATE SOLUTION OF EQ.(42)

XBL 6911-6000

Fig. 6

of the line gives information about the boundary layer thickness δ, which depends on the diffusivity of the solute, the viscosity of the liquid, and the conditions of fluid flow, but only slightly on the growth rate. However, the experimental results shown in Fig. 6 for the initial liquid composition of 0.25 mole fraction stilbene indicate the steady state condition was not reached.

VI. EXPERIMENTAL RESULTS

A. Experimental Data

All the experimentally measured data and reduced data for the study of the crystal growth are listed in the following tables.

Table XII. Experimental Results, Pure Salol

Run No.	$V \times 10^4$ (cm/sec)	$(\Delta T)_2^2$ °C	T_e °C	Note
I - 72	0.97	3.84	42.14	degassed, isothermal stage
I - 72	0.83	4.99	42.14	degassed, isothermal stage
I - 73	13.00	40.87	42.14	degassed, isothermal stage
I - 73	7.58	20.25	42.14	degassed, isothermal stage
I - 74	17.30	64.00	42.14	degassed, isothermal stage
I - 75	0.79	2.97	42.14	degassed, isothermal stage

Table XIII. Experimental Results, Pure m-Terphenyl

Run No.	$V \times 10^4$ (cm/sec)	$(\Delta T)^2$	$(\Delta T_1)^2$	$(\Delta T_2)^2$	T_e °C	Note
IV - 38	9.81	9.92	7.72	12.34	85.61	zone refined, T.G.M.S.
IV - 39	8.00	5.33	4.97	5.67	85.61	zone refined, T.G.M.S.
IV - 40	5.68	3.57	3.46	3.69	85.61	zone refined, T.G.M.S.
IV - 41	4.05	3.27	2.53	4.12	85.61	zone refined, T.G.M.S.
IV - 42	2.91	3.20	2.89	3.50	85.61	zone refined, T.G.M.S.
IV - 45	14.20	9.49	7.18	12.18	85.61	zone refined, T.G.M.S.
IV - 47	1.06	1.85	0.49	4.04	85.61	zone refined, T.G.M.S.
IV - 48	21.30	9.06	8.29	9.86	85.61	zone refined, T.G.M.S.

Table XIV. Experimental Results, Pure Thymol

Run No.	$V \times 10^4$ (cm/sec)	$(\Delta T)^2$	$(\Delta T_1)^2$	$(\Delta T_2)^2$	T_e °C	Note
I - 49	4.63	58.52			49.60	zone refined, isothermal stage
I - 50	6.25	58.22			49.60	
I - 51	1.05	15.76			49.60	
I - 52	0.58	8.57			49.60	
I - 55	0.34	4.48			49.60	
I - 56	0.08	1.03			48.66	as received, isothermal stage
I - 56	4.05	72.29			48.66	
I - 56	2.20	34.00			48.66	
I - 56	1.97	30.02			48.66	

(continued)

Table XIV. continued

Run No.	$V \times 10^4$ (cm/sec)	$(\Delta T)^2$	$(\Delta T_1)^2$	$(\Delta T_2)^2$	T_e °C	Note
I - 60	2.11	32.30			49.60	zone refined, isothermal stage
I - 61	7.63	74.42			49.60	
I - 88	0.31	4.30			49.51	sublimed, isothermal stage
I - 90	2.35	30.54			49.51	
I - 92	8.54	87.33			49.51	
I - 94	3.67	56.25			49.51	
I - 95	1.70	21.48			49.51	
I - 96	10.80	175.75			49.51	
I - 97	10.80	152.80			49.51	
I - 98	12.90	142.10			49.51	
I - 99	21.40	232.83			49.51	
I -114	1.45	14.50	13.57	15.49	49.51	sublimed, T.G.M.S.
I -116	1.51	22.80	21.10	25.90	49.51	
I -119	2.33	28.73	22.66	35.52	49.51	
I -120	2.59	34.22	33.52	34.81	49.51	
I -121	1.02	22.18	13.32	33.29	49.51	
I -122	0.70	9.00	7.34	10.82	49.51	
I -123	0.69	12.67	10.20	15.50	49.51	
I -125	0.42	10.11	8.10	12.30	49.51	
I -128	4.00	52.85	51.41	54.32	49.51	
I -131	5.31	62.25	61.31	63.20	49.51	

Table XV. Experimental Results for Salol-Thymol System using T.G.M.S.

Run No.	$(V/y_i)\times10^4$	T_i	T_1	T_2	y_i	ΔT_i[a]	$(\Delta T)^2$	$(\Delta T_1)^2$	$(\Delta T_2)^2$	T_e[b]	x_i[c]
	cm/sec-mf	°C	°C	°C	mf	°C				°C	mf
$y_0 = y(\infty) = 0.90$ mole fraction, thymol											
II - 4	4.82	29.80	29.92	29.67	0.8790	1.20	89.30	87.05	91.78	40.45	0.8894
II - 5	4.88	27.60	27.81	27.40	0.8582	1.25	109.80	105.47	114.06	39.33	0.8778
II - 7	2.12	30.85	31.53	30.16	0.8623	0.60	68.06	57.30	79.92	39.70	0.9211
II - 9	1.03	33.26	34.35	32.17	0.8796	0.20	46.79	33.06	62.88	40.30	0.9165
II - 10	1.58	31.16	31.93	30.30	0.8517	0.31	54.32	43.03	67.08	38.80	0.9159
II - 11	3.50	28.44	28.57	28.31	0.8306	0.80	76.74	74.48	79.03	38.00	0.8643
II - 13	3.32	30.01	30.39	29.64	0.8407	0.80	49.56	44.35	54.91	37.85	0.8652
II - 14	6.20	29.37	29.46	29.28	0.8558	1.30	76.21	74.65	77.79	39.40	0.8714
II - 16	5.96	23.58	23.99	23.16	0.8602	1.40	216.70	204.80	229.20	39.70	0.8723
II - 17	7.68	26.35	26.66	26.03	0.8873	1.50	182.30	173.98	191.00	41.35	0.8987
II - 20	4.51	28.25	28.44	28.06	0.8687	1.10	109.30	105.30	113.20	39.80	0.8880
II - 21	2.92	29.68	29.97	29.39	0.8719	0.80	100.40	94.67	106.30	40.50	0.8944

[a] Interfacial temperature rise, measurements made on isothermal stage.

[b] Equilibrium temperature from the phase diagram based on y_i.

[c] Diffusivity, $D = 0.74 \times 10^{-6}$ cm^2/sec at 29.5° C was used and corrected with temperature for computing x_i using flux balance method.

Table XVI. Experimental Results for Salol-Thymol System using T.G.M.S.

Run No.	$(V/y_i)\times10^4$ cm/sec-mf	T_i °C	T_1 °C	T_2 °C	y_i mf	ΔT_i[a] °C	$(\Delta T)^2$	$(\Delta T_1)^2$	$(\Delta T_2)^2$	T_e[b] °C	x_i[c] mf
$y_0 = y(\infty) = 0.90$ mole fraction, salol											
II - 23	10.60	28.19	28.30	28.09	0.8889	1.80	33.76	32.49	34.93	35.80	
II - 24	6.51	28.07	28.18	27.96	0.8920	1.10	43.30	41.86	44.76	35.75	0.8970
II - 25	4.57	31.05	31.47	30.64	0.8881	0.70	11.56	8.88	14.52	35.15	0.8972
II - 28	9.70	27.66	28.82	26.49	0.9000	0.95	60.68	43.96	80.28	36.40	
II - 29	9.93	28.49	28.63	28.34	0.8950	0.95	45.70	43.82	47.75	36.20	
II - 31	2.56	28.61	28.88	28.34	0.8800	0.20	40.82	37.45	44.36	35.20	
II - 33	1.10	32.73	33.17	32.30	0.8892	0.10	8.94	6.40	11.56	35.80	0.9046
II - 34	3.62	30.56	30.90	30.23	0.8901	0.60	21.16	18.15	24.30	35.76	0.8970

[a] Interfacial temperature rise, measurements made on isothermal stage.

[b] Equilibrium temperature from the phase diagram based on y_i.

[c] Diffusivity, $D = 0.74\times10^{-6}$ cm^2/sec at 29.5° C was used and corrected with temperature for computing x_i using flux balance method.

Table XVII. Experimental Results, Pure trans-Stilbene using T.G.M.S.

Run No.	$V \times 10^3$ (cm/sec)	T_i °C	T_1 °C	T_2 °C	$(\Delta T)^2$	$(\Delta T_1)^2$	$(\Delta T_2)^2$	T_e [a]	Note
IV - 16	0.68	121.58	122.04	121.12	2.01	0.92	3.53	123.0	zone refined
IV - 17	0.36	121.73	122.28	121.19	1.61	0.52	3.28	123.0	zone refined
IV - 21	3.00	119.91	120.23	119.59	9.55	7.67	11.63	123.0	zone refined
IV - 22	2.08	120.55	120.73	120.37	6.00	5.15	6.91	123.0	zone refined
IV - 23	1.43	120.33	120.50	120.16	7.13	6.25	8.06	123.0	zone refined

[a] Melting point measured using Buchi apparatus.

Table XVIII. Effective Distribution Coefficient K^* Calculated from Eq. (IV-12)

Run No.	V (cm/sec)×10^3	K_A^{*a}	K_B^{*a}	K_A^{*b}	K_B^{*b}	K_A^{c}	K_B^{c}
$y_{BO} = y_B(\infty)$ = 0.15 mole fraction stilbene							
III- 72	0.68	0.982	1.115	0.983	1.108	0.694	3.038
III- 73	1.00	0.988	1.077	d	d	0.686	3.008
III- 75	1.92	0.994	1.039	0.978	1.134	0.711	3.107
III- 76	0.51	0.949	1.352	d	d	0.693	3.035
III- 77	0.50	0.978	1.137	0.944	1.343	0.699	3.060
III- 99	0.74	0.970	1.207	d	d	0.696	3.046
III-101	0.34	0.949	1.346	0.977	1.156	0.702	3.071
III-102	0.40	0.963	1.233	0.939	1.385	0.704	3.079
III-103	0.15	0.914	1.542	0.870	1.822	0.707	3.089
III-104	0.13	0.897	1.633	0.869	1.806	0.698	3.056
III-105	0.39	0.964	1.221	0.920	1.487	0.704	3.077
III-106	0.21	0.958	1.248	0.841	1.938	0.715	3.122
III-107	0.31	0.962	1.228	0.911	1.534	0.697	3.050
III-140	0.42	0.973	1.165	0.940	1.359	0.692	3.033
III-141	0.35	0.966	1.219	0.937	1.392	0.707	3.089
III-143	0.23	0.954	1.280	0.932	1.416	0.691	3.027
III-144	0.15	0.924	1.450	0.864	1.825	0.700	3.061
III-145	0.09	0.941	1.344	0.811	2.103	0.694	3.040
III-146	0.03	0.793	2.227	0.724	2.635	0.711	3.106

(continued)

Table XVIII. continued

Run No.	V $(cm/sec)\times10^3$	K_A^{*a}	K_B^{*a}	K_A^{*b}	K_B^{*b}	K_A^{c}	K_B^{c}
$y_{BO} = y_B(\infty) = 0.15$ mole fraction stilbene							
III-147	0.20	0.925	1.474	0.898	1.640	0.704	3.080
III-148	0.73	0.993	1.039	0.905	1.554	0.737	3.209
III-149	0.25	0.941	1.361	0.884	1.713	0.710	3.102
IV - 1	0.21	0.940	1.315	0.863	1.701	0.699	3.058
IV - 2	0.15	0.913	1.525	0.896	1.627	0.689	3.019
IV - 3	0.10	0.870	1.779	0.816	2.103	0.701	3.067
IV - 4	0.07	0.832	2.012	0.801	2.199	0.699	3.058
IV - 5	0.79	0.990	1.061	0.991	1.052	0.678	2.976
IV - 6	0.65	0.983	1.108	0.954	1.285	0.702	3.069
IV - 7	0.35	0.970	1.186	0.920	1.504	0.708	3.095
IV - 8	0.15	0.950	1.455	0.840	1.912	0.703	3.077
IV - 9	0.24	0.976	1.142	0.893	1.627	0.692	3.033
IV - 10	0.12	0.895	1.633	0.861	1.844	0.695	3.044

[a]Calculated from experimentally determined $y_i(0)$ and $x_i(0)$.

[b]With k_B^F calculated from Eq. (IV-21) using $\chi = 0.01$, and $\Delta T = T_e - T(0)$ for computing step density f to determine g_B.

[c]Equilibrium distribution coefficient based on measured interface temperature.

[d]Not computed because of negative ΔT due to error in the measurement of $T(0)$.

Table XIX. Effective Distribution Coefficient K^* Calculated from Eq. (IV-12)

Run No.	V (cm/sec)×10^3	K_A^{*a}	K_B^{*a}	K_A^{*b}	K_B^{*b}	K_A^{c}	K_B^{c}
$y_{BO} = y_B(\infty)$ = 0.25 mole fraction stilbene							
III- 78	0.48	0.954	1.151	0.868	1.439	0.574	2.585
III- 79	0.87	0.972	1.093	0.982	1.059	0.555	2.514
III- 80	1.33	0.986	1.047	0.946	1.183	0.566	2.556
III- 81	1.62	0.991	1.028	0.947	1.172	0.571	2.572
III- 84	0.16	0.866	1.442	0.847	1.505	0.558	2.525
III- 85	0.52	0.974	1.081	0.864	1.429	0.563	2.546
III- 86	1.24	0.981	1.063	0.950	1.161	0.562	2.542
III- 89	0.89	0.974	1.088	0.957	1.144	0.566	2.554
III- 91	2.00	0.991	1.028	0.947	1.170	0.572	2.576
III- 92	0.71	0.967	1.115	0.962	1.132	0.566	2.555
III- 93	0.96	0.979	1.071	0.937	1.211	0.571	2.573
III- 94	0.57	0.974	1.086	0.883	1.384	0.572	2.576
III- 96	0.10	0.774	1.739	0.913	1.285	0.549	2.492
III- 97	0.06	0.620	2.218	0.773	1.728	0.549	2.492
III- 98	0.13	0.792	1.672	0.731	1.868	0.565	2.551

[a] Calculated from experimentally determined $y_i(0)$ and $x_i(0)$.

[b] With k_B^F calculated from Eq. (IV-21) using $\chi = 0.01$, and $\Delta T = T_e - T(0)$ for computing step density f to determine g_B.

[c] Equilibrium distribution coefficient based on measured interface temperature.

[d] Not computed because of negative ΔT due to error in the measurement of $T(0)$.

Table XX. Effective Distribution Coefficient K^* Calculated from Eq. (IV-12)

Run No.	V	K_A^{*a}	K_B^{*a}	K_A^{*b}	K_B^{*b}	K_A^{c}	K_B^{c}
	$(cm/sec)\times10^3$						
$y_{BO} = y_B(\infty) = 0.45$ mole fraction stilbene							
III-108	0.83	0.959	1.054	0.874	1.163	0.409	1.818
III-109	0.58	0.931	1.089	0.990	1.013	0.400	1.779
III-110	0.39	0.920	1.101	0.722	1.352	0.410	1.823
III-113	0.16	0.882	1.148	0.526	1.595	0.420	1.865
III-115	0.76	0.930	1.092	0.779	1.292	0.422	1.872
III-116	0.34	0.888	1.142	0.725	1.351	0.409	1.817
III-117	0.29	0.891	1.137	0.702	1.375	0.407	1.809
III-118	0.15	0.729	1.340	0.638	1.453	0.404	1.796
III-119	0.14	0.710	1.384	0.521	1.633	0.428	1.903
III-132	0.86	0.926	1.097	0.675	1.428	0.451	2.005[e]
III-133	0.47	0.896	1.140	d	d	0.387	1.721
III-134	0.72	0.950	1.064	0.861	1.176	0.405	1.801
III-135	2.08	0.988	1.016	0.931	1.087	0.408	1.810
III-136	2.99	0.991	1.012	0.987	1.129	0.421	1.872
III-137	1.49	0.979	1.026	0.888	1.143	0.412	1.830
III-138	2.06	0.983	1.022	0.904	1.124	0.416	1.847
III-139	0.45	0.920	1.106	d	d	0.387	1.721

[a]Calculated from experimentally determined $y_i(0)$ and $x_i(0)$.

[b]With k_B^F calculated from Eq. (IV-21) using $\chi = 0.01$, $\Delta T = T_e - T(0)$ for computing step density f to determine g_B.

(continued)

Table XX. continued

[c]Equilibrium distribution coefficient based on measured interface temperature.

[d]Not computed because of negative ΔT due to error in the measurement of $T(0)$.

[e]Measured interface temperature $T(0)$ was in error.

B. Sample Calculations

1. Bibenzyl-Stilbene System

a. Measured Data for Bibenzyl-Stilbene System. Measured quantities, α, β, γ, s, t_i, ΔN, and $(dw/dv)_{v=0}$ were measured for each fringe pattern taken by Polaroid picture (see Fig. 4 of Chapter II). They were tabulated in Tables XXI, XXII, and XXIII. Since it was very difficult to measure the slope of a fringe at interface by eye, each fringe line was fitted with a least-squares second-order polynomial and the slope at interface was then computed from the fitted curve. The fringe shift, ΔN, at the interface, equal to (OB/OA) in Fig. 4 of Chapter II, was measured on the Polaroid pictures. The average ΔN was computed from measurements of as many as four fringe shifts.

The measured refractive indices of the binary mixtures of bibenzyl-stilbene system, tabulated in Table V, were comparable to the values obtained from the fitted equation by Kirwan (1967).

$$n = 1.5735 - 4.56 \times 10^{-4} T_i + 9.67 \times 10^{-2} y_{BO} - 1.15 \times 10^{-4} T_i y_{BO} + 9.30 \times 10^{-3} y_{BO}^2 \quad .$$

Thus,

$$\frac{\partial n}{\partial y})_T = 9.67 \times 10^{-2} - 1.15 \times 10^{-4} T_i + 1.86 \times 10^{-2} y_{BO} \ ,$$

where T_i = interfacial temperature in deg C.

b. Calculation of Interfacial Liquid Composition.

$$y_B(0) = y_B(\infty) - \Delta N \frac{\lambda_0}{2\, t_i (\partial n/\partial y)_T} \ .$$

For Run No. III-107, $\Delta N = 0.56$, $t_i = 0.3$ mm, $T_i = 63.28°$ C, $y_{BO} = 0.15$ mole fraction, stilbene.

$$(\partial n/\partial y)_T = 9.67 \times 10^{-2} - 1.15 \times 10^{-4} T_i + 1.86 \times 10^{-2} y_{BO} = 9.20 \times 10^{-2}$$

$$y_B(0) = 0.15 - (0.56) \frac{6.328 \times 10^{-4}}{2(0.31)(9.20 \times 10^{-2})} = 0.1436 \text{ mole fraction.}$$

c. Calculation of Interfacial Solid Composition. From Eq. (3) of Chapter II,

$$x_B(0) = y_B(0) + \frac{D}{V(\rho_S/\rho_L)} \quad \frac{dy}{dz})_{z=0}$$

$y_B(0) = 0.1436$, $\rho_S/\rho_L \sim 1$. From Eq. (4) of Chapter II and $V = 3.1 \times 10^{-4}$ cm/sec, $D = 7.594 \times 10^{-6}$ sq cm/sec and other measured values listed in Table XXI.

$$\frac{dy}{dz})_i = \frac{(6.328 \times 10^{-4})(0.115)}{2(1.53 \times 10^{-2})(0.3)(\cos 2.5)(\sin 128 + 0.115 \cos 128)(9.20 \times 10^{-2})}$$

$$= 0.12(\text{mm})^{-1} = 1.20(\text{cm})^{-1} \ .$$

$$x_B(0) = 0.1436 + \frac{7.59 \times 10^{-6}}{3.1 \times 10^{-4}} (1.2) = 0.1736 \text{ mole fraction.}$$

Table XXI. Experimental Measurements, Bibenzyl-Stilbene System

Run No.	$V \times 10^3$	t_i	$s \times 10^2$	α	β	γ	ΔN	$\left(\frac{dw}{dv}\right)_i$	$\left(\frac{dy}{dz}\right)_i$
	cm/sec	mm	mm		degrees				$(mm)^{-1}$
$y_{B0} = y(\infty) = 0.15$ mole fraction, stilbene									
III- 72	0.68	0.32	1.50	2.6	47.0	44.5	1.34	0.149	0.128
III- 73	1.00	0.32	1.50	3.0	43.5	49.0	1.69	0.136	0.124
III- 75	1.92	0.32	1.50	3.0	65.0	27.0	1.04	0.168	0.123
III- 76	0.51	0.32	1.50	3.0	125.0	30.0	2.21	0.263	0.284
III- 77	0.50	0.32	1.50	4.0	62.0	31.0	0.83	0.156	0.117
III- 99	0.74	0.29	1.65	4.0	107.0	21.5	1.92	0.292	0.242
III-101	0.34	0.29	1.65	2.5	118.0	30.0	1.73	0.207	0.190
III-102	0.40	0.29	1.50	0.0	91.0	0.0	1.10	0.195	0.154
III-103	0.15	0.29	1.50	2.0	32.0	55.0	1.14	0.105	0.134
III-104	0.13	0.30	1.62	2.5	45.0	40.5	0.90	0.166	0.143
III-105	0.39	0.30	1.62	2.5	38.5	48.0	0.74	0.154	0.147
III-106	0.21	0.30	1.53	1.3	124.0	35.0	0.42	0.097	0.093
III-107	0.31	0.30	1.53	2.5	128.0	40.0	0.56	0.115	0.120
III-140	0.42	0.24	1.44	11.1	146.0	44.0	0.45	0.060	0.119
III-141	0.35	0.24	1.44	14.3	135.0	31.0	1.02	0.101	0.126
III-143	0.23	0.24	1.44	12.3	137.7	36.0	0.69	0.067	0.109
III-144	0.15	0.24	1.44	14.3	40.2	59.0	0.62	0.081	0.167

(continued)

Table XXI. continued

Run No.	$V \times 10^3$	t_i	$s \times 10^2$	α	β	γ	ΔN	$\left(\frac{dw}{dv}\right)_i$	$\left(\frac{dy}{dz}\right)_i$
	cm/sec	mm	mm		degrees				$(mm)^{-1}$
$y_{BO} = y(\infty)$ mole fraction, stilbene									
III-145	0.09	0.24	1.50	13.3	45.3	58.0	0.27	0.042	0.056
III-146	0.03	0.24	1.50	13.8	33.3	70.0	0.38	0.044	0.074
III-147	0.20	0.24	1.47	12.2	28.5	75.0	0.63	0.071	0.133
III-148	0.73	0.24	1.41	13.8	44.0	32.5	0.24	0.034	0.050
III-149	0.25	0.24	1.44	12.7	28.7	72.0	0.71	0.083	0.152
IV - 1	0.21	0.24	1.47	12.9	27.2	75.0	0.50	0.068	0.130
IV - 2	0.15	0.24	1.47	12.0	25.6	75.0	0.53	0.067	0.135
IV - 3	0.10	0.24	1.47	13.7	27.5	75.0	0.48	0.072	0.137
IV - 4	0.07	0.24	1.47	12.2	27.5	75.0	0.53	0.303	0.130
IV - 5	0.79	0.24	1.50	11.5	38.5	63.0	0.49	0.670	0.082
IV - 6	0.65	0.24	1.50	13.2	56.5	34.0	0.67	0.104	0.168
IV - 7	0.35	0.24	1.50	13.2	51.5	51.0	0.83	0.645	0.110
IV - 8	0.15	0.24	1.48	13.2	35.1	67.5	0.58	0.733	0.116
IV - 9	0.24	0.24	1.41	12.0	120.0	18.0	0.29	0.475	0.058
IV - 10	0.12	0.24	1.46	11.3	139.5	37.5	0.57	0.798	0.136

Note: V is the value corrected for the angle γ.

Table XXII. Experimental Measurements, Bibenzyl-Stilbene System

Run No.	$V \times 10^3$	t_i	$s \times 10^2$	α	β	γ	ΔN	$\frac{dw}{dv})_i$	$\frac{dy}{dz})_i$
	cm/sec	mm	mm		degrees				$(mm)^{-1}$
$y_{B0} = y(\infty) = 0.25$ mole fraction, stilbene									
III- 78	0.48	0.32	1.50	4.5	131.0	36.4	1.75	0.152	0.166
III- 79	0.87	0.32	1.50	8.0	129.0	30.5	1.81	0.170	0.183
III- 80	1.33	0.32	1.50	7.0	65.0	31.6	2.14	0.191	0.139
III- 81	1.62	0.32	1.50	7.0	56.0	41.0	1.38	0.133	0.106
III- 84	0.16	0.29	1.71	15.0	30.0	74.3	1.47	0.149	0.170
III- 85	0.52	0.29	1.71	13.0	41.0	61.0	0.82	0.101	0.097
III- 86	1.24	0.29	1.71	13.0	41.0	35.5	1.22	0.205	0.179
III- 89	0.89	0.30	1.71	11.5	77.0	24.7	1.97	0.268	0.177
III- 91	2.00	0.29	1.71	12.5	57.0	21.0	0.92	0.168	0.127
III- 92	0.71	0.29	1.71	12.0	101.0	0.0	2.15	0.241	0.182
III- 93	0.96	0.29	1.71	11.0	66.0	13.8	1.73	0.218	0.153
III- 94	0.57	0.29	1.71	12.0	109.0	7.3	1.44	0.141	0.111
III- 96	0.10	0.29	1.70	4.0	19.0	67.0	1.32	0.114	0.183
III- 97	0.06	0.29	1.65	0.0	19.0	69.0	1.05	0.111	0.185
III- 98	0.13	0.29	1.65	0.0	18.0	72.0	1.12	0.123	0.207

Note: V is the value corrected for the angle γ.

Table XXIII. Experimental Measurements, Bibenzyl-Stilbene System

Run No.	$V \times 10^3$	t_i	$s \times 10^2$	α	β	γ	ΔN	$\left(\frac{dw}{dv}\right)_i$	$\left(\frac{dy}{dz}\right)_i$
	cm/sec	mm	mm		degrees				$(mm)^{-1}$
$y_{BO} = y(\infty) = 0.45$ mole fraction, stilbene									
III-108	0.83	0.30	1.53	1.0	97.0	7.5	1.35	0.196	0.149
III-109	0.58	0.26	1.53	1.0	95.5	6.0	1.11	0.200	0.174
III-110	0.39	0.30	1.50	0.0	106.0	15.0	0.79	0.165	0.134
III-113	0.16	0.30	1.50	3.5	61.5	24.5	0.57	0.101	0.081
III-115	0.76	0.30	1.52	4.5	63.5	21.5	1.72	0.328	0.233
III-116	0.34	0.30	1.53	3.0	33.5	53.0	0.91	0.153	0.165
III-117	0.29	0.30	1.53	3.0	130.0	42.0	0.65	0.127	0.136
III-118	0.15	0.30	1.53	3.0	143.0	55.0	0.54	0.128	0.187
III-119	0.14	0.30	1.56	0.0	61.0	28.5	1.71	0.276	0.196
III-132	0.86	0.24	1.44	14.5	131.0	25.5	1.31	0.180	0.282
III-133	0.47	0.24	1.47	15.0	42.5	61.0	1.60	0.179	0.220
III-134	0.72	0.24	1.41	12.5	41.0	61.0	0.63	0.112	0.154
III-135	2.08	0.24	1.41	10.5	106.5	6.0	0.63	0.101	0.109
III-136	2.99	0.24	1.41	12.0	87.5	15.0	0.51	0.113	0.114
III-137	1.49	0.24	1.50	13.5	59.0	44.0	0.80	0.126	0.131
III-138	2.06	0.24	1.50	13.0	58.0	45.0	0.99	0.147	0.152
III-139	0.45	0.24	1.50	12.0	59.0	42.0	1.30	0.153	0.157

Note: V is the value corrected for the angle γ.

2. Salol-Thymol System

a. Measured Data. All measured quantities necessary for the computation of interfacial compositions were listed in Table XXIV.

b. Calculation of Interfacial Liquid Composition. For Run II-9, $t_i = 0.24$ mm, $\Delta N = 1.05$, $y_0 = 0.90$ mole fraction of thymol, $(\partial n/\partial y)_T = 6.8 \times 10^{-2}$. Since the refractive index of salol melt is higher than that of pure thymol melt, growing a crystal richer in thymol results in depletion of the liquid interfacial concentration of thymol. Consequently the fringe shift owing to the increase in refractive index of the binary melt at interface will move toward thinner edge of the wedge, according to Eq. (2) of Chapter II. The fringe shift will be in opposite direction of what is shown in Fig. 4 of Chapter II.

$$y(0) = 0.90 - (1.05)\frac{6.328 \times 10^{-4}}{2(0.24)(6.8\times10^{-2})} = 0.8796 \text{ mole fraction.}$$

c. Calculation of Interfacial Solid Composition. For Run II-9, $T_i = 33.26°$ C, $s = 1.08 \times 10^{-2}$ mm, $\alpha = 7.0$ degrees, $\beta = 79.0$ degrees, $V = (1.03)(0.8796) \times 10^{-4} = 9.06 \times 10^{-5}$ cm/sec, and $D = 0.74 \times 10^{-6}$ $(306.41/302.65) = 0.749 \times 10^{-6}$ sq cm/sec.

$$\left(\frac{dy}{dz}\right)_i = \frac{(6.328\times10^{-4})(0.232)}{2(1.08\times10^{-2})(0.24)(\cos 7)(\sin 79 + 0.23 \cos 79)(6.8 \times 10^{-2})}$$

$$= 0.448 \text{ (mm)}^{-1} = 4.48 \text{ (cm)}^{-1}$$

$x(0) = 0.8796 + (0.749\times10^{-6}/9.06\times10^{-5})(4.48) = 0.9165$ mole fraction, thymol.

Table XXIV. Experimental Measurements, Salol-Thymol System

Run No.	$(V/y_i)\times10^4$	t_i	$s \times 10^2$	α	β	ΔN	$\left(\frac{dw}{dv}\right)_i$	$\left(\frac{dy}{dz}\right)_i$
	cm/sec-mf	mm	mm	degrees				$(mm)^{-1}$
$y_0 = y(\infty) = 0.90$ mole fraction, thymol								
II - 4	4.82	0.23	1.14	7.0	82.5	1.04	0.312	0.590
II - 5	4.88	0.24	1.14	4.0	76.5	2.16	0.551	1.114
II - 7	2.12	0.24	0.96	9.5	85.5	1.95	0.668	1.449
II - 9	1.03	0.24	1.08	7.0	79.0	1.05	0.232	0.448
II - 10	1.58	0.22	1.38	3.5	85.5	2.28	0.714	1.165
II - 11	3.50	0.22	1.20	6.0	87.5	3.28	0.726	1.329
II - 13	3.32	0.23	0.99	4.0	105.0	2.93	0.495	0.927
II - 14	6.20	0.23	1.23	5.0	88.0	2.18	0.662	1.119
II - 16	5.96	0.20	1.62	6.0	116.5	1.71	0.718	0.851
II - 19	7.68	0.26	1.20	2.0	72.0	0.71	0.553	1.057
II - 20	4.51	0.20	1.23	2.5	107.0	1.34	0.612	1.020
II - 21	2.92	0.24	1.20	5.5	59.0	1.45	0.329	0.776
$y_0 = y(\infty) = 0.90$ mole fraction, salol								
II - 24	6.51	0.25	1.29	0.0	102.0	0.43	0.249	0.388
II - 25	4.57	0.20	1.29	0.0	103.5	0.51	0.250	0.494
II - 33	1.10	0.46	1.20	9.0	80.0	1.07	0.205	0.201
II - 34	3.62	0.31	1.53	15.6	92.0	0.66	0.294	0.303

Note: V is the value corrected for the angle γ, i.e. the normal velocity of the interface.

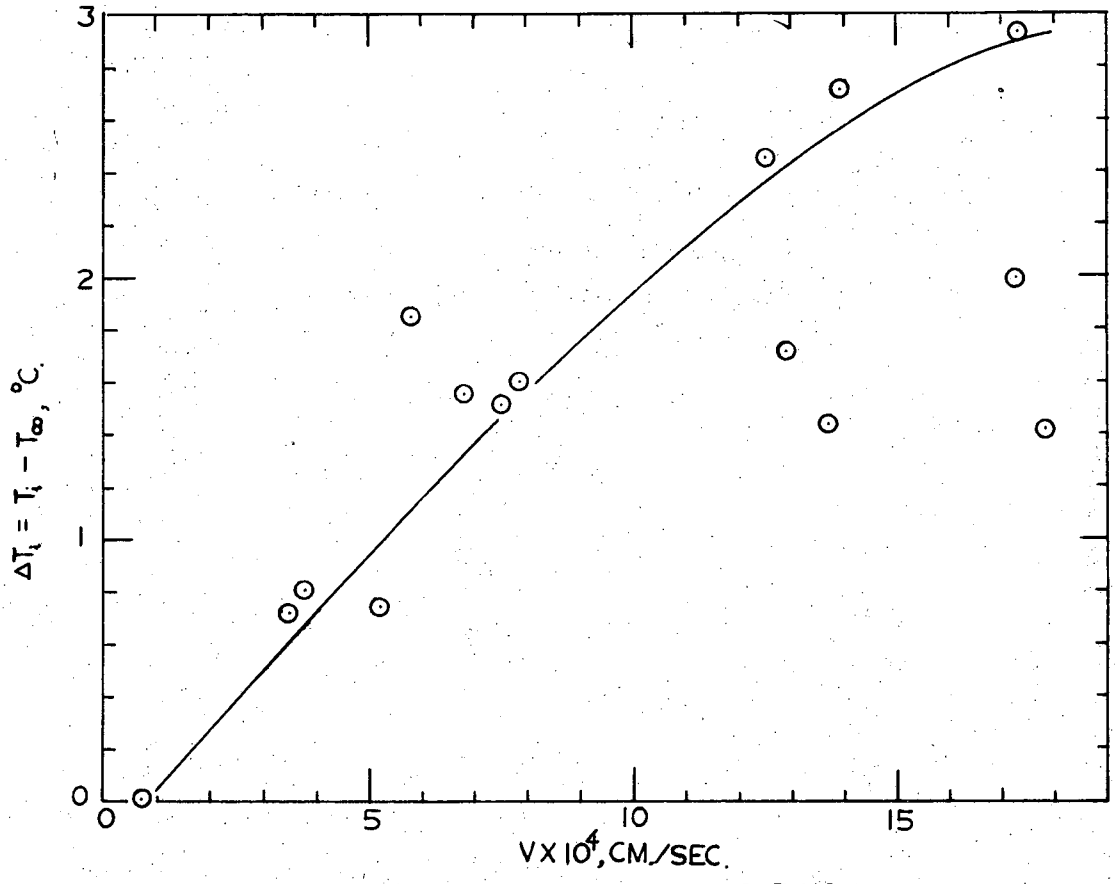

INTERFACIAL TEMPERATURE RISE DURING
THE GROWTH OF PURE SALOL

XBL 6911-6504

Fig. 7

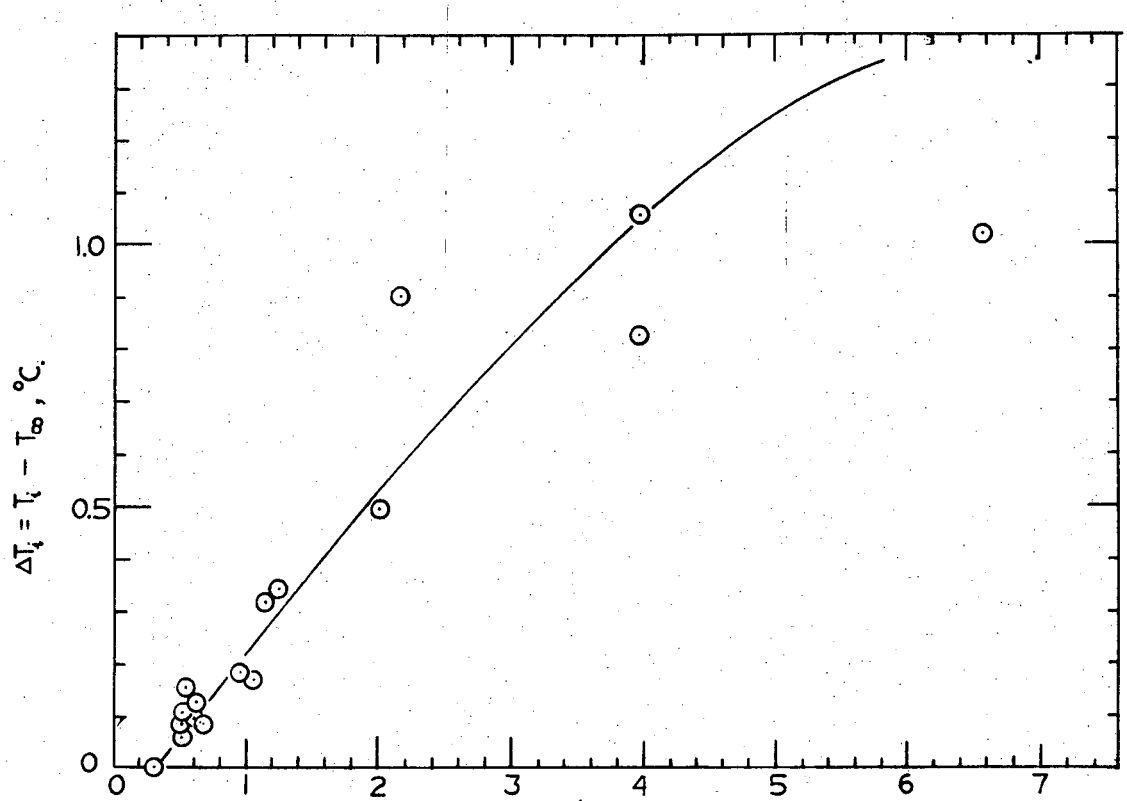

INTERFACIAL TEMPERATURE RISE DURING THE GROWTH OF PURE THYMOL

XBL 6911-6505

Fig. 8

C. Measurement of Interfacial Temperature Rise

1. Salol-Thymol System. When either pure salol or pure thymol grew in its own melt, any fringe shift at the interface was due to temperature rise. Measurements were made for the growth of pure salol and for pure thymol on an isothermal microscope stage; the results were plotted in Fig. 7 for salol and in Fig. 8 for thymol. For salol highly scattered results were noticed at higher growth rates.

2. Bibenzyl-Stilbene System. Measurements of the rates of growth of pure trans-stilbene using the temperature-gradient microscope stage did not reveal any observable fringe shift. Therefore the effect of interface temperature rise on the growth of bibenzyl-stilbene system was not considered.

LITERATURE CITED

Chapter I

Burton, W., Cabrera, N., and Frank, F. C., Phil. Trans. Roy. Soc. (London) A243, 299 (1951).

Cabrera, N., in "Crystal Growth" edited by H. S. Peiser, Pergamon Press (1967).

Frank, F. C., in "Growth and Perfection of Crystals", John Wiley and Sons, New York (1958).

Glasston, S., Laidler, K., and Eyring, H., "Theory of Rate Processes", McGraw-Hill, New York (1941).

Hillig, W. B., and Turnbull, D., J. Chem. Phys. 24, 914 (1956).

Hunt, J. D., Jackson, K. A., and Brown, H., Rev. Sci. Instr. 37, 805 (1966).

Kirwan, D. J., and Pigford, R. L., A.I.Ch.E.J. 15, 442 (1969).

Mott, N. F., Disc. Far. Soc. 5, 11 (1948).

Powers, J. E., Hydrocarbon Process. Petrol. Refiner. 45, 97 (1966).

Turnbull, D., Scientific American, 212, 38 (1965).

LITERATURE CITED

Chapter II

Berg, W., Proc. Roy. Soc. (London) 164A, 79 (1938).

Bunn, C. W., Disc. Far. Soc. 5, 132 (1949).

Cheng, C. T., Ph.D. Thesis in Chemical Engineering, University of California (1969).

Hillig, W. B., and Turnbull, D. J., Chem. Phys. 24, 914 (1956).

Humphreys-Owen, S. Proc. Roy. Soc. (London) 197A, 218 (1948).

Hunt, J. D., Jackson, K. A., and Brown, H., Rev. Sci. Instr. 37, 805 (1966).

Kirwan, D. J., and Pigford, R. L., A.I.Ch.E.J. 15, 442 (1969).

Kirwan, D. J., Ph.D. Thesis in Chemical Engineering, University of Delaware (1967).

Nishijima, Y., and Oster, G., J. Polymer Sci. 19, 337 (1956).

Secor, R., A.I.Ch.E.J. 11, 452 (1965).

Timmermans, J., "Physico-Chemical Constants of Binary Systems in Concentrated Solutions", Vol. II, p. 1169, Interscience, New York (1959).

Wilke, C. R., and Chang, P., A.I.Ch.E.J. 1, 264 (1955).

LITERATURE CITED

Chapter III

Andrew, J. N., and Ubbelohde, A. R., Proc. Roy. Soc. (London) A228, 435 (1955).

Burton, W., Cabrera, N., and Frank, F. C., Phil. Trans. Roy. Soc. (London) A243, 299 (1951).

Cheng, C. T., and Pigford, R. L., Paper submitted for publication.

Clifton, D., Ph.D. Thesis, University of Utah (1957).

Cohen, M. H., and Turnbull, D., J. Chem. Phys. 31, 1164 (1959).

Frank, F. C., Disc. Fard. Soc. 5, 48 (1948).

Glasstone, S., Laidler, K., and Eyring, H., "Theory of Rate Processes", McGraw-Hill, New York (1941).

Greet, R. J., J. Crystal Growth 1, 195 (1967).

Greet, R. J., and Turnbull, D., J. Chem. Phys. 46, 1243 (1967).

Greet, R. J., and Turnbull, D., J. Chem. Phys. 47, 2185 (1967).

Hildebrand, J. H., and Rotariu, G. J., J. Am. Chem. Soc. 73, 2524 (1951).

Hillig, W. B, and Turnbull, D., J. Chem. Phys. 24, 914 (1956).

Kirwan, D. J., and Pigford, R. L., A.I.Ch.E.J. 15, 442 (1969).

Magill, J. H., and Plazek, D. J., J. Chem. Phys. 46, 3757 (1967).

Magill, J. H., and Ubbelohde, A. R., Trans. Fard. Soc. 54, 1811 (1958).

Plazek, D. J., and Magill, J. H., J. Chem. Phys. 45, 3038 (1966).

Turnbull, D., in "Solid State Physics", Vol. III, Academic Press, New York (1958).

Whitaker, S., and Pigford, R. L., Ind. Eng. Chem. 50, 1026 (1958).

LITERATURE CITED

Chapter IV

Bondi, A., J. Chem. Phys. 14, 591 (1936).

Burton, W., Cabrera, N., and Frank, F. C., Phil Trans. Roy. Soc. A243, 299 (1951).

Cahn, J., Hillig, W., and Sears, G., Acta Meta. 12, 1421 (1964).

Chalmers, B., "Principles of Solidification", J. Wiley and Sons, New York (1964).

Cheng, C. T., and Pigford, R. L., Paper submitted for publication.

Cheng, C. T., Ph.D. Thesis, Chem. Eng. Dept., University of California (1969).

Chernov, A. A., "The Spiral Growth of Crystals", Soviet Physics Uspekhi 4, 116 (1961).

Clifton, D, Ph.D. Thesis, University of Utah (1957).

Frank, F. C., Disc. Fard. Soc. 5, 48 (1948).

Glasston, S., Laidler, K., and Eyring, H., "Theory of Rate Processes", McGraw-Hill, New York (1941).

Hillig, W. B., and Turnbull, D., J. Chem. Phys. 12, 914 (1956).

Jackson, K. A., Uhlmann, D. R., and Hunt, J. D., J. Crystal Growth 1, 1 (1967).

Jackson, K. A., in "Growth and Perfection of Crystals", J. Wiley and Sons, New York (1958).

Jackson, K. A., "A Review of the Fundamental Aspects of Crystal Growth" in "Crystal Growth", Pergamon, Oxford (1967).

Jackson, K. A., "Current Concepts in Crystal Growth from the Melt" in "Progress in Solid State Chemistry" Vol. IV, (1967).

Kirwan, D. J., and Pigford, R. L., A.I.Ch.E.J. 15, 442 (1969).

Kirwan, D. J., Ph.D. Thesis, Chem. Eng. Dept., University of Delaware (1967).

Kolosov, N. Ia., Soviet Physics-Crystallography 3, 707 (1958).

Turnbull, D., in "Solid State Physics", Vol. III, Academic Press, New York (1958).

Van Hook, A., "Crystallization", Rheinhold Publ. Co., New York (1963).

Vignes, A., Ind. Eng. Chem. Fund. 5, 189 (1966).

Whitaker, S., and Pigford, R. L., Ind. Eng. Chem. 50, 1026 (1958).

Wilke, C. R., and Chang, P., A.I.Ch.E.J. 1, 264 (1955).

LITERATURE CITED

Chapter V

Andrews, J. N., and Ubbelohde, A. R., Proc. Roy. Soc. (London) A228, 435 (1955).

Flachsbart, I., Naturwiss. 44, 348 (1957).

Gainer, J. L., and Metzner, A. B., Proc. A.I.Ch.E.-I.Chem.E. (London) Joint Meeting, London 6, 74 (1965).

Greet, R. J., J. Crystal Growth 1, 195 (1967).

Greet, R. J., and Turnbull, D., J. Chem. Phys. 46, 1243 (1967).

Hulme, K. F., Proc. Phys. Soc. (London) B68, 393 (1955).

Jantsch, O., Z. fur. Krist. 108, 185 (1956).

Kirwan, D. J., Ph.D. Thesis, Chem. Eng. Dept., University of Delaware (1967).

Kolosov, H. Ia., Soviet Phys. - Crystallogrophy 3, 707 (1958).

Magill, J. H., and Plazek, D. J., J. Chem. Phys. 46, 3757 (1967).

Memelink, D. W., Phillips Res. Rept. 11, 183 (1956).

Pigford, R. L., private communication, University of California, 1969.

Plazek, D. J., and Magill, J. H., J. Chem. Phys. 45, 3038 (1966).

Slavyanski, V. T., J. General Chem. (USSR) 18, 1259 (1948).

Smith, V. G., Tiller, W. A., and Rutter, J. W., Can. J. Phys. 33, 723 (1955).

Timmermans, J., "Physico-Chemical Constants of Pure Organic Compounds", Elsevier Pub. Co., New York (1950).

Timmermans, J., "Physico-Chemical Constants of Binary Systems in Concentrated Solutions", Vol. II, p. 1169, Interscience, New York (1959).

Vignes, A., Ind. Eng. Chem. Fund. 5, 189 (1966).

Wilke, C. R., and Chang, P., A.I.Ch.E.J. 1, 264 (1955).

ACKNOWLEDGMENTS

The author is grateful to Professor R. L. Pigford for his encouragement, guidance, assistance in this research, and also for his warm personal concern during the course of this work.

These studies were supported by AEC Contract w-7405-eng-48. The author thanks the Atomic Energy Commission for its financial support.

Thanks are due Mr. Fred Wiltens for help with his creative suggestions in modifying the experimental apparatus and to Mr. G. G. Young for making the optical wedge for the isothermal crystal growth study.

The author is indebted to Mr. Ray G. Clem who performed the ultra violet absorption analysis for the determination of the mixed crystals composition.

The excellent typing and editing done by Mrs. Kathy Wissmar is thankfully acknowledged.

Above all, the author is most grateful to his wife, Lin, for her understanding and encouragement throughout the entire course of this work. Her help in assuming most of the responsibility to take good care of our four children while her husband works day and sometimes nights is greatly appreciated.

TECHNICAL INFORMATION DIVISION
LAWRENCE RADIATION LABORATORY
UNIVERSITY OF CALIFORNIA
BERKELEY, CALIFORNIA 94720